Appendix B: CSIRO Environmental Modelling Suite: Scientific description of the optical, carbon chemistry and biogeochemical models (BGC1p0).

Mark E. Baird[1], Matthew P. Adams[2], John Andrewartha[1], Nagur Cherukuru[1], Malin Gustafsson[3], Scott Hadley[1], Mike Herzfeld[1], Emlyn Jones[1], Nugzar Margvelashvili[1], Mathieu Mongin[1], John Parlsow[1], Peter J. Ralph[3], Farhan Rizwi[1], Barbara Robson[4], Uwe Rosebrock[1], Pavel Sakov[1], Thomas Schroeder[1], Jenny Skerratt[1], Andrew D. L. Steven[1], and Karen A. Wild-Allen[1]

[1]CSIRO, Oceans and Atmosphere, Hobart, Australia
[2]School of Chemical Engineering, The University of Queensland, Brisbane, Australia
[3]Plant Functional Biology and Climate Change Cluster, Faculty of Science, University of Technology Sydney, Sydney, Australia
[4]CSIRO, Land and Water, Canberra, Australia

June 1, 2017

Contents

List of Tables

List of Figures

1 Abstract

Over 20 years, Australia's Commonwealth Science Industry and Research Organisation (CSIRO) has developed a biogeochemical model for coupling with a hydrodynamic and sediment model for application in shallow and shelf seas, and applied this model around the Australian continent. With the focus on shallow seas, the model includes more detailed representations of benthic plants such as seagrass, macroalgae and corals than other marine biogeochemical models, and a detailed spectrally-resolved optical model. A second focus has been on, where possible, the geometric derivation of ecological rates. Thus nutrient uptake by microalgae considers the divergence of the gradient of the nutrient field in the vicinity of the cell, zooplankton grazing considers encounter rates based on summing relative motion, chlorophyll synthesis includes a geometrically-derived self-shading term, and the bottom coverage of benthic plants is generically-related to their biomass using a form derived from geometric arguments. This approach has led to an algebraically-complicated, and unfamiliar, set of equations, when compared to other biogeochemical models. But while being algebraically-complicated, the model has fewer unconstrained parameters and is therefore numerically simpler than it would otherwise be. Thus at this mature point in the model's developed, a full mathematical description of the model, including the rationale for many of the geometric derivations used, is required. The model is now being applied on the Great Barrier Reef, northeast Australia in a near real time capacity.

2 Overview

The CSIRO Environmental Modelling Suite (EMS) has been developed over 20 years to model coupled physical, sediment, chemical and biogeochemical processes in marine and estuarine environments. Recently the biogeochemical model has been significantly improved through the addition of a spectrally-resolved optical model and a number of new biogeochemical processes (carbon chemistry, coral processes, multiple seagrass species etc). This document provides a summary of the science used for the optical and biogeochemical models in the eReefs project, and a precise description of the equations used in the simulations. The implementation of the optical and biogeochemical models within the larger eReefs marine modelling workpackage is summarised in Fig. 1.

2.1 Spectrally-resolved optical model

The optical model undertakes calculations at distinct wavelengths of light (say 395, 405, 415, 705 nm) representative of individual wavebands (say 400-410, 410-420 nm etc.), and can be modified for the particular application. First the spectrally-resolved Inherent Optical Properties (IOPs) of

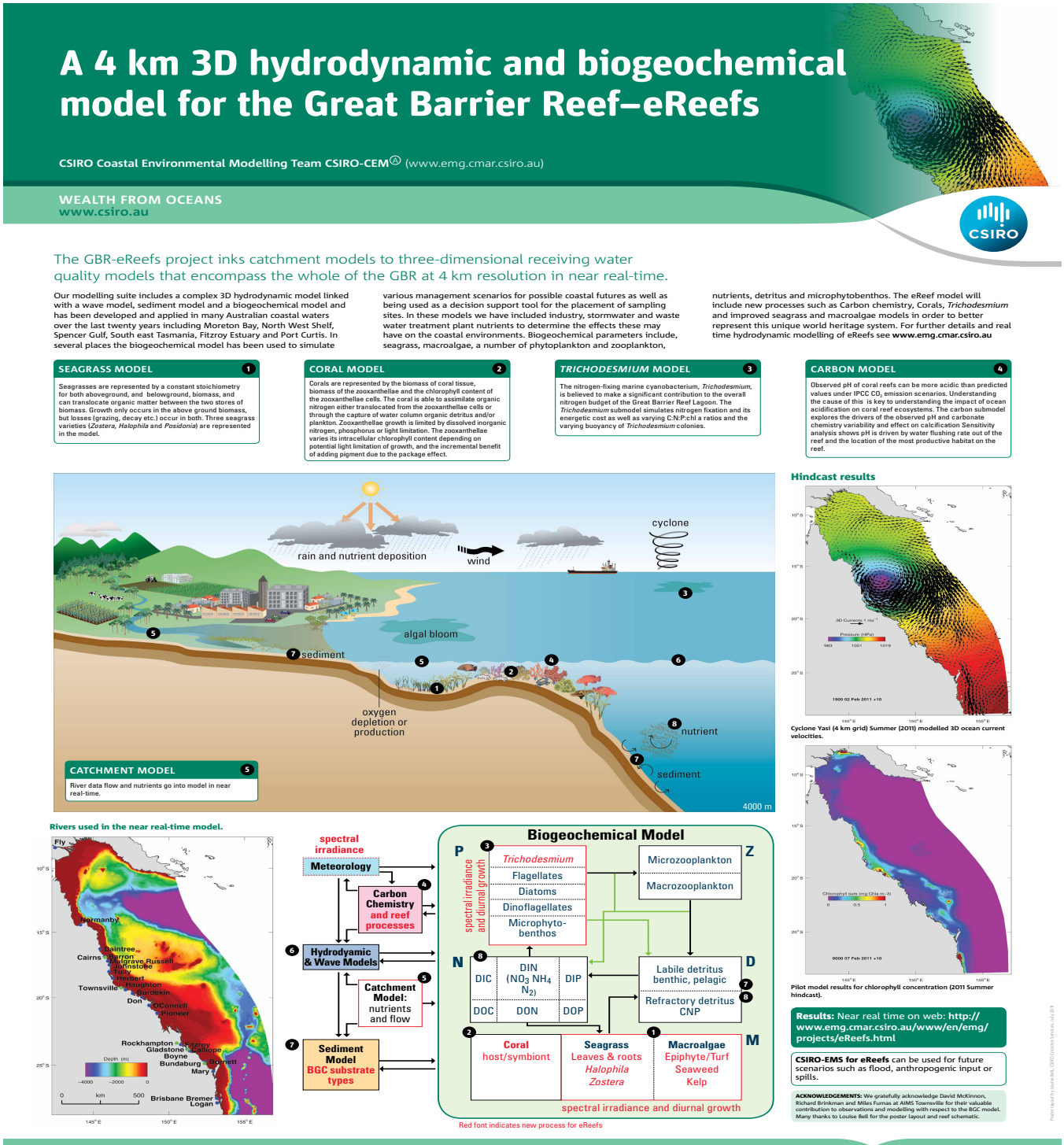

Figure 1: Australian Marine Science Association annual conference poster presentation, July 2013.

the water column are calculated from the model biogeochemical state (phytoplankton biomass, particulate concentrations etc). These include the absorption and scattering properties of clear water, colour dissolved organic matter, suspended solids and each microalgal population.

Using the calculated IOPs, as a well as sun angle, surface albedo and refraction, the spectrally-resolved light field (downwelling and scalar irradiance) is calculated for each grid cell in the model. From this light field phytoplankton absorption is calculated. The light that reaches the bottom is absorbed by epibenthic flora as a function of wavelength, depending on the absorbance of each individual flora. From the calculation of the light field other apparent optical properties (AOPs), such as remote-sensing reflectance, can be determined, and compared to remotely-sensed products. As AOPs can be recalculated from IOPs post-simulation, the model can be run for one set of wavelengths to optimise the integration speed and accuracy, and the AOPs re-calculated at another set of wavelengths for comparison with hyperspectral observations such as those used to calculate chlorophyll from the MODIS ocean color sensors.

The use of remote-sensing reflectance introduces a novel means of model assessment - simulated true colour. The model output can be processed to produce simulated true colour images of the water surface, with features such as bottom reflectance, river plumes and microalgal blooms easily characterised by their colour.

2.2 Biogeochemical model

The ecological model is organised into 3 zones: pelagic, epibenthic and sediment. Depending on the grid formulation the pelagic zone may have one or several layers of similar or varying thickness. The epibenthic zone overlaps with the lowest pelagic layer and the top sediment layer and shares the same dissolved and suspended particulate material fields. The sediment is modelled in multiple layers with a thin layer of easily resuspendable material overlying thicker layers of more consolidated sediment.

Dissolved and particulate biogeochemical tracers are advected and diffused throughout the model domain in an identical fashion to temperature and salinity. Additionally, biogeochemical particulate substances sink and are resuspended in the same way as sediment particles. Biogeochemical processes are organized into pelagic processes of phytoplankton and zooplankton growth and mortality, detritus remineralisation and fluxes of dissolved oxygen, nitrogen and phosphorus; epibenthic processes of growth and mortality of macroalgae, seagrass and corals, and sediment based processes of plankton mortality, microphytobenthos growth, detrital remineralisation and fluxes of dissolved substances (Fig. 2).

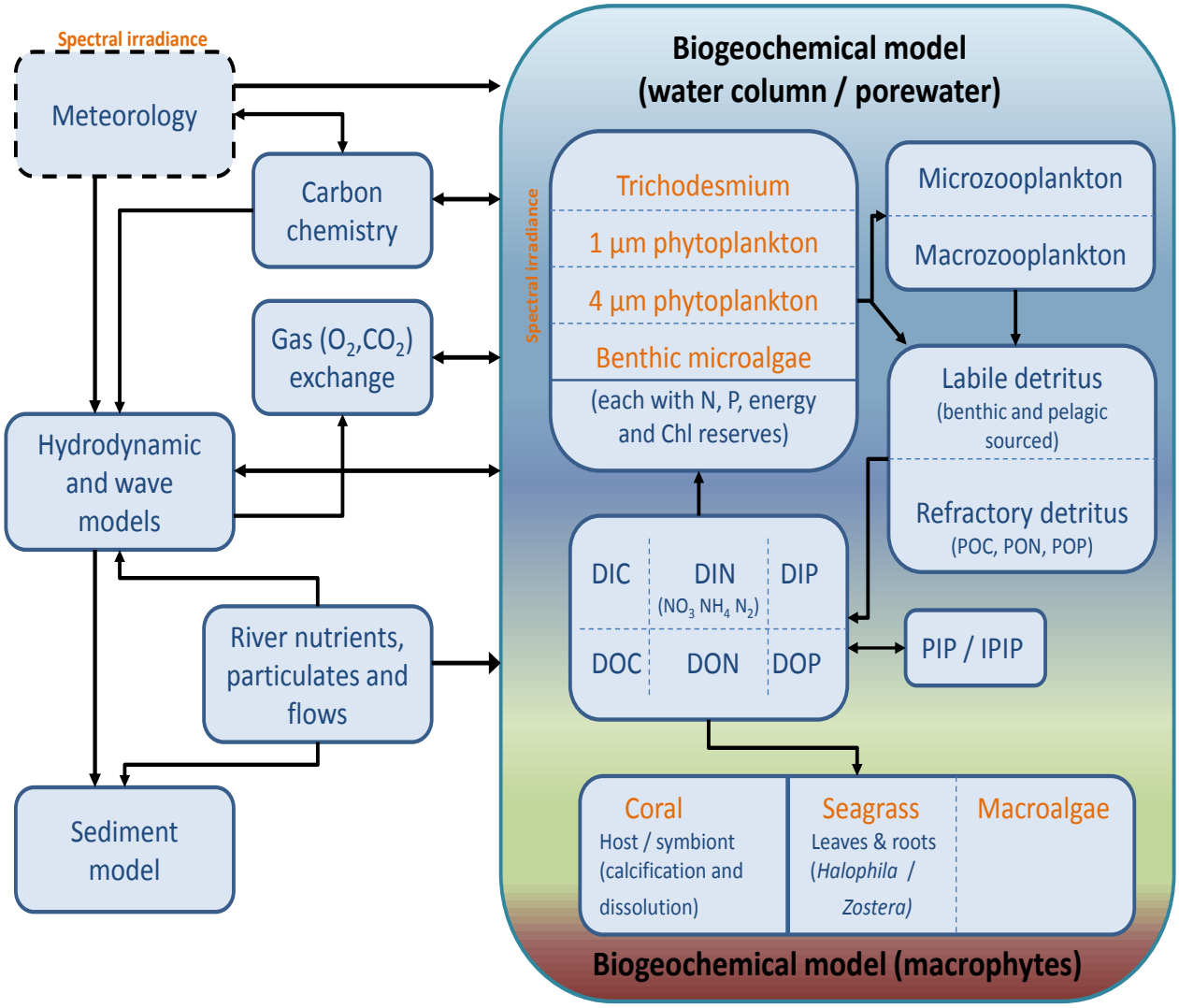

Figure 2: Schematic of CSIRO Environmental Modelling Suite. This document describes the biogeochemical processes in the water column, epipelagic and sediment zones.

The biogeochemical model considers four groups of microalgae (small and large phytoplankton, microphytobenthos and *Trichodesmium*), three macrophytes types (seagrass types corresponding to *Zostera* and *Halophila*, macroalgae) and coral communities. Photosynthetic growth is determined by concentrations of dissolved nutrients (nitrogen and phosphate) and photosynthetically active radiation. Autotrophs take up dissolved ammonium, nitrate, phosphate and inorganic carbon. Microalgae incorporate carbon (C), nitrogen (N) and phosphorus (P) at the Redfield ratio (106C:16N:1P) while macrophytes do so at the Atkinson ratio (550C:30N:1P). Microalgae contain two pigments (chlorophyll *a* and an accessory pigment), and have variable carbon:pigment ratios determined using a photoadaptation model.

Micro- and meso-zooplankton graze on small and large phytoplankton respectively, at rates determined by particle encounter rates and maximum ingestion rates. Additionally large zooplankton consume small zooplankton. Of the grazed material that is not incorporated into zooplankton biomass, half is released as dissolved and particulate carbon, nitrogen and phosphate, with the remainder forming detritus. Additional detritus accumulates by mortality. Detritus and dissolved organic substances are remineralised into inorganic carbon, nitrogen and phosphate with labile detritus transformed most rapidly (days), refractory detritus slower (months) and dissolved organic material transformed over the longest timescales (years). The production (by photosynthesis) and consumption (by respiration and remineralisation) of dissolved oxygen is also included in the model and depending on prevailing concentrations, facilitates or inhibits the oxidation of ammonia to nitrate and its subsequent denitrification to di-nitrogen gas which is then lost from the system.

Additional water column chemistry calculations are undertaken to solve for the equilibrium carbon chemistry ion concentrations necessary to undertake ocean acidification (OA) studies, and to consider sea-air fluxes of oxygen and carbon dioxide. The adsorption and desorption of phosphorus onto inorganic particles as a function of the oxic state of the water is also considered.

In the sediment porewaters, similar remineralisation processes occur as found in the water column (Fig. 3). Additionally, nitrogen is denitrified and lost as N_2 gas while phosphorus can become adsorbed onto inorganic particles, and become permanently immobilised in sediments.

2.3 Outline of document

The description of the optical and biogeochemical models is divided into the primary environmental zones: pelagic, epibenthic and sediment. Within these zones, descriptions are sorted by processes, such as microalgae growth, coral processes, food web interactions etc. This organisation allows the model to be explained, with notation, in self-contained chunks. For each process the complete set

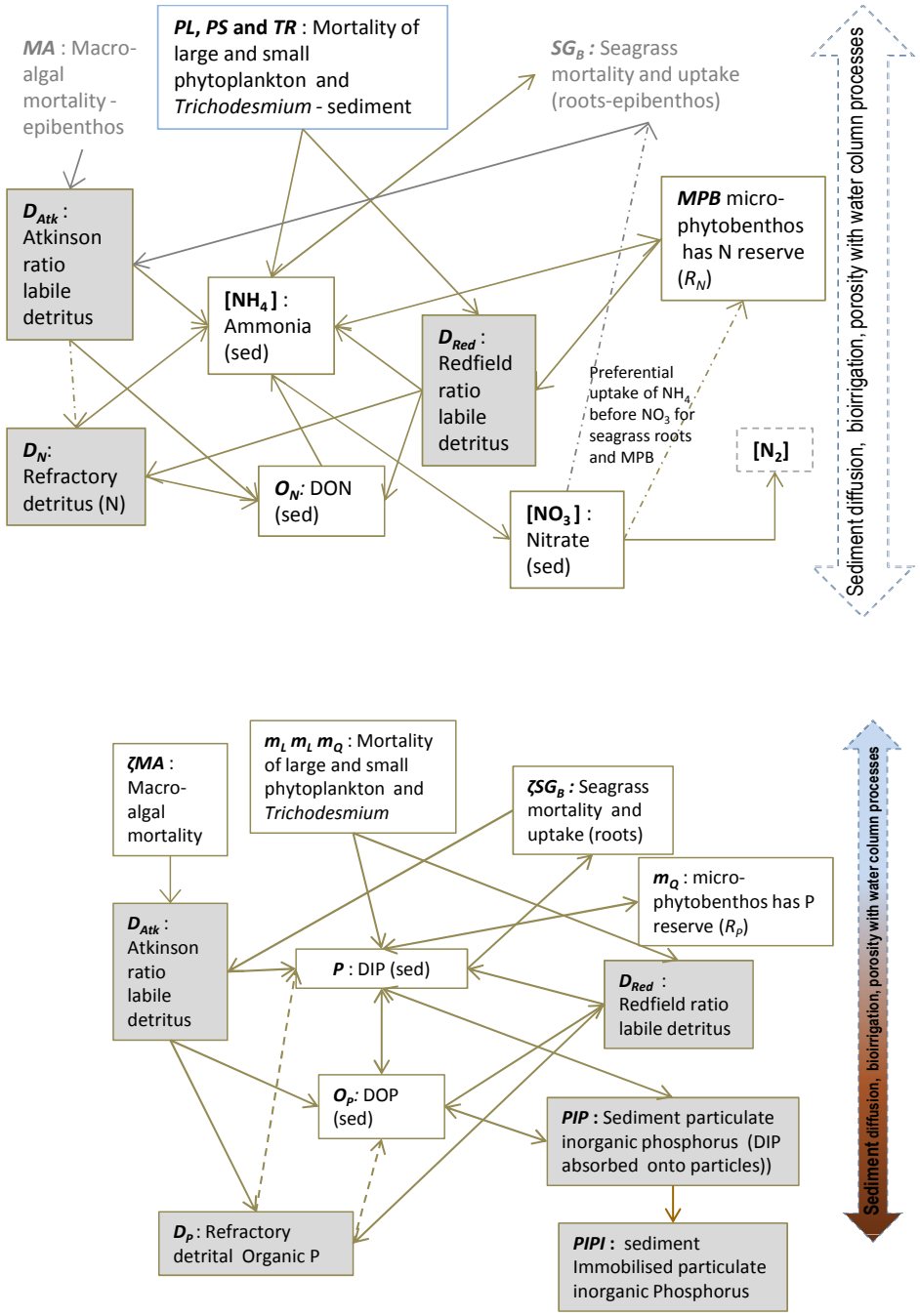

Figure 3: Schematic of sediment nitrogen and phosphorus pools and fluxes. Processes represented include phytoplankton mortality, detrital decomposition, denitification (nitrogen only), phosphorus adsorption (phosphorus only) and microphytobenthic growth.

of model equations, parameter values and state variables are given. As the code itself allows the inclusion / exclusion of processes at runtime, the process-based structuring of this document aligns with the structure of the code. To investigate the complete equation for a single state variable, such as nitrate concentration, the reader will need to combine the individual terms affecting the variable from all processes.

A number of text boxes appear in the description. These are additional explanations which may be useful for the reader, but are not essential for the description of the model itself.

Section 7 gives some of the details of the numerical methods that solve the model equations, and Section 8 lists peer-reviewed publications from the CSIRO EMS modelling suite.

Enjoy.

3 Pelagic processes

3.1 Transport

The local rate of change of concentration of each dissolved and particulate constituent, C, contains sink/source terms, S_C, which are described in length in this document, and the advection, diffusion and sinking terms:

$$\frac{\partial C}{\partial t} + \mathbf{v} \cdot \nabla^2 C = \nabla \cdot (K \nabla C) + w_{sink} \frac{\partial C}{\partial z} + S_C \tag{1}$$

where the symbol $\nabla = \left(\frac{\partial}{\partial x}, \frac{\partial}{\partial y}, \frac{\partial}{\partial z}\right)$, $\mathbf{v}$ is the velocity field, K is the eddy diffusion coefficient which varies in space and time, and w_C is the local sinking rate (positive downwards) and the z co-ordinate is positive upwards. The calculation of $\mathbf{v}$ and K is described in the hydrodynamic model (Herzfeld, 2006; Gillibrand and Herzfeld, 2016).

The microalgae are particulates that contain internal concentrations of dissolved nutrients and pigments that are specified on a per cell basis. To conserve mass, the local rate of change of the concentration of microalgae, B, multiplied by the internal concentration, R, is given by:

$$\frac{\partial (BR)}{\partial t} + \mathbf{v} \cdot \nabla^2 (BR) = \nabla \cdot (K \nabla (BR)) + w_C \frac{\partial (BR)}{\partial z} + S_{BR} \tag{2}$$

For more information see Sec. 3.3.5 and Section 3.1 of Baird et al. (2004a).

3.2 Optical model

The optical model considers the processes of absorption and scattering by clear water, coloured dissolved organic matter (CDOM), non-algal particulates (NAP) and phytoplankton cells. First the inherent optical properties (IOPs), such as total phytoplankton absorption at a specific wavelength, are calculated from the model state variables (e.g. phytoplankton chlorophyll biomass) and model parameters (e.g. cell radius). The optical model then solves for the apparent optical properties (AOPs), such as the spectrally-resolved scalar irradiance, from the surface downwelling light field and the IOPs. Finally, the AOPs can be directly compared to remotely-sensed products such as remote-sensing reflectance and simulated true colour images.

3.2.1 Inherent optical properties (IOPs)

Phytoplankton absorption. The absorption-cross section (α) of a spherical cell of radius (r), pigment-specific absorption coefficient (γ), and homogeneous intracellular pigment concentration (c_i), calcu-

	Symbol	Value
Constants		
Speed of light	c	2.998×10^8 m s^{-1}
Planck constant	h	6.626×10^{-34} J s^{-1}
Avagadro constant	A_V	6.02×10^{23} mol^{-1}
[a]Total scattering coefficient of phytoplankton	b_{phy}	0.2 (mg Chl a m^{-2})$^{-1}$
[b]Azimuth-independent scattering coefficient	g_i	0.402
[b]Azimuth-dependent scattering coefficient	g_{ii}	0.180
[c]CDOM-specific absorption coefficient at 443 nm	$k^*_{CDOM,443}$	0.02 m^2 mg C^{-1}
[c]Spectral slope of CDOM absorption	S_{CDOM}	0.012 nm^{-1}
[d]Linear remote-sensing reflectance coefficient	g_0	0.0895
[d]Quadratic remote-sensing reflectance coefficient	g_1	0.1247
[e]Backscatter ratio of non-algal particles	$\tilde{b}_{b,NAP}$	0.02

Table 1: Constants and parameter values used in the optical model.[a] Kirk (1994).[b] Kirk (1991) using an average cosine of scattering of 0.924 (Mobley, 1994). [c] Blondeau-Patissier et al. (2009). [d] Brando et al. (2012). [e] Vaillancourt et al. (2004).

lated using geometric optics (i.e., ray tracing) without considering internal scattering, is given by (Duysens, 1956; Kirk, 1975):

$$\alpha = \pi r^2 \left(1 - \frac{2(1-(1+2\gamma c_i r)e^{-2\gamma c_i r})}{(2\gamma c_i r)^2}\right) \tag{3}$$

where πr^2 is the projected area of a sphere, and the bracketed term is 0 for no absorption ($\gamma c_i r = 0$) and approaches 1 as the cell becomes fully opaque ($\gamma c_i r \to \infty$). The pigment-specific absorption coefficient (γ) is wavelength-dependent (Fig. 4), and later α will be calculated at specific wavelengths. Note that the bracketed term in Eq. 3 is mathematically equivalent to the dimensionless efficiency factor for absorption, Q_a (used in Morel and Bricaud (1981), Finkel (2001) and Bohren and Huffman (1983)), of homogeneous spherical cells with an index of refraction close to that of the surrounding water.

The use of an absorption cross-section of an individual cell has two significant advantages. Firstly, the same model parameters used here to calculated absorption in the water column are used to determine photosynthesis by individual cells, including the effect of packaging of pigments within cells. Secondly, the dynamic chlorophyll concentration determined later can be explicitly included in the calculation of phytoplankton absorption. Thus the absorption of a population of n cell m^{-3} is given by $n\alpha$ m^{-1}, while an individual cell absorbs αE_o light, where E_o is the scalar irradiance.

Coloured Dissolved Organic Matter (CDOM) absorption. Two equations for CDOM absorption are presently being trialed. It is possible a one may be applied in the the GBR4 and GBR1 grids, and

	Symbol	Units
Downwelling irradiance at depth z, wavelength λ	$E_{d,z,\lambda}$	W m^{-2}
Scalar irradiance at depth z, wavelength λ	$E_{o,z,\lambda}$	W m^{-2}
In water azimuth angle	θ	rad
Backscattering as a fraction of total absorption and scattering	u_λ	-
Below-surface remote-sensing reflectance	$r_{rs,\lambda}$	sr^{-1}
Above-surface remote-sensing reflectance	$R_{rs,\lambda}$	sr^{-1}
Thickness of model layer	h	m
Optical depth weighting function	$w_{z,\lambda}$	
Vertical attenuation coefficient	K_λ	m^{-1}
Total absorption coefficient	$a_{T,\lambda}$	m^{-1}
Total scattering coefficient	$b_{T,\lambda}$	m^{-1}
Absorption cross-section	α_λ	m^2 cell^{-1}
Concentration of cells	n	cell m^{-3}

Table 2: State and derived variables in the water column optical model.

another within the finer scale grids. The two schemes are:

Scheme 1. The absorption of CDOM, $a_{CDOM,\lambda}$, is determined from a relationship with salinity in the region (Schroeder et al., 2012):

$$a_{CDOM,443} = -0.0332S + 1.2336 \tag{4}$$

where S is the salinity. In order to avoid unrealistic extrapolation, the salinity used in this relationship is the minimum of the model salinity and 36. In some cases coastal salinities exceed 36 due to evaporation. The absorption due to CDOM at other wavelengths is calculated using a CDOM spectral slope for the region (Blondeau-Patissier et al., 2009):

$$a_{CDOM,\lambda} = a_{CDOM,443} \exp\left(-S_{CDOM}\left(\lambda - 443.0\right)\right) \tag{5}$$

where S_{CDOM} is an approximate spectral slope for CDOM, with observations ranging from 0.01 to 0.02 nm^{-1} for significant concentrations of CDOM. Lower spectral slope values generally occur at high concentrations of CDOM (Blondeau-Patissier et al., 2009).

Scheme 2. The absorption of CDOM, $a_{CDOM,\lambda}$, is directly related to the concentration of dissolved organic carbon, D_C.

$$a_{CDOM,\lambda} = k^*_{CDOM,443} D_C \exp\left(-S_{CDOM}\left(\lambda - 443.0\right)\right) \tag{6}$$

where $k^*_{CDOM,443}$ is the dissolved organic carbon-specific CDOM absorption coefficient at 443 nm.

Both schemes have drawbacks. Scheme 2, using the concentration of dissolved organic carbon, is closer to reality, but is likely to be sensitive to poorly-known parameters such as remineralisation rates and initial detritial concentrations. Scheme 1, a function of salinity, will be more stable, but perhaps less accurate, especially in estuaries where hypersaline waters may have large estuarine loads of coloured dissolved organic matter.

Absorption due to non-algal particulate material. In the model, optically-active non-algal particulates (NAPs) include the mineral particulates (such as sand and mud, see Sec. 5.1) and detritus.

$$a_{NAP,\lambda} = c_1 NAP^{c_2} \tag{7}$$

where c_1 and c_2 are spectrally-resolved coefficients determine from in situ observations and the concentrations of NAPs, NAP is given by:

$$NAP = Mud + FineSed + \left(\frac{550}{30}\frac{12}{14} D_{Atk} + \frac{106}{16}\frac{12}{14} D_{Red} + D_C \right) / 10^6 \tag{8}$$

where NAP, Mud and $FineSed$ are all quantified in kg m^{-3}, D_{Atk} and D_{Red} are quantified in mg N m^{-3} and D_C is quantified in mg C m^{-3}. Only refractory detrital carbon, D_C, is considered as by weight it is the component.

Total absorption. The total absorption, $a_{T,\lambda}$, is given by:

$$a_{T,\lambda} = a_{w,\lambda} + a_{NAP,\lambda} + a_{CDOM,\lambda} + \sum_{x=1}^{N} n_x \alpha_{x,\lambda} \tag{9}$$

where $a_{w,\lambda}$ is clear water absorption (Fig. 4) and N is the number of phytoplankton classes (see Table 3).

Scattering. The total scattering coefficient is given by

$$b_{T,\lambda} = b_{w,\lambda} + c_1 NAP^{c_2} + b_{phy,\lambda} \sum_{x=1}^{N} n_x c_{i,x} V_x \tag{10}$$

where NAP is the concentration of non-algal particulates, $b_{w,\lambda}$ is the scattering coefficient due to clear water (Fig. 4), c_1 and c_2 are two coefficients and phytoplankton scattering is the product of the chlorophyll-specific phytoplankton scattering coefficient, $b_{phy,\lambda}$, and the water column chlorophyll concentration of all classes, $\sum n_x c_{i,x} V_x$ (where c_i is the chlorophyll concentration in the cell, and V is the cell volume). The value for $b_{phy,\lambda}$ is set to 0.2 (mg Chl a m^{-2})$^{-1}$ for all wavelengths, a typical value for marine phytoplankton (Kirk, 1994). For more details see Baird et al. (2007).

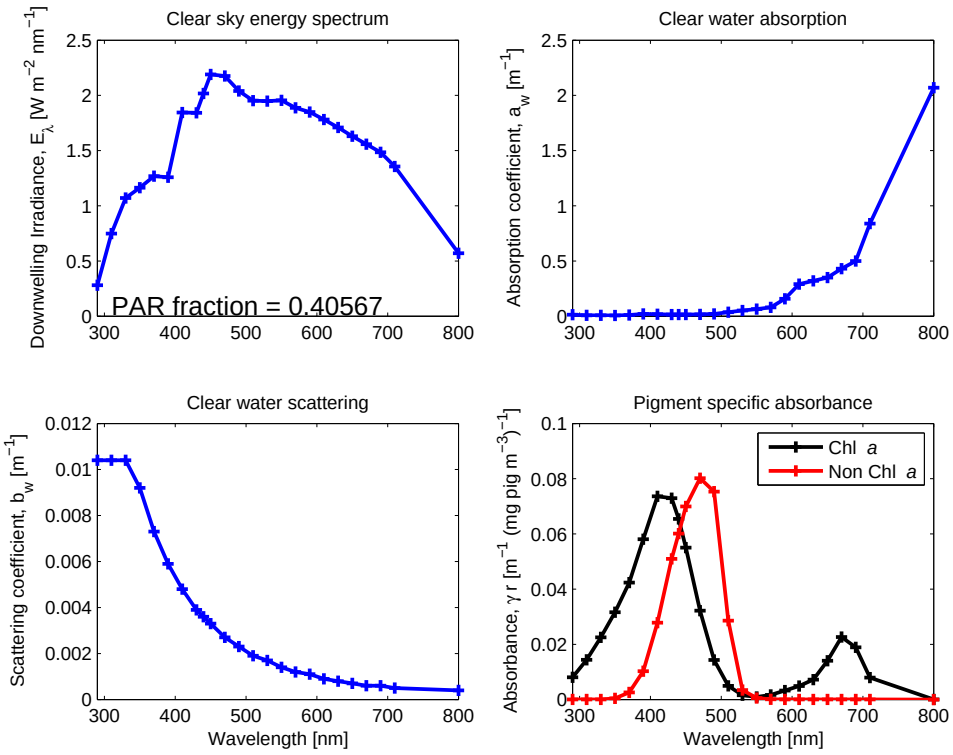

Figure 4: Spectrally-resolved energy distribution of sunlight, clear water absorption, clear water scattering (Smith and Baker, 1981) and pigment-specific absorbance of Chl *a* and photosynthetic carotenoids (Ficek et al., 2004). The fraction of solar radiation between 400 and 700 nm for clear sky irradiance at the particular spectral resolution is given in the top left panel. The centre of each waveband used in the model simulations is identified by a cross on each curve.

3.2.2 Apparent optical properties (AOPs)

The optical model is forced with the downwelling short wave radiation just above the sea surface, based on remotely-sensed cloud fraction observations and calculations of top-of-the-atmosphere clear sky irradiance and solar angle. The calculation of downwelling radiation and surface albedo (a function of solar elevation and cloud cover) is detailed in the hydrodynamic model description (Sec. 9.1.1).

The downwelling irradiance just above the water interface is split into wavebands using the weighting for clear sky irradiance (Fig. 4). Snell's law is used to calculate the azimuth angle of the mean light path through the water, θ_{sw}, as calculated from the atmospheric azimuth angle, θ_{air}, and the refraction of light at the air/water interface (Kirk, 1994):

$$\frac{\sin\theta_{air}}{\sin\theta_{sw}} = 1.33 \tag{11}$$

Calculation of in-water light field. Given the IOPs determined above, the exact solution for AOPs would require a radiative transfer model (Mobley, 1994), which is too computationally-expensive for a complex ecosystem model such as developed here. Instead, the in-water light field is solved for using empirical approximations of the relationship between IOPs and AOPs (Kirk, 1991; Mobley, 1994).

The vertical attenuation coefficient at wavelength λ when considering absorption and scattering, K_λ, is given by:

$$K_\lambda = \frac{a_{T,\lambda}}{\cos\theta_{sw}}\sqrt{1 + (g_i\cos\theta_{sw} - g_{ii})\frac{b_{T,\lambda}}{a_{T,\lambda}}} \tag{12}$$

The term outside the square root quantifies the effect of absorption, where $a_{T,\lambda}$ is the total absorption. The term within the square root of Eq. 12 represents scattering as an extended pathlength through the water column, where g_i and g_{ii} are empirical constants and take values of 0.402 and 0.180 respectively. The values of g_i and g_{ii} depend on the average cosine of scattering. For filtered water with scattering only due to water molecules, the values of g_i and g_{ii} are quite different to natural waters. But for waters ranging from coastal to open ocean, the average cosine of scattering varies by only a small amount (0.86 - 0.95, Kirk (1991)), and thus uncertainties in g_i and g_{ii} do not strongly affect K_λ.

The downwelling irradiance at wavelength λ at the bottom of a layer h thick, $E_{d,\lambda,bot}$, is given by:

$$E_{d,bot,\lambda} = E_{d,top,\lambda}e^{-K_\lambda h} \tag{13}$$

where $E_{d,top,\lambda}$ is the downwelling irradiance at wavelength λ at the top of the layer and K_λ is the vertical attenuation coefficient at wavelength λ, a result of both absorption and scattering processes.

Assuming a constant attenuation rate within the layer, the average downwelling irradiance at wavelength λ, $E_{d,\lambda}$, is given by:

$$E_{d,\lambda} = \frac{1}{h}\int_{bot}^{top} E_{d,z,\lambda} e^{-K_\lambda h} dz = \frac{E_{d,top,\lambda} - E_{d,bot,\lambda}}{K_\lambda h} \tag{14}$$

We can now calculate the scalar irradiance, E_o, for the calculation of absorbing components, from downwelling irradiance, E_d. The light absorbed within a layer must balance the difference in downwelling irradiance from the top and bottom of the layer (since scattering in this model only increases the pathlength of light), thus:

$$E_{o,\lambda} a_{T,\lambda} h = E_{d,top,\lambda} - E_{d,bot,\lambda} = E_{d,\lambda} K_\lambda h \tag{15}$$

Canceling h, and using Eq. 12, the scalar irradiance as a function of downwelling irradiance is given by:

$$E_{o,\lambda} = \frac{E_{d,\lambda}}{\cos\theta_{sw}} \sqrt{1 + \left(g_i \cos\theta_{sw} - g_{ii}\right) \frac{b_{T,\lambda}}{a_{T,\lambda}}} \tag{16}$$

This correction conserves photons within the layer, although it is only as a good as the original approximation of the impact of scattering and azimuth angle on vertical attenuation (Eq. 12).

Vertical attenuation of heat. The vertical attenuation of heat is given by:

$$K_{heat} = -\int \frac{1}{E_{d,z,\lambda}} \frac{\partial E_{d,z,\lambda}}{\partial z} d\lambda \tag{17}$$

and the local heating by:

$$\frac{\partial T}{\partial t} = -\frac{1}{\rho c_p} \int \frac{\partial E_{d,\lambda}}{\partial z} d\lambda \tag{18}$$

where T is temperature, ρ is the density of water, and $c_p = 4.1876$ J m^{-3} K^{-1} is the specific heat of water. This calculation does not feed back to the hydrodynamic model.

3.2.3 Remote-sensing reflectance

In addition to the IOPs calculated above, the calculation of remote-sensing reflectance uses a backscattering coefficient, b_b, which has a component due to pure seawater, and a component due to particulates. The particulate component for phytoplankton is strongly related to cell carbon (and therefore cell size) and the number of cells (Vaillancourt et al., 2004):

$$b^*_{bphy,\lambda} = 5 \times 10^{-15} m_C^{1.002} \quad (R^2 = 0.97) \tag{19}$$

where m_C is the carbon content of the cells, here in pg cell^{-1}.

The total backscatter then becomes:

$$b_{b,\lambda} = \tilde{b}_w b_{w,\lambda} + b^*_{bphy,\lambda} n + \tilde{b}_{b,NAP,\lambda} c_3 NAP_4^c \tag{20}$$

where the backscatter ratio of pure seawater, $\tilde{b}_w$, is 0.5, n is the concentration of cells, and for particulate matter (NAP, detritus, microalgae), $\tilde{b}_{b,NAP,\lambda}$, is variable (Vaillancourt et al., 2004), but takes a value of ~ 0.02 (Table 1), $c_3 NAP_4^c$ is described in above for total scattering. To account for a greater backscattering ratio, and therefore backscatter, at low wavelengths (Fig. 4 of Vaillancourt et al. (2004)), we linearly increased the backscatter ratio from 0.02 at 555 nm to 0.04 at 470 nm. Above and below 555 nm and 470 nm respectively the backscatter ratio remained constant.

The ratio of the backscattering coefficient to the sum of backscattering and absorption coefficients for the water column, u_λ, is:

$$u_\lambda = \sum_{z'=1}^{N} \frac{w_{\lambda,z'} b_{b,\lambda,z'}}{a_{\lambda,z'} + b_{b,\lambda,z'}} \tag{21}$$

where $w_{\lambda,z'}$ is a weighting representing the component of the remote-sensing reflectance due to the absorption and scattering in layer number z', and N is the number of layers.

The weighting fraction in layer z' is given by:

$$w_{\lambda,z'} = \frac{1}{z_1 - z_0} \left(\int_0^{z_1} \exp\left(-2K_{\lambda,z}\right) dz - \int_0^{z_0} \exp\left(-2K_{\lambda,z}\right) dz \right) \tag{22}$$

$$= \frac{1}{z_1 - z_0} \int_{z_0}^{z_1} \exp\left(-2K_{\lambda,z}\right) dz \tag{23}$$

where K_λ is the vertical attenuation coefficient at wavelength λ described above, and the factor of 2 accounts for the pathlength of both downwelling and upwelling light. The integral of $w_{\lambda,z}$ to infinite depth is 1. In areas where light reaches the bottom, the integral of $w_{\lambda,z}$ to the bottom is less than one, and bottom reflectance is important (see Sec. 5.2.2).

The below-surface remote-sensing reflectance, r_{rs}, is given by:

$$r_{rs,\lambda} = g_0 u_\lambda + g_1 u_\lambda^2 \tag{24}$$

where $g_0 = 0.0895$ and $g_1 = 0.1247$ are empirical constants for the nadir-view in oceanic waters (Lee et al., 2002; Brando et al., 2012), and these constants result in a change of units from the unitless u to a per unit of solid angle, sr^{-1}, quantity $r_{rs,\lambda}$.

The above-surface remote-sensing reflectance, through rearranging Lee et al. (2002), is given by:

$$R_{rs,\lambda} = \frac{0.52 r_{rs,\lambda}}{1 - 1.7 r_{rs,\lambda}} \tag{25}$$

At open ocean values, $R_{rs} \sim 0.06u$ sr^{-1}. Thus if total scattering and absorption are approximately equal, $u = 0.5$ and $R_{rs} \sim 0.03$ sr^{-1}.

3.3 Microalgae

The model contains four function groups of suspended microalgae: small and large phytoplankton, microphytobenthos and *Trichodesmium*. The growth model for each of the functional groups is identical and explained below. The differences in the ecological interactions of the four functional groups are summarised in Table 3.

	small phyto.	large phyto.	benthic phyto.	*Trichodesmium*
Radius (μm)	1	4	5	5
Maximum growth rate (d^{-1})	1.25	2	1.35	1
Sink rate (m d^{-1})				variable
Surface sediment growth	×	×	√	×
Nitrogen fixation	×	×	×	√
Water column mort.	√	√	×	√
Sediment mort.	√	√	√	√
[a]Ratio of xanthophyll to Chl *a*	0.51	0.81	0.81	0.50

Table 3: Traits of suspended microalgae cells.[a] Values for *Trichodesmium* from Subramaniam et al. (1999), other values from CSIRO parameter library.

3.3.1 Growth

The microalgae model considers the diffusion limited supply of dissolved inorganic nutrients (N and P) and the absorption of light, delivering N, P and fixed C to the internal reserves of the cell. The growth rate of a microalgae cell is given by the maximum growth rate, μ^{max}, multiplied by the normalised reserves, R^*, of each N, P and energy:

$$\mu = \mu^{max} R_N^* R_P^* R_I^* \tag{26}$$

The internal reserves are consumed to form structural material at the Redfield ratio (Redfield et al., 1963):

$$106CO_2 + 16NO_3^- + PO_4^{3-} + 122H_2O + 19H^+ \xrightarrow{1060 \text{ photons}} (CH_2O)_{106}(NH_3)_{16}H_3PO_4 + 138O_2 \tag{27}$$

The mass of the reserves (and therefore the total C:N:P:Chl *a* ratio) of the cell depends on the interaction of the supply and consumption rates. When consumption exceeds supply, and the supply rates are non-Redfield, the normalised internal reserves of the non-limiting nutrients approach 1 while the limiting nutrient becomes depleted. Thus the model behaves like a 'Law of the Minimum' growth model, except during fast changes in nutrient supply rates.

Variable	Symbol	Units
Scalar irradiance	E_o	W m^{-2}
Dissolved inorganic nitrogen (DIN)	N	mg N m^{-3}
Dissolved inorganic phosphorus (DIP)	P	mg P m^{-3}
Dissolved inorganic carbon (DIC)	DIC	mg C m^{-3}
Dissolved oxygen	$[O_2]$	mg O m^{-3}
Reserves of nitrogen	R_N	mg N cell^{-1}
Reserves of phosphorus	R_P	mg P cell^{-1}
Reserves of energy	R_I	mmol photon cell^{-1}
Maximum reserves of nitrogen	$R_N^{\max}$	mg N cell^{-1}
Maximum reserves of phosphorus	$R_P^{\max}$	mg P cell^{-1}
Maximum reserves of energy	$R_I^{\max}$	mmol photon cell^{-1}
Normalised reserves of nitrogen	$R_N^* \equiv R_N/R_N^{\max}$	-
Normalised reserves of phosphorus	$R_P^* \equiv R_P/R_P^{\max}$	-
Normalised reserves of energy	$R_I^* \equiv R_I/R_I^{\max}$	-
Intracellular Chl a concentration	c_i	mg m^{-3}
Structural phytoplankton biomass	B	mg N m^{-3}
Absorption cross-section	α	m^2 cell^{-1}
Diffusion shape factor	ψ	m cell^{-1}
Wavelength	λ	nm
Maximum Chl a synthesis rate	$k_{\text{Chl}}^{\max}$	mg Chl m^{-3} d^{-1}
Photon absorption-weighted opaqueness	$\overline{\Theta}$	-
Non-dimensional absorbance	$\rho_\lambda = \gamma_\lambda c_i r$	-

Table 4: State and derived variables for the microalgae growth model. DIN is given by the sum of nitrate and ammonia concentrations, $[NO_3]$+$[NH_4]$.

The molar ratio of a cell is given by:

$$\text{C} : \text{N} : \text{P} = 106(1 + R_I^*) : 16(1 + R_N^*) : 1 + R_P^* \tag{28}$$

3.3.2 Nutrient uptake

The diffusion-limited nutrient uptake to a single phytoplankton cell, J, is given by:

$$J = \psi D \left(C_b - C_w\right) \tag{29}$$

where ψ is the diffusion shape factor ($= 4\pi r$ for a sphere), D is the molecular diffusivity of the nutrient, C_b is the average extracellular nutrient concentration, and C_w is the concentration at the

wall of the cell. The diffusion shape factor is determined by equating the divergence of the gradient of the concentration field to zero ($\nabla^2 C = 0$).

A semi-empirical correction to Eq. 29, to account for fluid motion around the cell, and the calculation of non-spherical diffusion shape factors, has been applied in earlier work (Baird and Emsley, 1999). For the purposes of biogeochemical modelling these uncertain corrections for small scale turbulence and non-spherical shape are not quantitatively important, and have not been pursued here.

Numerous studies have considered diffusion-limited transport to the cell surface at low nutrient concentrations saturating to a physiologically-limited nutrient uptake from the cell wall (Hill and Whittingham, 1955; Pasciak and Gavis, 1975; Mann and Lazier, 2006) at higher concentrations. The physiological limitation is typically considered using a Michaelis-Menton type equation. Here we simply consider the diffusion-limited uptake to be saturated by the filling-up of reserves, $(1 - R^*)$. Thus, nutrient uptake is given by:

$$J = \psi D C_b \, (1 - R^*) \tag{30}$$

where R^* is the reserve of the nutrient being considered. As shown later when considering preferential ammonia uptake, under extreme limitation relative to other nutrients, R^* approaches 0, and uptake approaches the diffusion limitation.

3.3.3 Light capture and chlorophyll synthesis

Light absorption by microalgae cells has already been considered above Eq. 3. The same absorption cross section, α, is used to calculate the capture of photons:

$$\frac{\partial R_I^*}{\partial t} = (1 - R_I^*) \, \frac{(10^9 hc)^{-1}}{A_V} \int \alpha_\lambda E_{o,\lambda} \lambda \, d\lambda \tag{31}$$

where $(1 - R_I^*)$ accounts for the reduced capture of photons as the reserves becomes saturated, and $\frac{(10^9 hc)^{-1}}{A_V}$ converts from energy to photons. The absorption cross-section is a function of intracellular pigment concentration, which is a dynamic variable determined below. While a drop-off of photosynthesis occurs as the energy reserves become replete, this formulation does not consider photoinhibition due to photooxidation, although it has been considered elsewhere (Gustafsson et al., 2014).

The dynamic C:Chl component determines the rate of synthesis of pigment based on the incremental benefit of adding pigment to the rate of photosynthesis. This calculation includes both the reduced benefit when energy reserves are replete, $(1 - R_I^*)$, and the reduced benefit due to self-shading, χ. The factor χ is calculated for the derivative of the absorption cross-section per unit projected area, α / PA, with non-dimensional group $\rho = \gamma c_i r$. For a sphere of radius r (Baird et al., 2013):

$$\frac{1}{PA} \frac{\partial \alpha}{\partial \rho} = \frac{1 - e^{-2\rho}(2\rho^2 + 2\rho + 1)}{\rho^3} = \chi \tag{32}$$

where χ represents the area-specific incremental rate of change of absorption with ρ. The rate of chlorophyll synthesis is given by:

$$\frac{\partial c_i}{\partial t} = k_{\text{Chl}}^{\max}(1 - R_i^*)\overline{\chi} \quad \text{if C : Chl} > \theta_{min} \tag{33}$$

where $k_{\text{Chl}}^{\max}$ is the maximum rate of synthesis and θ_{min} is the minimum C:Chl ratio. Below θ_{min}, pigment synthesis is zero. Both self-shading, and the rate of photosynthesis itself, are based on photon absorption rather than energy absorption (Table 5), as experimentally shown in Nielsen and Sakshaug (1993).

The model considers two pigments, Chl *a*, and photosynthetic xanthophyll, with distinct absorbance spectra (Fig. 4, Ficek et al. (2004)). Two spectrally-distinct absorbing pigments are necessary as the C:Chl model calculates the pigment concentration based on that required to maximise photosynthesis. If only Chl *a* was represented, the model would predict a Chl *a* concentration that was accounting for both the absorption of Chl *a* and auxiliary pigments, thus over-predicting the Chl *a* concentration when compared to observations.

The state variables, equations and parameter values are listed in Tables 4, 5 and 6 respectively. The equations in Table 4 described nitrogen uptake from the DIN pool, where the partitioning between nitrate and ammonia due to preferential ammonia uptake is described in Sec. 6.1.

3.3.4 Carbon fixation / respiration

When photons are captured (photosynthesis) there is an increase in reserves of energy, $k_I(1 - R_I^*)$, and an accompanying uptake of dissolved inorganic carbon, $\frac{106}{1060}12k_I(1 - R_I^*)$, and release of oxygen, $\frac{138}{1060}32k_I(1 - R_I^*)$, per cell to the water column (Table 5).

Additionally, there is a basal respiration, representing a constant cost of cell maintenance. The loss of internal reserves, $\mu_B^{\max} m_I \phi R_I^*$ results in a gain of water column dissolved inorganic carbon per cell, $\frac{106}{1060}\frac{12}{14}\mu_B^{\max}\phi R_I^*$, as well as a loss in water column dissolved oxygen per cell, $\frac{138}{1060}\frac{32}{14}\mu_B^{\max}\phi R_I^*$ (Table 5). The loss in water column dissolved oxygen per cell represents an instantaneous respiration of the fixed carbon of the reserves. Basal respiration decreases internal reserves, and therefore growth rate, but does not directly lead to cell mortality at zero energy reserves. Implicit in this scheme is that the basal cost is higher when the cell has more energy reserves, R_I^*.

A linear mortality term, considering both the loss of structural material and energy reserves, is considered later.

3.3.5 Conservation of mass of microalgae model

The conservation of mass during transport, growth and mortality is proven in Baird et al. (2004a). Briefly, for microalgal growth, total concentration of nitrogen in microalgae cells is given by $B + BR_N^*$. For conservation of mass, the time derivatives must equate to zero:

$$\frac{\partial B}{\partial t} + \frac{\partial \left(R_N B / R_N^{max}\right)}{\partial t} = 0. \tag{34}$$

using the product rule to differentiate the second term on the LHS:

$$\frac{\partial B}{\partial t} + \frac{\partial B}{\partial t}\frac{R_N}{R_N^{max}} + \frac{B}{R_N^{max}}\frac{\partial R_N}{\partial t} = 0 \tag{35}$$

Where:

$$\frac{\partial B}{\partial t} = +\mu_B^{max} R_I^* R_N^* R_P^* B \tag{36}$$

$$\frac{\partial B}{\partial t}\frac{R_N}{R_N^{max}} = +\mu_B^{max} R_I^* R_N^* R_P^* B \frac{R_N}{R_N^{max}} \tag{37}$$

$$\frac{B}{R_N^{max}}\frac{\partial R_N}{\partial t} = -B(1 + R_N^*)\mu_B^{max} R_I^* R_N^* R_P^* \frac{R_N}{R_N^{max}} \tag{38}$$

Thus demonstrating conservation of mass when $m_{B,N} = R_N^{max}$, as used here.

$$\frac{\partial N}{\partial t} = -\psi D_N N(1-R_N^*)\,(B/m_N) \tag{39}$$

$$\frac{\partial P}{\partial t} = -\psi D_P P(1-R_P^*)\,(B/m_N) \tag{40}$$

$$\frac{\partial DIC}{\partial t} = -\left(\frac{106}{1060}12k_I(1-R_I^*) - \frac{106}{16}\frac{12}{14}\mu_B^{\max}\phi R_I^*\right)(B/m_N) \tag{41}$$

$$\frac{\partial [\mathrm{O_2}]}{\partial t} = \left(\frac{138}{1060}32k_I(1-R_I^*) - \frac{138}{16}\frac{32}{14}\mu_B^{\max}\phi R_I^*\right)(B/m_N) \tag{42}$$

$$\frac{\partial R_N}{\partial t} = \psi D_N N(1-R_N^*) - \mu_B^{\max}\,(m_N+R_N)\,R_P^*R_N^*R_I^* \tag{43}$$

$$\frac{\partial R_P}{\partial t} = \psi D_P P(1-R_P^*) - \mu_B^{\max}\,(m_P+R_P)\,R_P^*R_N^*R_I^* \tag{44}$$

$$\frac{\partial R_I}{\partial t} = k_I(1-R_I^*) - \mu_B^{\max}\,(m_I+R_I)\,R_P^*R_N^*R_I^* - \mu_B^{\max}\phi m_I R_I^* \tag{45}$$

$$\frac{\partial B}{\partial t} = \mu_B^{\max}R_P^*R_N^*R_I^*B \tag{46}$$

$$\frac{\partial c_i}{\partial t} = k_{\mathrm{Chl}}^{\max}(1-R_I^*)\overline{\chi} - \mu_P^{\max}R_P^*R_N^*R_I^*c_i \tag{47}$$

$$\psi = 4\pi r \tag{48}$$

$$k_I = \frac{(10^9hc)^{-1}}{A_V}\int \alpha_\lambda E_{o,\lambda}\lambda\,d\lambda \tag{49}$$

$$\alpha_\lambda = \pi r^2\left(1-\frac{2(1-(1+2\rho_\lambda)e^{-2\rho_\lambda})}{4\rho_\lambda^2}\right) \tag{50}$$

$$\overline{\chi} = \int \chi_\lambda E_{o,\lambda}\lambda\ d\lambda \Big/ \int E_{o,\lambda}\lambda\ d\lambda \tag{51}$$

$$\chi_\lambda = \frac{1}{\pi r^2}\frac{\partial \alpha_\lambda}{\partial \rho_\lambda} = \frac{1-e^{-2\rho_\lambda}(2\rho_\lambda^2+2\rho_\lambda+1)}{\rho_\lambda^3} \tag{52}$$

$$\rho_\lambda = c_i\,(\gamma_{\mathrm{Chl}a,\lambda} + f_{\mathrm{xan}}\gamma_{\mathrm{xan},\lambda})\,r \tag{53}$$

$$106\mathrm{CO_2} + 16\mathrm{NO_3^-} + \mathrm{PO_4^{3-}} + 122\mathrm{H_2O} + 19\mathrm{H^+} \xrightarrow{1060\ \text{photons}} (\mathrm{CH_2O})_{106}(\mathrm{NH_3})_{16}\mathrm{H_3PO_4} + 138\mathrm{O_2} \tag{54}$$

Table 5: Microalgae growth model equations. The term B/m_N is the concentration of cells. The equation for organic matter formation gives the stoichiometric constants; 12 g C mol C^{-1}; 32 g O mol $\mathrm{O_2^{-1}}$. The equations are for scalar irradiance specified as an energy flux.

	Symbol	Value
Constants		
Molecular diffusivity of NO_3	D_N	$f(T,S)$ m^2 s^{-1}
Molecular diffusivity of PO_4	D_P	$f(T,S)$ m^2 s^{-1}
Speed of light	c	2.998×10^8 m s^{-1}
Planck constant	h	6.626×10^{-34} J s^{-1}
Avagadro constant	A_V	6.02×10^{23} mol^{-1}
[a]Pigment-specific absorption coefficient	$\gamma_{\text{pig},\lambda}$	$f(\text{pig},\lambda)$ m^{-1} (mg m^{-3})$^{-1}$
[d]Minimum C:Chl ratio	θ_{min}	20.0 wt/wt
Allometric relationships		
[b]Carbon content	m_C	$12010 \times 9.14 \times 10^3 V$ mg C cell^{-1}
[c]Maximum intracellular Chl a concentration	$c_i^{\max}$	$2.09 \times 10^7 V^{-0.310}$ mg Chl m^{-3}
Nitrogen content of phytoplankton	m_N	$\frac{14}{12}\frac{16}{106} m_C$ mg N cell^{-1}

Table 6: Constants and parameter values used in the microalgae model. V is cell volume in μm^3. [a]Spectrally-resolved values of γ_λ for chlorophyll a, and diatoxanthin are based on idealised curves in Ficek et al. (2004),[b]Straile (1997),[c]Finkel (2001);[c] Sathyendranath et al. (2009) using HPLC determination which isolates chl a.

Earlier published versions of the microalgae model are described with multiple nutrient limitation (Baird et al., 2001), with variable C:N ratios (Wild-Allen et al., 2010) and variable C:Chl ratios (Baird et al., 2013). Further, demonstration of the conservation of mass during transport is given in Baird et al. (2004a). Here the microalgae model is presented with variable C:Chl ratios (with an additional auxiliary pigment), and both nitrogen and phosphorus limitation, and a preference for ammonia uptake when compared to nitrate. The strategy of dynamic supply and consumption rates of elements is a simple version of what is often called Dynamic Energy Budget (DEB) models in the ecological modelling literature (Kooijman, 2010).

3.4 Nitrogen-fixing *Trichodesmium*

The growth of *Trichodesmium* follows the microalgae growth and C:Chl model above, with the following additional processes of nitrogen fixation and physiological-dependent buoyancy adjustment, as described in Robson et al. (2013). Additional parameter values for *Trichodesmium* are given in Table 7.

3.4.1 Nitrogen fixation

Nitrogen fixation occurs when the DIN concentration falls below a critical concentration, DIN_{crit}, typically 0.3 to 1.6 μmol L^{-1} (i.e. 4 to 20 mg N m^{-3},Robson et al. (2013)), at which point *Trichodesmium* produce nitrogenase to allow fixation of N_2. It is assumed that nitrogenase becomes available whenever ambient DIN falls below the value of DIN_{crit} and energy and phosphorus are available to support nitrogen uptake. The rate of change of internal reserves of nitrogen, R_N, due to nitrogen fixation if $DIN < DIN_{crit}$ is given by:

$$N_{fix} = \frac{\partial R_N}{\partial t}|_{N_{fix}} = \max\left(4\pi r D_{\mathrm{NO_3}} DIN_{crit} R_P^* R_I^* (1 - R_N^*) - 4\pi r D_{\mathrm{NO_3}} \left[\mathrm{NO_3} + \mathrm{NH_4}\right](1 - R_N^*), 0\right) \tag{55}$$

where N_{fix} is the rate of nitrogen fixation per cell. Using this formulation, *Trichodesmium* is able to maintain its nitrogen uptake rate at that achieved through diffusion limited uptake at DIN_{crit} even when DIN drops below DIN_{crit}, provided phosphorus and energy reserves, R_P^* and R_I^* respectively, are available.

The energetic cost of nitrogen fixation is represented as a fixed proportion of carbon fixation, f_{Nfix}, equivalent to a reduction in quantum efficiency, and as a proportion, $f_{nitrogenase}$, of the nitrogen fixed:

$$\frac{\partial R_I}{\partial t} = -(1 - f_{Nfix})(1 - f_{nitrogenase}) k_I \tag{56}$$

where k_I is the rate of photon absorption per cell obtain from the microalgal growth model (Table 5).

3.4.2 Buoyancy adjustment

The rate of change of *Trichodesmium* biomass, B, as a result of density difference between the cell and the water, is approximated by Stokes' Law:

$$\frac{\partial B}{\partial t} = -\frac{2}{9}\frac{g r^2}{\mu}\left(\rho - \rho_w\right)\frac{\partial B}{\partial z} \tag{57}$$

where z is length in the vertical (+ve up), μ is the dynamic viscosity of water, g is acceleration due to gravity, r is the equivalent spherical radius of the cell, ρ_w is the density of water, and ρ is the cell density is given by:

$$\rho = \rho_{min} + R_I^* \left(\rho_{max} - \rho_{min}\right) \tag{58}$$

where R_I^* is the normalised energy reserves of the cell (see above), and ρ_{min} and ρ_{max} are the densities of the cell when there is no energy reserves and full energy reserves respectively. Thus, when light reserves are depleted, the cell is more buoyant, facilitating the retention of *Trichodesmium* in the surface waters.

	Symbol	Value
Maximum growth rate	μ^{max}	1 d^{-1}
[b]Ratio of xanthophyll to Chl *a*	f_{xan}	0.5
Linear mortality	m_L	0.14 d^{-1}
Quadratic mortality	m_Q	0.15 d^{-1} (mg N m^{-3})$^{-1}$
Radius	r	5 μm
Max. cell density	ρ_{max}	1060 kg m^{-3}
Min. cell density	ρ_{min}	990 kg m^{-3}
Critical threshold for N fixation	DIN_{crit}	4 mg N m^{-3}
Fraction of energy used for nitrogenase	$f_{nitrogenase}$	0.07
Fraction of energy used for N fixation	f_{Nfix}	0.33
Nitrogen gas in equilibrium with atm.	$[N_2]$	2 $\times 10^4$ mg N m^{-3}

Table 7: Parameter values used in the *Trichodesmium* model (Robson et al., 2013). [b] The major accessory pigments in *Trichodesmium* are the red-ish phycourobilin and phycoerythrobilin (Subramaniam et al., 1999). For simplicity in this model their absorption cross-section is approximated by photosynthetic xanthophyll, which has an absorption peak approximately 10 nm less than the phycourobilin.

3.5 Water column inorganic chemistry

3.5.1 Carbon chemistry

The major pools of dissolved inorganic carbon species in the ocean are HCO_3^-, CO_3^-, and dissolved CO_2, which influence the speciation of H^+, and OH^- ions, and therefore pH. The interaction of these ions reaches an equilibrium in seawater within a few tens of seconds (Zeebe and Wolf-Gladrow, 2001). In the biogeochemical model here, where calculation timesteps are of order tens of minutes, it is reasonable to assume that the carbon chemistry system is at equilibrium.

The Ocean-Carbon Cycle Model Intercomparison Project (OCMIP) has developed numerical methods to quantify air-sea carbon fluxes and carbon dioxide system equilibria (Najjar and Orr, 1999). Here we uses a modified version of the OCMIP-2 Fortran code developed for MOM4 (GFDL Modular Ocean Model version 4, (Griffies et al., 2004)). The OCMIP procedures quantify the state of the carbon dioxide (CO_2) system using two prognostic variables, the concentration of dissolved inorganic carbon, DIC, and total alkalinity, A_T. The value of these prognostic variables, along with salinity and temperature, are used to calculate the pH and partial pressure of carbon dioxide, pCO_2, in the surface waters using a set of governing chemical equations which are solved using a Newton-Raphson method (Najjar and Orr, 1999).

One alteration from the global implementation of the OCMIP scheme is to increase search space for the iterative scheme from ±0.5 pH units (appropriate for global models) to ±2.5. With this change, the OCMIP scheme converges over a broad DIC and A_T values (Munhoven, 2013).

For more details see Mongin and Baird (2014); Mongin et al. (2016).

Variable	Symbol	Units
Ammonia concentration	$[NH_4]$	mg N m^{-3}
Water column Dissolved Inorganic Carbon (DIC)	DIC	mg C m^{-3}
Water column Dissolved Inorganic Phosphorus (DIP)	P	mg P m^{-3}
Water column Particulate Inorganic Phosphorus (PIP)	PIP	mg P m^{-3}
Water column Non-Algal Particulates (NAP)	NAP	kg m^{-3}
Water column dissolved oxygen concentration	$[O_2]$	mg O m^{-3}

Table 8: State and derived variables for the water column inorganic chemistry model.

$$\mathrm{NH_4^+ + 2O_2 \longrightarrow NO_3^- + H_2O + 2H^+} \tag{59}$$

$$\frac{\partial[\mathrm{NH_4}]}{\partial t} = -\tau_{nit,wc}[\mathrm{NH_4}]\frac{[\mathrm{O_2}]}{K_{nit,\mathrm{O}} + [\mathrm{O_2}]} \tag{60}$$

$$\frac{\partial[\mathrm{O_2}]}{\partial t} = -2\tau_{nit,wc}[\mathrm{NH_4}]\frac{[\mathrm{O_2}]}{K_{nit,\mathrm{O}} + [\mathrm{O_2}]} \tag{61}$$

$$\frac{\partial[\mathrm{NO_3}]}{\partial t} = \tau_{nit,wc}[\mathrm{NH_4}]\frac{[\mathrm{O_2}]}{K_{nit,\mathrm{O}} + [\mathrm{O_2}]} \tag{62}$$

$$\frac{\partial P}{\partial t} = \tau_{Pabs}\left(\frac{PIP}{k_{Pads,wc}NAP} - \frac{[\mathrm{O_2}]P}{K_{\mathrm{O_2,abs}} + [\mathrm{O_2}]}\right) \tag{63}$$

$$\frac{\partial PIP}{\partial t} = -\tau_{Pabs}\left(\frac{PIP}{k_{Pads,wc}NAP} - \frac{[\mathrm{O_2}]P}{K_{\mathrm{O_2,abs}} + [\mathrm{O_2}]}\right) \tag{64}$$

Table 9: Equations for the water column inorganic chemistry.

Description	Symbol	Units
Maximum rate of nitrification in the water column	$\tau_{nit,wc}$	0.1 d^{-1}
Oxygen half-saturation constant for nitrification	$K_{nit,O}$	500 mg O m^{-3}
Rate of P adsorbed/desorbed equilibrium	τ_{Pabs}	0.001 d^{-1}
Isothermic const. P adsorption for NAP	$k_{Pads,wc}$	30 kg NAP^{-1}
Oxygen half-saturation for P adsorption	$K_{O_2,abs}$	74 mg O m^{-3}

Table 10: Constants and parameter values used in the water column inorganic chemistry.

3.5.2 Nitrification

Nitrification is the oxidation of ammonia with oxygen, to form nitrite followed by the rapid oxidation of these nitrites into nitrates. This is represented in a one step processes, with the rate of nitrification given by:

$$\frac{\partial[\mathrm{NH_4}]}{\partial t} = -\tau_{nit,wc}[\mathrm{NH_4}]\frac{[\mathrm{O_2}]}{K_{nit,\mathrm{O}} + [\mathrm{O_2}]} \tag{65}$$

where the equations and parameter values are defined in Tables 9 and 10.

3.5.3 Phosphorus absorption - desorption

The rate of phosphorus desorption from particulates is given by:

$$\frac{\partial P}{\partial t} = \tau_{Pabs}\left(\frac{PIP}{k_{Pads,wc}NAP} - \frac{[\mathrm{O_2}]P}{K_{\mathrm{O_2,abs}} + [\mathrm{O_2}]}\right) = -\frac{\partial PIP}{\partial t} \tag{66}$$

where $[\mathrm{O_2}]$ is the concentration of oxygen, P is the concentration of dissolved inorganic phosphorus, PIP is the concentration of particulate inorganic phosphorus, NAP is the sum of the fine sediment and mud concentrations, and τ_{Pabs}, $k_{Pads,wc}$ and $K_{\mathrm{O_2,abs}}$ are model parameters described in Table 10.

At steady-state, the PIP concentration is given by:

$$PIP = k_{Pads,wc}P\frac{[\mathrm{O_2}]}{K_{\mathrm{O_2,abs}} + [\mathrm{O_2}]}NAP \tag{67}$$

As an example for rivers flowing into the eReefs configuration, $[\mathrm{O_2}] = 7411$ mg m^{-3} (90% saturation at T = 25, S = 0), $NAP = 0.231$ kg m^{-3}, $k_{Pads,wc} = 30$ kg NAP^{-1}, $K_{\mathrm{O_2,abs}} = 74$ mg O m^{-3}, $P = 4.2$ mg m^{-3}, thus the ratio $PIP/DIP = 6.86$ (see Fig. 5).

Limited available observations of absorption-desorption include from the Johnstone River (Pailles and Moody, 1992) and the GBR (Monbet et al., 2007).

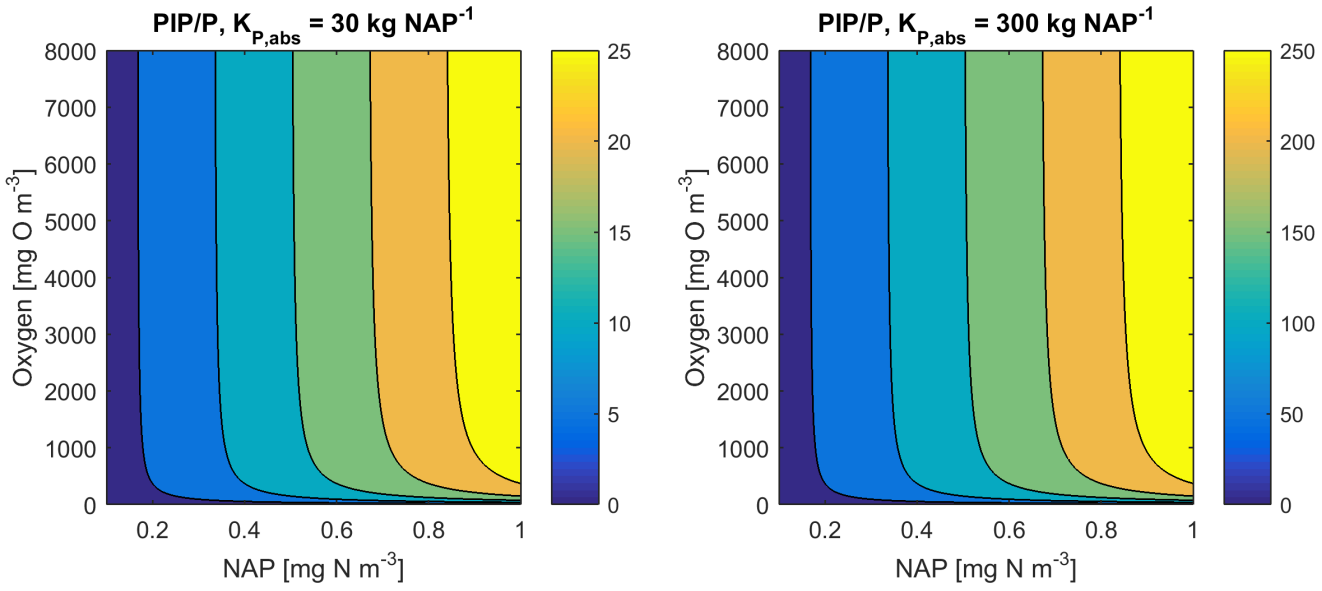

Figure 5: Phosphorus adsorption - desorption equilibria, $K_{\mathrm{O_2,abs}} = 74$ mg O m^{-3}.

3.6 Zooplankton herbivory

The simple food web of the model involves small zooplankton consuming small phytoplankton, and large zooplankton consuming large phytoplankton, microphytobenthos and *Trichodesmium*. For simplicity the state variables and equations are only given for small plankton grazing (Tables 11, 13), but the parameters are given for all grazing terms (Table 12).

The rate of zooplankton grazing is determined by the encounter rate of the predator and all its prey up until the point at which it saturates the growth of the zooplankton, and then it is constant. This is effectively a Hollings Type I grazing response (Gentleman, 2002). Under the condition of multiple prey types, there is no preferential grazing other than that determined by the chance of encounter. The encounter rate is the result of the relative motion brought about by diffusive, shear, and swimming-determined relative velocities (Jackson, 1995; Baird, 2003).

This formulation of grazing, originally proposed by Jackson (1995) but rarely used in biogeochemical modelling, is developed from considering the encounter of individuals, not populations. One particular advantage of formulating the encounter on individuals is that should the number of populations considered in the model change (i.e. an additional phytolankton class is added), there is no need to re-parameterise. In contrast, almost all biogeochemical models, as typified by Fasham et al. (1990), consider the grazing of populations of plankton, parameterised using a saturating curve constrained by a half saturation constant. Awkwardly, the half saturation constant only has meaning for one particular diet of phytoplankton. This is best illustrated by dividing a single population into two identical populations of half the number, in which case, for the same specification of half-saturation constant, the grazing rate increases. That is:

$$\frac{\mu P}{k+P} \neq \frac{\mu P/2}{k+P/2} + \frac{\mu P/2}{k+P/2} \tag{68}$$

As the zooplankton are grazing on the phytoplankton that contain internal reserves of nutrients an addition flux of dissolved inorganic nutrients (gR^*_N for nitrogen) is returned to the water column (for more details see Sec. 3.6.1).

3.6.1 Conservation of mass in zooplankton grazing

It is important to note that the microalgae model presented above represents internal reserves of nutrients, energy and chlorophyll as a per cell quantity. Using this representation there are no losses of internal quantities with either grazing or mortality. However the implication of their presence is represented in the (gR^*_N) terms (Table 13) that return the reserves to the water column. These terms represent the fast return of a fraction of phytoplankton nitrogen due to processes like "sloppy eating".

Variable	Symbol	Units
Ammonia concentration	$[NH_4]$	mg N m^{-3}
Water column dissolved Inorganic Carbon (DIC)	DIC	mg C m^{-3}
Water column dissolved Inorganic Phosphorus (DIP)	P	mg P m^{-3}
Water column dissolved oxygen concentration	$[O_2]$	mg O m^{-3}
Reserves of phytoplankton nitrogen	R_N	mg N $cell^{-1}$
Reserves of phytoplankton phosphorus	R_P	mg P $cell^{-1}$
Reserves of phytoplankton energy	R_I	mmol photon $cell^{-1}$
Maximum reserves of nitrogen	$R_N^{\max}$	mg N $cell^{-1}$
Maximum reserves of phosphorus	$R_P^{\max}$	mg P $cell^{-1}$
Maximum reserves of energy	$R_I^{\max}$	mmol photon $cell^{-1}$
Normalised reserves of nitrogen	$R_N^* \equiv R_N/R_N^{\max}$	-
Normalised reserves of phosphorus	$R_P^* \equiv R_P/R_P^{\max}$	-
Normalised reserves of energy	$R_I^* \equiv R_I/R_I^{\max}$	-
Phytoplankton structural biomass	B	mg N m^{-3}
Zooplankton biomass	Z	mg N m^{-3}
Detritus at the Redfield ratio	D_{Red}	mg N m^{-3}
Zooplankton grazing rate	g	mg N m^{-3} s^{-1}
Encounter rate coefficient due to molecular diffusion	ϕ_{diff}	m^3 s^{-1} cell Z^{-1}
Encounter rate coefficient due to relative motion	ϕ_{rel}	m^3 s^{-1} cell Z^{-1}
Encounter rate coefficient due to turbulent shear	ϕ_{shear}	m^3 s^{-1} cell Z^{-1}
Phytoplankton cell mass	m_B	mg N $cell^{-1}$
Zooplankton cell mass	m_Z	mg N $cell^{-1}$

Table 11: State and derived variables for the zooplankton grazing. Zooplankton cell mass, $m_Z = 16000 \times 14.01 \times 10.5 V_Z$ mg N $cell^{-1}$, where V_Z is the volume of zooplankton (Hansen et al., 1997).

An alternative and equivalent formulation would be to consider total concentration of reserves in the water column, then the change in water column concentration of reserves due to mortality (either grazing or natural mortality) must be considered. This alternate representation will not be undertaken here as the above considered equations are fully consistent, but it is worth noting that the numerical solution of the model within the EMS package represents total water column concentrations of internal reserves, and therefore must include the appropriate loss terms due to mortality.

Description	Symbol	Small	Large
Maximum growth rate of zooplankton at T_{ref} (d^{-1})	μ_Z	3.0	1.15
Nominal cell radius of zooplankton (μm)	r_Z	12	500
Growth efficiency of zooplankton	E_Z	0.304	0.341
Fraction of growth inefficiency lost to detritus	γ_Z	0.5	0.5
Swimming velocity ($\mu m\ s^{-1}$)	U_Z	200	2000
Constants			
Boltzmann's constant	κ	1.38066×10^{-23}	$J\ K^{-1}$
Viscosity	ν	10^{-6}	$m^2\ s^{-1}$
Dissipation rate of TKE	ϵ	10^{-6}	$m^3\ s^{-1}$
Oxygen half-saturation for aerobic respiration	K_{OA}	500	mg O m^{-3}

Table 12: Constants and parameter values used for zooplankton grazing. Dissipation rate of turbulent kinetic energy (TKE) is considered constant.

3.7 Zooplankton carnivory

Large zooplankton consume small zooplankton. This process uses similar encounter rate and consumption rate limitations calculated for zooplankton herbivory (Table 13). As zooplankton contain no internal reserves, the equations are simplified from the herbivory case to those listed in Table 14). Assuming that the efficiency of herbivory, γ, is equal to that of carnivory, and therefore assigned the same parameter, the additional process of carnivory adds no new parameters to the biogeochemical model.

3.8 Zooplankton respiration

In the model there is no change in water column oxygen concentration if organic material is exchanged between pools at a constant ratio. Thus, when zooplankton plankton consume phytoplankton no oxygen is consumed due to the consumption of phytoplankton structural material (B_P). However, the excess energy reserves represent a pool of fixed carbon, which when released from the phytoplankton must consume oxygen. Further, zooplankton mortality and growth inefficiency results in detritial production, which when remineralised consumes oxygen. Additionally, carbon released to the dissolved inorganic pool during inefficiency grazing on phytoplankton structural material also consumes oxygen. Thus zooplankton respiration is implicitly captured in these associated processes.

3.9 Non-grazing plankton mortality

The rate of change of phytoplankton biomass, B, as a result of natural mortality is given by:

$$\frac{\partial B}{\partial t} = -m_L B - m_Q B^2 \tag{90}$$

where m_L is the linear mortality coefficient and m_Q is the quadratic mortality coefficient.

A combination of linear and quadratic mortality rates are used in the model. When the mortality term is the sole loss term, such as zooplankton in the water column or benthic microalgae in the sediments, a quadratic term is employed to represent increasing predation / viral disease losses in dense populations.

Linear terms have been used to represent a basal respiration rate.

As described in Sc 3.3.5, the mortality terms need to account for the internal properties of lost microalgae.

For definitions of the state variables see Tables 15 & 16.

$$
\begin{aligned}
\frac{\partial[\mathrm{NH_4}]}{\partial t} &= g(1-E)\,(1-\gamma) + gR_N^* && (69)\\
\frac{\partial P}{\partial t} &= g\frac{1}{16}\frac{31}{14}(1-E)\,(1-\gamma) + \frac{1}{16}\frac{31}{14}gR_P^* && (70)\\
\frac{\partial DIC}{\partial t} &= g\frac{106}{16}\frac{12}{14}(1-E)\,(1-\gamma) + \frac{106}{16}\frac{12}{14}gR_I^* && (71)\\
\frac{\partial B}{\partial t} &= -g && (72)\\
\frac{\partial Z}{\partial t} &= Eg && (73)\\
\frac{\partial D_{Red}}{\partial t} &= g(1-E)\gamma && (74)\\
\frac{\partial[\mathrm{O_2}]}{\partial t} &= -\frac{\partial DIC}{\partial t}\frac{138}{106}\frac{32}{12}\frac{[\mathrm{O_2}]}{K_{OA}+[\mathrm{O_2}]} && (75)\\
g &= \min\left[\mu_Z^{max} Z/E, \frac{Z}{m_Z}\left(\phi_{diff}+\phi_{rel}+\phi_{shear}\right)B\right] && (76)\\
\phi &= \phi_{diff}+\phi_{rel}+\phi_{shear} && (77)\\
\phi_{diff} &= (2\kappa T/(3\rho\nu))(1/r_Z+1/r_B)(r_B+r_Z) && (78)\\
\phi_{rel} &= \pi(r_Z+r_B)^2 U_{eff} && (79)\\
\phi_{shear} &= 1.3\sqrt{\epsilon/\nu}(r_Z+r_B)^3 && (80)\\
U_{eff} &= (U_B^2+3U_Z^2)/3U_Z && (81)
\end{aligned}
$$

Table 13: Equations for zooplankton grazing. The terms represent a predator Z consuming a phytoplankton B. Notes (1) If the zooplankton diet contains multiple phytoplankton classes, and grazing is prey saturated, then phytoplankton loss must be reduced to account for the saturation by other types of microalgae; (2) $\frac{Z}{m_Z}$ is the number of individual zooplankton; (3) Phytoplankton pigment is lost to water column without being conserved. Chl *a* has chemical formulae $C_{55}H_{72}O_5N_4Mg$, and a molecular weight of 893.49 g mol^{-1}. The uptake (and subsequent remineralisation) of molecules for chlorophyll synthesis could make up a maximum (at C:Chl = 12) of $660/(893\times12)$ and $56/(893\times12\times(16/106)\times(14/12))$, or ∼6 and ∼3 per cent of the exchange of C and N between the cell and water column, and will cancel out over the lifetime of a cell. Thus the error in ignoring chlorophyll loss to the water column is small.

$$
\begin{aligned}
\frac{\partial[\mathrm{NH_4}]}{\partial t} &= g(1-E)\,(1-\gamma) && (82)\\
\frac{\partial P}{\partial t} &= g\frac{1}{16}\frac{31}{14}(1-E)\,(1-\gamma) && (83)\\
\frac{\partial DIC}{\partial t} &= g\frac{106}{16}\frac{12}{14}(1-E)\,(1-\gamma) && (84)\\
\frac{\partial Z_S}{\partial t} &= -g && (85)\\
\frac{\partial Z_L}{\partial t} &= Eg && (86)\\
\frac{\partial D_{Red}}{\partial t} &= g(1-E)\gamma && (87)\\
\frac{\partial[\mathrm{O_2}]}{\partial t} &= -\frac{\partial DIC}{\partial t}\frac{138}{106}\frac{32}{12}\frac{[\mathrm{O_2}]}{K_{OA}+[\mathrm{O_2}]} && (88)\\
g &= \min\left[\mu_{Z_L}^{max} Z_L/E, \frac{Z_L}{m_Z}\left(\phi_{diff}+\phi_{rel}\phi_{shear}\right) Z_S\right] && (89)
\end{aligned}
$$

Table 14: Equations for zooplankton carnivory, represent large zooplankton Z_L consuming small zooplankton Z_S. The parameters values and symbols are given in Table 12 and Table 11

.

Description	water column		sediment	
	linear d^{-1}	quadratic d^{-1} $(\mathrm{mg\ N\ m^{-3}})^{-1}$	linear d^{-1}	quadratic d^{-1} $(\mathrm{mg\ N\ m^{-3}})^{-1}$
Small phytoplankton	0.01	-	0.01	-
Large phytoplankton	0.01	-	0.01	-
Microphytobenthos	-	-	-	0.0004
Trichodesmium	0.14	0.15	-	-

Table 15: Constants and parameter values used for plankton mortality.

$$
\begin{aligned}
\frac{\partial[\mathrm{NH_4}]}{\partial t} &= m_{L,B} B R_N^* && (91)\\
\frac{\partial DIP}{\partial t} &= \frac{1}{16}\frac{31}{14} m_{L,B} B R_P^* && (92)\\
\frac{\partial DIC}{\partial t} &= \frac{106}{16}\frac{12}{14} m_{L,B} B R_I^* && (93)\\
\frac{\partial[\mathrm{O_2}]}{\partial t} &= -\frac{\partial DIC}{\partial t}\frac{138}{106}\frac{32}{12}\frac{[\mathrm{O_2}]}{K_{OA}+[\mathrm{O_2}]} && (94)\\
\frac{\partial B}{\partial t} &= -m_{L,B} B && (95)\\
\frac{\partial D_{Red}}{\partial t} &= m_{L,B} B && (96)
\end{aligned}
$$

Table 16: Equations for linear phytoplankton mortality.

$$
\begin{aligned}
\frac{\partial Z_S}{\partial t} &= -m_{Q,ZS} Z_S^2 && (97)\\
\frac{\partial Z_L}{\partial t} &= -m_{Q,ZL} Z_L^2 && (98)\\
\frac{\partial D_{Red}}{\partial t} &= f_{Z2det}\left(m_{Q,ZS} Z_S^2 + m_{Q,ZL} Z_L^2\right) && (99)\\
\frac{\partial[\mathrm{NH_4}]}{\partial t} &= (1-f_{Z2det})\left(m_{Q,ZS} Z_S^2 + m_{Q,ZL} Z_L^2\right) && (100)
\end{aligned}
$$

Table 17: Equations for the zooplankton mortality. f_{Z2det} is the fraction of zooplankton mortality that is remineralised, and is equal to 0.5 for both small and large zooplankton.

3.10 Gas exchange

Gas exchange is calculated using a cubic relationship between wind speed (Wanninkhof and McGillis, 1999), the saturation state of the gas (described below) and the Schmidt number of the gas (Wanninkhof, 1992). The transfer coefficient, k, is given by:

$$k = \frac{0.0283}{360000} u_{10}^3 \left(\mathrm{Sc}/660\right)^{-1/2} \tag{101}$$

where 0.0283 cm hr^{-1} is an empirically-determined constant (Wanninkhof and McGillis, 1999), u_{10}^3 is the short-term steady wind at 10 m above the sea surface [m s^{-1}], the Schmidt number, Sc, is the ratio of the diffusivity of momentum and that of the exchanging gas, and is given by a cubic temperature relationship (Wanninkhof, 1992). Finally, a conversion factor of 360000 m s^{-1} (cm hr^{-1})$^{-1}$ is used.

In practice the hydrodynamic model can contain thin surface layers as the surface elevation moves between z-levels. Further, physical processes of advection and diffusion and gas fluxes are done sequentially, allowing concentrations to build up through a single timestep. To avoid unrealistic changes in the concentration of gases in thin surface layers, the shallowest layer thicker than 20 cm receives all the surface fluxes.

3.10.1 Oxygen

The saturation state of oxygen $[\mathrm{O}_2]_{sat}$ is determined as a function of temperature and salinity following Weiss (1970). The change in concentration of oxygen in the surface layer due to a sea-air oxygen flux (+ve from sea to air) is given by:

$$\frac{\partial[\mathrm{O}_2]}{\partial t} = k_{\mathrm{O}_2} \left([\mathrm{O}_2]_{sat} - [\mathrm{O}_2]\right)/h \tag{102}$$

where k_{O_2} is the transfer coefficient for oxygen (Eq. 101), $[\mathrm{O}_2]$ is the dissolved oxygen concentration in the surface waters, and h is the thickness of the surface layer of the model into which sea-air flux flows.

Bubble production. Highly productive benthic communities can produce enough oxygen to form gas bubbles (Hermand et al., 1998) which are not measured by dissolved oxygen sensors. Hermand et al. (1998) found for a seagrass meadow that dissolved oxygen reached a maximum of 120 % saturation, with additional oxygen being accounted for by bubble formation that could be detected by acoustic means.

In the model we assume that above $\upsilon = 1.20$ of oxygen saturation, bubbles form at a rate proportional to the concentration above $\upsilon[\mathrm{O}_2]_{sat}$, and that the time scale of bubble formation is $\tau = 1$

hour. Further, bubbles that form are lost to the air through positive buoyancy. Thus, the change in concentration of oxygen in the bottom water layer due to bubble formation is given by:

$$\frac{\partial[\mathrm{O}_2]}{\partial t} = \tau\left([\mathrm{O}_2] - \upsilon[\mathrm{O}_2]_{sat}\right) \tag{103}$$

An implicit assumption is that once bubbles have formed the oxygen is instantaneously and permanently lost to the air. This will not produce an error in dissolved oxygen prediction in the model if the bubbles take a finite time to reach the surface. However an error will be introduced if in reality oxygen in bubbles moves back to the dissolved state.

3.10.2 Carbon dioxide

The change in surface dissolved inorganic carbon concentration, DIC, resulting from the sea-air flux (+ve from sea to air) of carbon dioxide is given by:

$$\frac{\partial DIC}{\partial t} = k_{\mathrm{CO}_2}\left([\mathrm{CO}_2]_{atm} - [\mathrm{CO}_2]\right)/h \tag{104}$$

where k_{CO_2} the transfer coefficient for carbon dioxide (Eq. 101), $[\mathrm{CO}_2]$ is the dissolved carbon dioxide concentration in the surface waters determined from DIC and A_T using the carbon chemistry equilibria calculations described above, $[\mathrm{CO}_2]_{atm}$ is the partial pressure of carbon dioxide in the atmosphere, and h is the thickness of the surface layer of the model into which sea-air flux flows.

Note the carbon dioxide flux is not determined by the gradient in DIC, but the gradient in $[\mathrm{CO}_2]$. At pH values around 8, $[\mathrm{CO}_2]$ makes up only approximately 1/200th of DIC in seawater, significantly reducing the air-sea exchange. Counteracting this reduced gradient, note that changing DIC results in an approximately 10 fold change in $[\mathrm{CO}_2]$ (quantified by the Revelle factor (Zeebe and Wolf-Gladrow, 2001)). Thus, the gas exchange of CO_2 is approximately $1/200 \times 10 = 1/20$ of the oxygen flux for the same proportional perturbation in DIC and oxygen. At a Sc number of 524 (25°C seawater) and a wind speed of 12 m s^{-1}, 1 m of water equilibrates with air with an e-folding timescale of approximately 1 day.

4 Epibenthic processes

In the model, benthic communities are quantified as a biomass per unit area, or areal biomass. At low biomass, the community is composed of a few specimens spread over a small fraction of the bottom, with no interaction between the nutrient and energy acquisition of individual specimens. Thus, at low biomass the areal fluxes are a linear function of the biomass.

As biomass increases, the individuals begin to cover a significant fraction of the bottom. For nutrient and light fluxes that are constant per unit area, such as downwelling irradiance and sediment releases, the flux per unit biomass decreases with increasing biomass. Some processes, such as photosynthesis in a thick seagrass meadow or nutrient uptake by a coral reef, become independent of biomass (Atkinson, 1992) as the bottom becomes completely covered. To capture the non-linear effect of biomass on benthic processes, we use an effective projected area fraction, A_{eff}.

To restate, at low biomass, the area on the bottom covered by the benthic community is a linear function of biomass. As the total leaf area approaches and exceeds the projected area, the projected area for the calculation of water-community exchange approaches 1, and becomes independent of biomass. This is represented using:

$$A_{eff} = 1 - \exp(-\Omega_B \ B) \tag{105}$$

where A_{eff} is the effective projected area fraction of the benthic community (m^2 m^{-2}), B is the biomass of the benthic community (g N m^{-2}), and Ω_B is the nitrogen-specific leaf area coefficient (m^2 g N^{-1}). For further explanation of Ω_B see **?**.

The parameter Ω_B is critical: it provides a means of converting between biomass and fractions of the bottom covered, and is used in calculating the absorption cross-section of the leaf and the nutrient uptake of corals and macroalgae. That Ω_B has a simple physical explanation, and can be determined from commonly undertaken morphological measurement (see below), gives us confidence in its use throughout the model.

4.1 Epibenthic optical model

The spectrally-resolved light field at the base of the water column is attenuated, in vertical order, by macroalgae, seagrass (*Zostera* then *Halophila*), followed by the zooxanthellae in corals. The downwelling irradiance at wavelength λ after passing through each macroalgae and seagrass species is given by, $E_{below,\lambda}$:

$$E_{below,\lambda} = E_{d,above,\lambda} e^{-A_\lambda \Omega_X X} \tag{106}$$

where $E_{above,\lambda}$ for macroalgae is $E_{d,bot,\lambda}$, the downwelling irradiance of the bottom water column layer, A_λ is the absorbance of the leaf, Ω is the nitrogen specific leaf area, and X is the leaf nitrogen

Variable	Symbol	Units
Downwelling irradiance	E_d	W m^{-2}
Macroalgae biomass	MA	g N m^{-2}
Water column detritus, C:N:P = 550:30:1	D_{Atk}	g N m^{-3}
Effective projected area of macroalgae	A_{eff}	m^2 m^{-2}
Leaf absorbance	$A_{L,\lambda}$	-
Bottom stress	τ	N m^{-2}
Wavelength	λ	nm
Bottom water layer thickness	h_{wc}	m

Table 18: State and derived variables for the macroalgae model. For simplicity in the equations all dissolved constituents are given in grams, although elsewhere they are shown in milligrams.

biomass.

The light absorbed by corals is assumed to be entirely due to zooxanthellae, and is given by:

$$E_{below,\lambda} = E_{above,\lambda} e^{-n\alpha_\lambda} \tag{107}$$

where $n = CS/m_{N,CS}$ is the areal density of zooxanthellae cells and $\alpha\lambda$ is the absorption-cross section of a cell.

The optical model for microphytobenthic algae, and the bottom reflectance due to sediment and bottom types, is described in Sec. 5.1.

4.2 Macroalgae

The macroalgae model considers the diffusion-limited supply of dissolved inorganic nutrients (N and P) and the absorption of light, delivering N, P and fixed C respectively. Unlike the microalgae model, no internal reserves are considered, implying that the macroalgae has a fixed stoichiometry that can be specified as:

$$550CO_2 + 30NO_3^- + PO_4^{3-} + 792H_2O \xrightarrow{5500 \text{ photons}} (CH_2O)_{550}(NH_3)_{30}H_3PO_4 + 716O_2 \tag{108}$$

where the stoichiometry is based on Atkinson and Smith (1983) (see also Baird and Middleton (2004); Hadley et al. (2015a,b)). In the next section will consider the maximum nutrient uptake and light absorption, and then bring them together to determine the realised growth rate.

4.2.1 Nutrient uptake

Nutrient uptake by macroalgae is a function of nutrient concentration, water motion (Hurd, 2000) and internal physiology. The maximum flux of nutrients is specified as a mass transfer limit per projected area of macroalgae and is given by (Falter et al., 2004; Zhang et al., 2011):

$$S_x = 2850 \left(\frac{2\tau}{\rho}\right)^{0.38} \mathrm{Sc_x}^{-0.6}, \mathrm{Sc_x} = \frac{\nu}{D_x} \tag{109}$$

where S_x is the mass transfer rate coefficient of element x = N, P, τ is the shear stress on the bottom, ρ is the density of water and $\mathrm{Sc_x}$ is the Schmidt number. The Schmidt number is the ratio of the diffusivity of momentum, ν, and mass, D_x, and varies with temperature, salinity and nutrient species. The rate constant S can be thought of the height of water cleared of mass per unit of time by the water-macroalgae exchange.

4.2.2 Light capture

The calculation of light capture by macroalgae involves estimating the fraction of light that is incident upon the leaves, and the fraction that is absorbed. The rate of photon capture is given by:

$$k_I = \frac{(10^9 hc)^{-1}}{A_V} \int E_{d,\lambda} \left(1 - \exp\left(-A_{L,\lambda} \Omega_{MA} MA\right)\right) \lambda d\lambda \tag{110}$$

where h, c and A_V are fundamental constants, 10^9 nm m^{-1} accounts for the typical representation of wavelength, λ in nm, and $A_{L,\lambda}$ is the spectrally-resolved absorbance of the leaf. As shown in Eq. 105, the term $1 - \exp\left(-\Omega_{MA} MA\right)$ gives the effective projected area fraction of the community. In the case of light absorption of macroalgae, the exponent is multiplied by the leaf absorbance, $A_{L,\lambda}$, to account for the transparency of the leaves. At low macroalgae biomass, absorption at wavelength λ is equal to $E_{d,\lambda} A_{L,\lambda} \Omega_{MA} MA$, increasing linearly with biomass as all leaves at low biomass are exposed to full light (i.e. there is no self-shading). At high biomass, the absorption by the community asymptotes to $E_{d,\lambda}$, at which point increasing biomass does not increase the absorption as all light is already absorbed.

For more details on the calculation of Ω_{MA} see the Sec. 4.3.2.

4.2.3 Growth

The growth rate combines nutrient, light and maximum organic matter synthesis rates following:

$$\mu_{MA} = \min\left[\mu_{MA}^{max}, \frac{30}{5500} 14 \frac{k_I}{MA}, \frac{S_N A_{eff} N}{MA}, \frac{30}{1}\frac{14}{31}\frac{S_P A_{eff} P}{MA}\right] \tag{111}$$

and the production of macroalgae is given by $\mu_{MA}MA$. Note, as per seagrass and corals, that the maximum growth rates sits within the minimum operator. This allows the growth of macroalgae to the independent of temperature at low light, but still have an exponential dependence at maximum growth rates (Baird et al., 2003).

$$\frac{\partial N}{\partial t} = -\mu_{MA}MA/h_{wc} \tag{112}$$

$$\frac{\partial P}{\partial t} = -\frac{1}{30}\frac{31}{14}\mu_{MA}MA/h_{wc} \tag{113}$$

$$\frac{\partial DIC}{\partial t} = -\frac{550}{30}\frac{12}{14}\mu_{MA}MA/h_{wc} \tag{114}$$

$$\frac{\partial [\mathrm{O_2}]}{\partial t} = \frac{716}{30}\frac{32}{14}\left(\mu_{MA}MA\right)/h_{wc} \tag{115}$$

$$\frac{\partial MA}{\partial t} = \mu_{MA}MA - \zeta_{MA}MA \tag{116}$$

$$\frac{\partial D_{Atk}}{\partial t} = \zeta_{MA}MA/h_{wc} \tag{117}$$

$$\mu_{MA} = \min\left[\mu_{MA}^{max}, \frac{30}{5500}14\frac{k_I}{MA}, \frac{S_N A_{eff} N}{MA}, \frac{30}{1}\frac{14}{31}\frac{S_P A_{eff} P}{MA}\right] \tag{118}$$

$$S_{\mathrm{x}} = 2850\left(\frac{2\tau}{\rho}\right)^{0.38}\mathrm{Sc}^{-0.6}, Sc = \frac{\nu}{D_{\mathrm{x}}} \tag{119}$$

$$k_I = \frac{\left(10^9 hc\right)^{-1}}{A_V}\int E_{d,\lambda}\left(1-\exp\left(-A_{L,\lambda}\Omega_{MA}MA\right)\right)\lambda d\lambda \tag{120}$$

$$A_{eff} = 1-\exp(-\Omega_{MA}\ MA) \tag{121}$$

$$550\mathrm{CO_2} + 30\mathrm{NO_3^-} + \mathrm{PO_4^{3-}} + 792\mathrm{H_2O} \xrightarrow{5500\ \text{photons}} (\mathrm{CH_2O})_{550}(\mathrm{NH_3})_{30}\mathrm{H_3PO_4} + 716\mathrm{O_2} + 391\mathrm{H^+} \tag{122}$$

Table 19: Equations for the macroalgae model. Other constants and parameters are defined in Table 20. 14 g N mol N^{-1}; 12 g C mol C^{-1}; 31 g P mol P^{-1}; 32 g O mol $\mathrm{O_2^{-1}}$.

	Symbol	Value	Units
Parameters			
Maximum growth rate of macroalgae	μ_{MA}^{max}	0.2	d^{-1}
Nitrogen-specific area of macroalgae	Ω_{MA}	2.0	$(g\ N\ m^{-2})^{-1}$
[a]Leaf absorbance	$A_{L,\lambda}$	~ 0.7	-
Mortality rate	ζ_{MA_A}	0.01	d^{-1}

Table 20: Constants and parameter values used to model macroalgae. [a]Spectrally-resolved values

4.2.4 Mortality

Mortality is defined as a simple linear function of biomass:

$$\frac{\partial MA}{\partial t} = -\zeta_{MA} MA \tag{123}$$

A quadratic formulation is not necessary as both the nutrient and light capture rates become independent of biomass as $MA \gg 1/\Omega_{MA}$. Thus the steady-state biomass of macroalgae under nutrient limitation is given by:

$$(MA)_{SS} = \frac{S_N A_{eff} N}{\zeta} \tag{124}$$

and for light-limited growth by:

$$(MA)_{SS} = \frac{k_I}{\zeta} \tag{125}$$

The full macroalgae equations, parameters and symbols are listed in Tables 18, 19 and 20.

4.3 Seagrass

Seagrasses are quantified per m^2 with a constant stoichiometry (C:N:P = 550:30:1) for both above-ground, SG_A, and below-ground, SG_B, biomass, and can translocate organic matter at this constant stoichiometry between the two stores of biomass. Growth occurs only in the above-ground biomass, but losses (grazing, decay etc.) occur in both. Two seagrass varieties, nominally *Zostera* and *Halophila*, are represented in the model. The varieties are modelled using the same equations for growth, respiration and mortality, but with different parameter values.

Variable	Symbol	Units
Downwelling irradiance	E_d	W m^{-2}
Porewater DIN concentration	N_s	g N m^{-3}
Porewater DIP concentration	P_s	g P m^{-3}
Water column DIC concentration	DIC	g C m^{-3}
Water column oxygen concentration	$[O_2]$	g O m^{-3}
Above-ground seagrass biomass	SG_A	g N m^{-2}
Below-ground seagrass biomass	SG_B	g N m^{-2}
Detritus at 550:30:1 in sediment	$D_{Atk,sed}$	g N m^{-3}
Effective projected area of seagrass	A_{eff}	m^2 m^{-2}
Bottom stress	τ	N m^{-2}
Thickness of sediment layer l	$h_{s,l}$	m
Bottom water layer thickness	h_{wc}	m
Wavelength	λ	nm
Translocation rate	Υ	g N m^{-2} s^{-1}
Porosity	ϕ	-

Table 21: State and derived variables for the seagrass model. For simplicity in the equations all dissolved constituents are given in grams, although elsewhere they are shown in milligrams. The bottom water column thickness varies is spatially-variable, depending on bathymetry. The 4 sediment layers have nominal thicknesses of 0.005, 0.02, 0.08, 0.295 m, which are altered through the simulation by deposition and resuspension.

4.3.1 Nutrient uptake

Dissolved inorganic nutrients are taken up by the root system following a Michaelis-Menton form:

$$k_N = \frac{\mu_{SG}^{\max} N_s}{K_{SG,N} + N_s} \tag{142}$$

where $\mu_{SG}^{\max}$ is the maximum growth rate of the above-ground seagrass biomass, N_s is the concentration of dissolved inorganic nitrogen in the sediment pore waters of porosity ϕ, and $K_{SG,N}$ is the concentration at which nutrient uptake is half the maximum.

Depth-resolved sediment nutrient uptake. Nutrients are taken from the sediment porewaters to a depth of z_{root}. The nutrient concentration used in Eq. 142 is weighted by the volume of porewater in each of L layers:

$$\overline{N_s} = \frac{\sum_{l=1}^{L} N_{s,l} h_{s,l} \phi_l}{\sum_{l=1}^{L} h_{s,l} \phi_l} \tag{143}$$

where $h_{s,l}$ and ϕ_l are the thickness and porosity of sediment layer l.

As a further caveat, ammonia is preferentially absorbed relative to nitrate (see Sec. 6.1).

The nutrient taken up from each layer, as a fraction of the total growth rate, $\mu_{SG} SG_A$, also matches this weighting. Thus the nutrient uptake from layer l is given by:

$$f_{N,l} = \frac{N_{s,l} h_{s,l} \phi_l}{\sum_{l=1}^{L} N_{s,l} h_{s,l} \phi_l} \mu_{SG} SG_A \tag{144}$$

4.3.2 Light capture

The spectrally-resolved leaf absorbance, $A_{L,\lambda}$, of two common Australian seagrass species, *Zostera capriconia* and *Halophila ovalis*, are given in Fig. 6. It is assumed that when co-existing *Zostera* shades *Halophila*.

Following Eq. 106, the light below successive seagrass canopies is given by:

$$E_{below,\lambda} = E_{d,above,\lambda} e^{-A_\lambda \Omega_{SG} SG_A \sin \beta_{blade}} \tag{145}$$

where $E_{d,above,\lambda}$ is the downwelling light above the canopy, $E_{d,below,\lambda}$, is the downwelling irradiance below the canopy, A_λ is the absorbance of the leaf, Ω_{SG} is the nitrogen-specific leaf area, SG is the leaf nitrogen biomass, and $\sin \beta_{blade}$ is the sine of the nadir bending angle of the leaf. This formulation captures the phenomena that seagrass biomass cannot be infinitely spread on the bottom, but must be in leaves that shade a fraction of the bottom, while the remaining light passes through the canopy without attenuation. For more information see the epibenthic light model (Sec. 5.2.2).

The rate of photon capture by seagrass is given by:

$$k_I = \frac{(10^9 hc)^{-1}}{A_V} \int E_{d,\lambda} \left(1 - \exp\left(-A_{L,\lambda} \Omega_{SG} SG_A \sin \beta_{blade}\right)\right) \lambda d\lambda \tag{146}$$

where h, c and A_V are fundamental constants, 10^9 nm m^{-1} accounts for the typical representation of wavelength, λ, in nm, and $A_{L,\lambda}$ is the spectrally-resolved absorbance of the seagrass leaf. As shown in Eq. 105, the term $1 - \exp(-\Omega_{SG} SG_A)$ gives the effective projected area fraction of the community. In the case of light absorption of seagrass, the exponential exponent is multiplied by the leaf absorbance, $A_{L,\lambda}$, to account for the transparency of the leaves, and $\sin \beta_{blade}$ to account for the orientation of the leaf. At low seagrass biomass, absorption at wavelength λ is equal to the $E_{d,\lambda} A_{L,\lambda} \Omega_{SG} SG_A \sin \beta_{blade}$, increasing linearly with biomass at low biomass as all leaves are exposed to full light (i.e. there is no self-shading). As biomass increases, the absorption by the community asymptotes to $E_{d,\lambda}$, at which point increasing biomass does not increase the absorption as all light is already absorbed. These end points arise for the same reasons as given in Eq. 105 for A_{eff}.

For *H. ovalis*, the leaf weighs 0.0035 g and has dimensions 15.4 mm × 8.5 mm, thus $\Omega_{SG,Halophila} = 1.9$ (g N m^{-2})$^{-1}$. Observations from Cairns Harbour suggest seagrass meadows of *Z. capriconia* can reach a leaf area of approximately 6 times their surface area (McKenzie, 1994). This corresponds to a biomass of 6 / Ω = 4 g N m^{-2}, or 200 g DW m^{-2}.

4.3.3 Respiration

The seagrass model does not consider internal reserves of energy and nutrients, and therefore cannot respire using energy from reserves like in the model representation of microalgae. Furthermore, growth is represented as net production, not gross production. Given growth timescales of many days, this is a reasonable approximation for the purposes of estimating seagrass biomass, and the daily fluxes of metabolites.

Nonetheless, the energy loss due to respiration needs to be taken into account. Observations from Port Curtis (Petrou et al., 2013) suggest that *Zostera* is unable to survive at less than 4.5 mol photon m^{-2} d^{-1} (Petrou et al., 2013). Presuming this is for a leaf without self-shading (i.e. absorption given by $A_L \Omega_{SG} SG_A$), the loss rate of photons through respiration as a turnover time becomes:

$$k_{resp} = 2 \left(E_{comp} A_L \Omega_{SG} \sin \beta_{blade} - \frac{5500}{30} \frac{1}{14} \zeta_{SG_A} \right) SG_A \tag{147}$$

where E_{comp} is the PAR-weighted by photons compensation scalar irradiance at which respiration equals gross production. Since the observed compensation irradiance will include other loss terms, the respiration turnover rate is calculated from the compensation irradiance minus twice the mortality rate. The factor of two accounts for mortality occurring throughout a 24 period, but photosynthesis only during the light.

The respiration rate, k_{resp}, is subtracted from the rate of absorption, k_I, to give the growth rate at a particular light intensity. If k_{resp} exceeds k_I, then no growth occurs (Table 22).

4.3.4 Seagrass net production

Gross production, the combination of C, N and P elements at 550:30:1 to form seagrass biomass, only occurs in the leaves, using 5500 photons. Net growth is the gross growth minus respiratory losses. As mentioned above, the realised net growth rate of the above-ground biomass, μ_{SG_A}, is represented using a law of the minimum formulation limited by either by nitrogen, phosphorus, light availability or the maximum growth rate:

$$\mu_{SG_A} = \min\left[\frac{\mu_{SG}^{max}\overline{N_s}}{K_{SG,N}+\overline{N_s}}, \frac{\mu_{SG}^{max}\overline{P_s}}{K_{SG,P}+\overline{P_s}}, \frac{30}{5500}14\frac{\max(0, k_I - k_{resp})}{SG_A}\right] \tag{148}$$

where μ_{SG}^{max} is the maximum growth rate of seagrass leaves. In the model, seagrass production occurs only in the day. Thus, μ_{SG}^{max} is equal to approximately twice that obtained from measurements of leaf growth over a 24-hour cycle, to account for zero growth at night in the model. Further, if the measurements of realised growth are obtained considering the change in biomass of both leaves and roots, then μ_{SG}^{max} must be multiplied by a further quantity, approximately 2 for a plant with a below-ground biomass to total biomass ratio, f_{below}, of 0.5, such that the net growth within the leaves can account for the biomass change in both the leaves and roots. Thus $\mu_{SG}^{max} = 0.4$ d^{-1}, as used for both *Zostera* and *Halophila* represents the maximum turnover of the whole plant over 24 hours of 0.1 d^{-1} (Table 23).

4.3.5 Translocation between above- and below-ground biomass

Translocation is modelled as a rate, Υ, with a time constant, τ_{tran}, at which the above and below ground biomasses approach a steady state, specified by a fraction of below ground biomass, f_{below}.

$$\Upsilon = \left(f_{below} - \frac{SG_B}{SG_B + SG_A}\right)(SG_A + SG_B)\,\tau_{tran} \tag{149}$$

4.3.6 Mortality

A linear mortality rate is defined for above ground biomass, ζ_{SG_A}, transforming above ground seagrass biomass into labile detritus at the Atkinson ratio. Additionally, seeds are represented as a component of the seagrass biomass which is unaffected by mortality. The fraction of the seagrass biomass at $1/\Omega_{SG}$ which is seeds is given byf_{seed}. Thus, the above (and similiarly below ground) mortality is:

$$\frac{\partial SG_A}{\partial t} = -\zeta_{SG_A}\left(SG_A - f_{seed}/\Omega_{SG}\left(1 - f_{below}\right)\right) \tag{150}$$

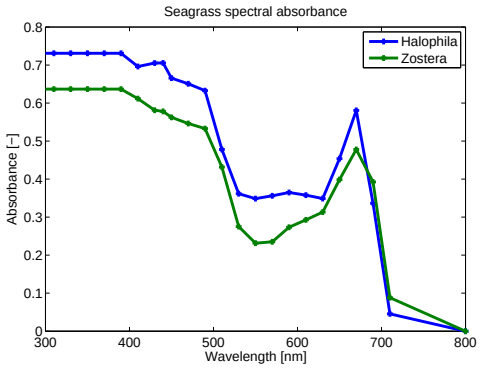

Figure 6: The spectrally-resolved leaf absorbance, $A_{L,\lambda}$, of two common Australian seagrass species (Petrou et al., 2013).

The below ground mortality is:

$$\frac{\partial SG_B}{\partial t} = -\zeta_{SG_B} \left(SG_B - \left(f_{seed} / \Omega_{SG} \right) f_{below} \right) \tag{151}$$

The inclusion of the term f_{below} in the above equations allows the mortality of both above and below ground biomass to asymptote to zero at a seed fraction, at which translocation is also zero.

$$\frac{\partial N_{s,l}}{\partial t} = -f_{N,l}/\left(h_{s,l}\phi_l\right) \quad (126)$$

$$\frac{\partial P_{s,l}}{\partial t} = -\frac{1}{30}\frac{31}{14}f_{P,l}/\left(h_{s,l}\phi_l\right) \quad (127)$$

$$\frac{\partial DIC}{\partial t} = -\frac{550}{30}\frac{12}{14}\left(\mu_{SG_A}SG_A\right)/h_{wc} \quad (128)$$

$$\frac{\partial [O_2]}{\partial t} = \frac{716}{30}\frac{32}{14}\left(\mu_{SG_A}SG_A\right)/h_{wc} \quad (129)$$

$$\frac{\partial SG_A}{\partial t} = \mu_{SG_A}SG_A - \zeta_{SG_A}\left(SG_A - \frac{f_{seed}}{\Omega_{SG}}\left(1 - f_{below}\right)\right) - \Upsilon \quad (130)$$

$$\frac{\partial SG_B}{\partial t} = -\zeta_{SG_B}\left(SG_B - \frac{f_{seed}}{\Omega_{SG}}f_{below}\right) + \Upsilon \quad (131)$$

$$\frac{\partial D_{Atk,sed}}{\partial t} = \left(\zeta_{SG_A}\left(SG_A - \frac{f_{seed}}{\Omega_{SG}}\left(1 - f_{below}\right)\right) + \zeta_{SG_B}\left(SG_B - \frac{f_{seed}}{\Omega_{SG}}f_{below}\right)\right)/\left(h_{sed}\phi\right) \quad (132)$$

$$\mu_{SG_A} = \min\left[\frac{\mu_{SG}^{max}\overline{N_s}}{K_{SG,N} + \overline{N_s}}, \frac{\mu_{SG}^{max}\overline{P_s}}{K_{SG,P} + \overline{P_s}}, \frac{30}{5500}14\frac{\max(0, k_I - k_{resp})}{SG_A}\right] \quad (133)$$

$$\overline{N_s} = \frac{\sum_{l=1}^{L} N_{s,l}h_{s,l}\phi_l}{\sum_{l=1}^{L} h_{s,l}\phi_l} \quad (134)$$

$$\overline{P_s} = \frac{\sum_{l=1}^{L} P_{s,l}h_{s,l}\phi_l}{\sum_{l=1}^{L} h_{s,l}\phi_l} \quad (135)$$

$$f_{N,l} = \frac{N_{s,l}h_{s,l}\phi_l}{\sum_{l=1}^{L} N_{s,l}h_{s,l}\phi_l}\mu_{SG}SG_A \quad (136)$$

$$f_{P,l} = \frac{P_{s,l}h_{s,l}\phi_l}{\sum_{l=1}^{L} P_{s,l}h_{s,l}\phi_l}\mu_{SG}SG_A \quad (137)$$

$$k_I = \frac{\left(10^9 hc\right)^{-1}}{A_V}\int E_{d,\lambda}\left(1 - \exp\left(-A_{L,\lambda}\Omega_{SG}SG_A\sin\beta_{blade}\right)\right)\lambda d\lambda \quad (138)$$

$$k_{resp} = 2\left(E_{comp}A_L\Omega_{SG}\sin\beta_{blade} - \frac{5500}{30}\frac{1}{14}\zeta_{SG_A}\right)SG_A \quad (139)$$

$$\Upsilon = \left(f_{below} - \frac{SG_B}{SG_B + SG_A}\right)\left(SG_A + SG_B\right)\tau_{tran} \quad (140)$$

$$550CO_2 + 30NO_3^- + PO_4^{3-} + 792H_2O \xrightarrow{5500\ \text{photons}} (CH_2O)_{550}(NH_3)_{30}H_3PO_4 + 716O_2 + 391H^+ \quad (141)$$

Table 22: Equations for the seagrass model. Other constants and parameters are defined in Table 23. The equation for organic matter formation gives the stoichiometric constants; 14 g N mol N^{-1};12 g C mol C^{-1}; 31 g P mol P^{-1}; 32 g O mol O_2^{-1}.

	Symbol	*Zostera capricorni*	*Halophila ovalis*	Units
Parameters				
[a]Maximum growth rate of seagrass	μ_{SG}^{max}	0.4	0.4	d^{-1}
[b]Nitrogen-specific area of seagrass	Ω_{SG}	1.5	1.9	$(g\ N\ m^{-2})^{-1}$
[c]Leaf absorbance	$A_{L,\lambda}$	~ 0.7	~ 0.7	-
[d]Fraction biomass below ground	f_{below}	0.5	0.278	-
[e]Translocation rate	τ_{tran}	0.033	0.033	d^{-1}
[f]Half-saturation P uptake	$K_{SG,P}$	96	96	$mg\ P\ m^{-3}$
[g]Half-saturation N uptake	$K_{SG,N}$	420	420	$mg\ N\ m^{-3}$
[h]Compensation scalar PAR irradiance	E_{comp}	4.5	2.8	$mol\ photon\ m^{-2}\ d^{-1}$
[h]Leaf loss rate	ζ_{SG_A}	0.04	0.08	d^{-1}
[h]Root loss rate	ζ_{SG_B}	0.004	0.004	d^{-1}
Seed biomass as a fraction of 63 % cover	f_{seed}	0.01	0.01	-
[i]Seagrass root depth	z_{root}	0.15	0.08	m
Sine of nadir canopy bending angle	$\sin\beta_{blade}$	0.5	1.0	-

Table 23: Constants and parameter values used to model seagrass. [a] ×2 for nighttime ×2 for roots; [b] Zostera - calculated from leaf characteristics in (Kemp et al., 1987; Hansen et al., 2000), *Halophia ovalis* - calculated from leaf dimensions in Vermaat et al. (1995) - Ω_{SG} can also be determined from specific leaf area such as determined in Cambridge and Lambers (1998) for 9 Australian seagrass species; [c] Spectrally-resolved values in Fig. 6; [d] Duarte and Chiscano (1999); [e] loosely based on Kaldy et al. (2013); [f] *Thalassia testudinum* Gras et al. (2003); [g] *Thalassia testudinum* (Lee and Dunton, 1999); [h] Chartrand et al. (2012); Longstaff (2003); [i] Roberts (1993).

4.4 Coral polyps

The coral polyp parameterisation consists of a microalgae growth model to represent zooxanthellae growth based on Baird et al. (2013), and the parameterisation of coral - zooxanthellae interaction based on the host - symbiont model of Gustafsson et al. (2013). In order to reduce complexity for implementation in an ecosystem model, stores of dissolved nutrients within the polyp, and variable elemental stoichiometry of both coral tissue and zooxanthellae cells, represented in Gustafsson et al. (2013) and Baird et al. (2013) respectively, are not considered here.

The state variables for the coral polyp model are the biomass of coral tissue, CH (g N m^{-2}), and zooxanthellae CS (mg N m^{-2}), and the chlorophyll content of the zooxanthellae cells, c_i (mg Chl m^{-2}) (Table 24). Exchanges between the coral community and the overlying water can alter the water column concentrations of nutrient, N and P, phytoplankton, B, zooplankton, Z, and detritus, D, where multiple nutrients, plankton and detritus types are resolved.

The coral is able to assimilate organic nitrogen either through translocated from the zooxanthellae cells or through the capture of water column organic detritus and/or plankton. The zooxanthellae varies its intracellular chlorophyll content depending on potential light limitation of growth, and the incremental benefit of adding pigment due to the package effect, following Baird et al. (2013). The coral tissue is assumed to have a Redfield C:N:P stoichiometry (Redfield et al., 1963), as shown by Muller-Parker et al. (1994). Although observations show elevated C:N ratios in nutrient-limited zooxanthellae (Muller-Parker et al., 1994), for simplicity we have assumed a Redfield ratio for zooxanthellae and coral tissue. Thus, fluxes of C and P with the overlying water column (nutrient uptake and detritial / mucus release) are directly calculated from N fluxes using the Redfield ratio. Finally, corals calcify, which removes alkalinity and dissolved inorganic carbon from the water column.

An explanation of the individual processes follows, with Tables summarizing the model state variables (Table 24), equations (Table 25), and parameters values (Table 26).

4.4.1 Effective projected area fraction of corals

Unlike other benthic habitats, coral communities are restricted to a size that is often much less than the grid size, due to their existence on the rims of reefs (Baird et al., 2004b). To consider this limitation, the effective projected area for corals is calculated by:

$$A_{eff} = A_{CH}\,(1 - \exp(-\Omega_{CH}\ CH/A_{CH})) \tag{152}$$

where A_{eff} is the effective projected area fraction of the coral community (m^2 m^{-2}), CH is the biomass of the coral host, and Ω_{CH} is the nitrogen-specific polyp area coefficient (m^2 g N^{-1}).

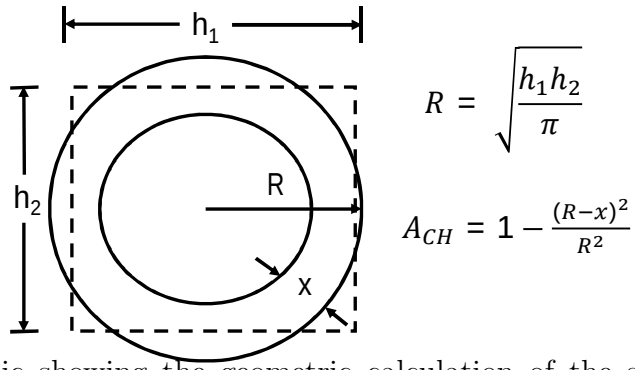

Figure 7: Schematic showing the geometric calculation of the sub-grid parameterisation of the effective projected area fraction of corals, A_{CH}. Nominal width of dense coral communities, $x = 200$ m, grid cell dimensions h_1 and h_2 are 4000 m for the 4 km grid, and R is the equivalent circular radius of the grid cell.

The area coefficient, A_{CH}, represents the fraction of a grid cell that the corals can occupy. In the case of 200 m grids, this will be up to 1, representing dense corals on the whole cell. For coarser grids, A_{CH} is reduced to represent that the cell contains both dense coral communities on the forereef / reef crest and also sparse coral communities on the reef flat / lagoon areas. In the 4 km grid, A_{CH} represents the fraction of the area of dense corals to total reef area, and is of order 0.1. The geometrically-derived equation for A_{CH} is given by (Fig. 7):

$$A_{CH} = 1 - \frac{(R-x)^2}{R^2}, \quad R = \sqrt{h_1 h_2/\pi}, \quad R > x \tag{153}$$

where x is the width of dense coral communities on the reef, and R is equivalent circular radius of the grid cell.

Thus, when $\Omega_{CH}\ CH/A_{CH}$ is small, $A_{CH} \sim \Omega_{CH}\ CH$ and A_{eff} has no impact. However, as $\Omega_{CH}\ CH/A_{CH} \to 1$, $A_{eff} = A_{CH}$. Therefore, if $A_{CH} < 1$ the coral biomass saturates due to space limitation at a lower biomass than it would for $A_{CH} = 1$.

For the case of macroalgae over-growing corals, the effective projected area occupied by corals is further reduced by the presence of macroalgal leaves:

$$A_{eff} = A_{CH}\,(1 - \exp(-\Omega_{MA}\ MA))\,(1 - \exp(-\Omega_{CH}\ CH/A_{CH})) \tag{154}$$

where MA is the biomass of macroalgae, and Ω_{MA} is the nitrogen-specific leaf area coefficient (m^2 g N^{-1}).

Variable	Symbol	Units
Downwelling irradiance	E_d	W m^{-2}
Aragonite saturation state	Ω_a	-
Total alkalinity	A_T	mmol m^{-3}
Dissolved inorganic nitrogen (DIN)	N	g N m^{-3}
Dissolved inorganic phosphorus (DIP)	P	g P m^{-3}
Intracellular pigment concentration	c_i	mg m^{-3}
Zooxanthellae biomass	CS	g N m^{-2}
Coral biomass	CH	g N m^{-2}
Suspended phytoplankton biomass	B	g N m^{-3}
Suspended zoooplankton biomass	Z	g N m^{-3}
Suspended detritus at 106:16:1	D_{Red}	g N m^{-3}
Temperature	T	°C
Absolute salinity	S_A	kg m^{-3}
Effective projected area fraction	A_{eff}	m^2 m^{-2}
Area density of zooxanthellae cells	n_{CS}	cell m^{-2}
Absorption cross-section	α	m^2 $cell^{-1}$
Rate of photon absorption	k_I	mol photon $cell^{-1}$ s^{-1}
Photon-weighted average opaqueness	$\overline{\chi}$	-
Maximum Chl. synthesis rate	$k_{\text{Chl}}^{\max}$	mg Chl m^{-3} d^{-1}
Light limitation factor	E_q	-
Density of water	ρ	kg m^{-3}
Bottom stress	τ	N m^{-2}
Schmidt number	Sc	-
Mass transfer rate coefficient for particles	S_{part}	m d^{-1}
Heterotrophic feeding rate	G	g N m^{-2} d^{-1}
Wavelength	λ	nm
Bottom water layer thickness	h_{wc}	m
Translocation fraction	f_{tran}	-

Table 24: State and derived variables for the coral polyp model. Note units of mass are g, not mg as per pelagic components of the model.

$$\frac{\partial N}{\partial t} = -\mu_{CS} CS/h_{wc} \tag{155}$$

$$\frac{\partial P}{\partial t} = -\frac{1}{30}\frac{31}{14}\mu_{CS} CS/h_{wc} \tag{156}$$

$$\frac{\partial DIC}{\partial t} = -\frac{550}{30}\frac{12}{14}\mu_{CS} CS/h_{wc} \tag{157}$$

$$\frac{\partial [\mathrm{O_2}]}{\partial t} = \frac{716}{30}\frac{32}{14}\mu_{CS} CS/h_{wc} \tag{158}$$

$$\frac{\partial CS}{\partial t} = (1 - f_{tran})\mu_{CS} CS - \zeta_{CS} CS + f_{remin}\frac{\zeta_{CH}}{A_{eff}} CH^2 \tag{159}$$

$$\frac{\partial CH}{\partial t} = G' - \frac{\zeta_{CH}}{A_{eff}} CH^2 \tag{160}$$

$$\frac{\partial c_i}{\partial t} = k_{\mathrm{Chl}}^{\max}(1 - E_q)\overline{\chi} - c_i(1 - f_{tran})\mu_{CS} \tag{161}$$

$$\frac{\partial B}{\partial t} = -S_{part} A_{eff} B \frac{G'}{G}/h_{wc} \tag{162}$$

$$\frac{\partial Z}{\partial t} = -S_{part} A_{eff} Z \frac{G'}{G}/h_{wc} \tag{163}$$

$$\frac{\partial D_{Red}}{\partial t} = \left(-S_{part} A_{eff} D_{Red}\frac{G'}{G} + (1 - f_{remin})\frac{\zeta_{CH}}{A_{eff}} CH^2\right)/h_{wc} \tag{164}$$

$$\tag{165}$$

$$k_I = \frac{(10^9 hc)^{-1}}{A_V}\int \alpha_\lambda E_{d,\lambda}\lambda \, d\lambda \tag{166}$$

$$f_{tran} = \frac{\pi r_{CS}^2 n_{CS}}{2CH\Omega_{CH}} \tag{167}$$

$$\mu_{CS} = \min\left[\mu_{CS}^{max}, \frac{k_I}{m_{CS,I}}, \frac{S_N A_{eff} N}{m_{CS,N}}, \frac{S_P A_{eff} P}{m_{CS,P}}\right] \tag{168}$$

$$S_{\mathrm{x}} = 2850\left(\frac{2\tau}{\rho}\right)^{0.38} \mathrm{Sc_x}^{-0.6}, \mathrm{Sc_x} = \frac{\nu}{D_{\mathrm{x}}} \tag{169}$$

$$G = S_{part} A_{eff}\left(B + Z + D_{Red}\right) \tag{170}$$

$$G' = \min\left[\min\left[\mu_{CH}^{max} CH - f_{tran}\mu_{CS} CS - \zeta_{CS} CS, 0\right], G\right] \tag{171}$$

$$106\mathrm{CO_2} + 16\mathrm{NO_3^-} + \mathrm{PO_4^{3-}} + 122\mathrm{H_2O} + 19\mathrm{H^+} \xrightarrow{1060\mathrm{photons}} (\mathrm{CH_2O})_{106}(\mathrm{NH_3})_{16}\mathrm{H_3PO_4} + 138\mathrm{O_2} \tag{172}$$

Table 25: Equations for the coral polyp model. The term CS/m_N is the concentration of zoothanxellae cells. The equation for organic matter formation gives the stoichiometric constants; 12 g C mol C^{-1}; 32 g O mol $\mathrm{O_2}^{-1}$. The equations are for scalar irradiance specified as an energy flux. Other constants and parameters are defined in Table 26.

	Symbol	Value
Constants		
Molecular diffusivity of NO_3	D	$f(T, S_A) \sim 17.5 \times 10^{-10}$ m^2 s^{-1}
Speed of light	c	2.998×10^8 m s^{-1}
Planck constant	h	6.626×10^{-34} J s^{-1}
Avagadro constant	A_V	6.02×10^{23} mol^{-1}
[a]Pigment-specific absorption coefficient	γ_λ	$f(\text{pig}, \lambda)$ m^{-1} (mg m^{-3})$^{-1}$
kinematic viscosity of water	ν	$f(T, S_A) \sim 1.05 \times 10^{-6}$ m^2 s^{-1}
Parameters		
[b]Nitrogen content of zooxanthellae cells	$m_{CS,N}$	5.77×10^{-12} mol N cell^{-1}
[c]Energy content of zooxanthellae cells	$m_{CS,I}$	(1060/16) m_N mol photon cell^{-1}
[d]Maximum intracellular Chl concentration	$c_i^{\max}$	3.15×10^6 mg Chl m^{-3}
Radius of zooxanthellae cells	r_{CS}	5 μm
Maximum growth rate of coral	μ_{CH}^{max}	0.05 d^{-1}
[e]Rate coefficient of particle capture	S_{part}	3.0 m d^{-1}
Maximum growth rate of zooxanthellae	μ_{CS}^{max}	0.4 d^{-1}
Quadratic mortality coefficient of polyps	ζ_{CH}	0.01 d^{-1} (g N m^{-2})$^{-1}$
Linear mortality of zooxanthellae	ζ_{CS}	0.04 d^{-1}
[g]Remineralised fraction of coral mortality	f_{remin}	0.5
nitrogen-specific host area coefficient of polyps	Ω_{CH}	2.0 m^2 g N^{-1}
[h]Maximum nighttime net coral calcification	k_{night}	0.013 mmol C m^{-2} s^{-1}
[h]Maximum daytime net coral calcification	k_{day}	0.007 mmol C m^{-2} s^{-1}
[i]Rate of net carbonate dissolution on uncovered sand	d_{sand}	8.1 $\times 10^{-5}$ mmol C m^{-2} s^{-1}
Solubility product of calcium carbonate	K_{sp}	$f(T, S_A)$

Table 26: Constants and parameter values used to model coral polyps. V is zooxanthellae cell volume in μm^3. [a]Spectrally-resolved values of γ_λ chlorophyll a, chlorophyll c based on idealised curves in Ficek et al. (2004),[b]Straile (1997),[c]Redfield et al. (1963) and Kirk (1994),[d]Finkel (2001),[e]Ribes and Atkinson (2007); Wyatt et al. (2010),[f,g]Gustafsson et al. (2013, 2014);[h]Anthony et al. (2011, 2013); [i]Cyronak et al. (2013).

4.4.2 Uptake of nutrients and particulate matter from the overlying water

The maximum flux of nutrients and prey to the surface of the coral is specified as a mass transfer limit per projected area of coral (Atkinson and Bilger, 1992; Baird et al., 2004b), as given by (Falter et al., 2004; Zhang et al., 2011):

$$S_x = 2850 \left(\frac{2\tau}{\rho}\right)^{0.38} \mathrm{Sc_x}^{-0.6}, \mathrm{Sc_x} = \frac{\nu}{D_x} \tag{173}$$

where S_x is the mass transfer rate coefficient of element x = N, P, τ is the shear stress on the bottom, ρ is the density of water and $\mathrm{Sc_x}$ is the Schmidt number. The Schmidt number is the ratio of the diffusivity of momentum, ν, and mass, D_x, and varies with temperature, salinity and nutrient species. The rate constant S can be thought of the height of water cleared of mass per unit of time by the water-coral exchange.

The capture of organic particles (phytoplankton, zooplankton, labile detritus) is also represented as an areal flux. Ribes and Atkinson (2007) considered whether mass transfer limits apply to particulate matter on reefs, and found for coral rubble communities only a weak velocity dependence, suggesting active pumping by filter feeders overcame any diffusion limitations (see also Monismith et al. (2010)). Thus, capture of organic particles, G, is represented by a constant rate coefficient, S_{Part}, multiplied by the concentration of each of organic constituents in the water column. The calculated capture rate is limited to the maximum growth rate of the coral tissue, $\mu_{CH}^{max} CH$.

The maximum fluxes of both nutrients and particulates from the overlying water are multiplied by the effective projected area fraction of the coral (A_{eff}).

4.4.3 Light capture by zooxanthellae

The rate of light absorption by a cell with an absorption cross-section α is αE_d. If the light is specified as a energy flux (W m^{-2}), the rate of photons absorbed across all wavelengths is given by:

$$k_I = \frac{(10^9 hc)^{-1}}{A_V} \int \alpha_\lambda E_{d,\lambda} \lambda \, d\lambda \tag{174}$$

where A_V, h and c are fundamental constants (Table 26). The rate of photon absorption per cell, k_I is used in the below equations to determine zooxanthellae growth.

The light incident upon the zooxanthellae, E_d, is assumed to be the downwelling irradiance from the bottom of the overlying water column. Using scalar irradiance microprobes, Wangpraseurt et al. (2012) found in coral tissue of 1 mm thickness that the scalar irradiance in deeper layers was 10% of the surface irradiance. Thus, in healthy coral, absorption is much greater than scattering, and

downwelling light is a reasonable approximation of scalar irradiance incident upon the zooxanthellae. In bleached corals (no zooxanthellae), scattering becomes greater than absorption in the coral tissue, and the scalar irradiance at the coral surface can reach 150% of the unbleached corals (Wangpraseurt et al., 2012). In such a case downwelling light is a poor approximation of scalar irradiance, but this has not been considered in the model.

The light field experienced by all zooxanthellae within a polyp is assumed to be the same, although in reality zooxanthellae are often found in two vertically-distinct layers (Gustafsson et al., 2013). Given this assumption of equal light exposure, and that zooxanthellae is the dominant attenuation term within the coral tissue, the average scalar irradiance at wavelength λ that the cells are exposed to, $E_{av,\lambda}$, is given by:

$$E_{d,\lambda} = \frac{E_{top,\lambda}\left(1 - e^{-\alpha_\lambda n_{CS}}\right)}{\alpha_\lambda n_{CS}} \tag{175}$$

where $E_{top,d,\lambda}$ is the downwelling irradiance above the corals, $E_{d,\lambda}$ is the mean downwelling irradiance experienced by all zooxanthellae, $n_{CS} = CS/m_{CS,N}$ is the areal density of zooxanthellae cells, where $m_{CS,N}$ is the nitrogen content of a single cell. The absorption cross-section of the zooxanthellae cells is calculated using geometric optics, and changes as a function the dynamic intracellular chlorophyll concentration as detailed in the next section.

4.4.4 Chlorophyll synthesis

Intracellular chlorophyll concentration is changed through the synthesis of pigment and the sharing of pigment between offspring during growth, as per the microalgal growth model. The mortality of both the entire polyp and the zooxanthellae impact on the chlorophyll per m^2, although because chlorophyll is specified as an intracellular concentration, these terms do not appear explicitly in the equations in Table 25. If chlorophyll were quantified per m^2 (as it is in the numerical solution), then the loss terms for chlorophyll due to polyp and zooxanthellae mortality would be $\zeta_{CS} c_i$ and $\zeta_{CH} CHc_i$ respectively. Since chlorophyll is considered a small proportion of the cellular nitrogen, neither the synthesis nor loss appear as terms in the equations for N.

The rate of chlorophyll synthesis is represented as a maximum rate, reduced by a factor representing the incremental benefit to absorption of adding further pigment, and a factor representing the degree of light limitation (identical to microalgae, Eq. 32). The rate of chlorophyll synthesis is given by:

$$\frac{\partial c_i}{\partial t} = k_{\text{Chl}}^{\max}\left(1 - E_q\right)\overline{\chi} \tag{176}$$

where $k_{\text{Chl}}^{\max}$ is the maximum synthesis rate of chlorophyll, $\overline{\chi}$ is the area-specific, PAR-weighted, incremental rate of change of absorption, and the degree of light limitation factor, E_q is given by:

$$E_q = \min\left[1, \frac{\frac{30}{5500}\frac{14}{12}k_I}{\mu_{CS}^{max} CS}, \frac{\frac{30}{5500}\frac{14}{12}k_I}{S_N A_{eff} N}, \frac{\frac{1}{5500}\frac{31}{12}k_I}{S_P A_{eff} P}\right] \tag{177}$$

where the second to fourth terms represent the ratio of light absorption to maximum growth rate, and light absorption to nitrogen and phosphorus uptake respectively. Should all these fractions be greater than 1, then the light limitation factor is set to 1. The maximum synthesis rate of chlorophyll, $k_{\text{Chl}}^{\max}$, is given by assuming that twice the maximum chlorophyll concentration, c_i^{max} can be synthesised each day (Baird et al., 2013).

4.4.5 Zooxanthellae growth

In the absence of internal reserves as resolved in Baird et al. (2013), zooxanthellae growth is consider as the minimum of the maximum fluxes of nutrient and energy to the cell, and the maximum growth rate (Everett et al., 2007):

$$\mu_{CS} = \min\left[\mu_{CS}^{max}, k_I/m_{CS,I}, S_N A_{eff} N/m_{CS,N}, S_P A_{eff} P/m_{CS,P}\right] \tag{178}$$

The flux of nutrients (Eq. 105 & 173) is assumed to be equally available to each zooxanthellae cell, and the flux of photons (Eq. 174) to be equal for all cells. This form of the growth limitation is similar to the law of the minimum (von Liebig, 1840), with the difference that the maximum growth rate appears within the minimum term. By including μ_{CS}^{max} within the minimum operator, the exponential temperature dependence of the maximum growth rate does not impact on the temperature-independent growth under-low light, or the non-linear temperature-dependent processes of diffusion of nutrient ions to the coral surface (Baird et al., 2003).

4.4.6 Translocation between zooxanthellae and coral tissue

Unlike seagrass (Sec. 4.3.5), where translocation represents a reallocation of mass within an individual plant, translocation here represents the one-way consumption of zooxanthellae organic matter produced through either zooxanthellae growth or mortality.

A fraction, f_{tran}, of zooxanthellae growth is translocated to the coral tissue. This fraction is equal to 0.5 when the projected area of the zooxanthellae cells ($\pi r_{CS}^2 CS/m_{CS,N}$) exceeds twice surface area of the coral polyp, $2CH\Omega_{CH}$ (Tab. 25). When $f_{tran} < 0.5$, zooxanthellae growth is primarily used for increasing symbiont population, and for $f_{tran} > 0.5$, it is primarily translocated. The initial number of symbiont cells is set so that $(\pi r_{CS}^2 CS/m_{CS,N}) \,/\, (2CH\Omega_{CH})$ is less than 1. Under this initial condition, as $(\pi r_{CS}^2 CS/m_{CS,N}) \,/\, (2CH\Omega_{CH})$ approaches 1, all symbiont growth is translocated, so f_{tran} never increases above 1.

This translocation formulation represents a geometrically-derived space limitation on zooxanthellae, being located within two layers of gastrodermal cells (Gustafsson et al., 2013).

4.4.7 Coral polyp net production

Coral host biomass, CH, grows at a rate, $\mu_{CH}^{max}CH$, conditional on the availability of organic matter either taken up from the water column as particulate organic matter by the host itself (Eq. 173), or through translocation from zooxanthellae. It is assumed that the growth rate of zooxanthellae is independent of the physiology of the coral host, and further, that the fraction of the zooxanthellae growth that is translocated depends only on the availability of space for the zooxanthellae population to reside in (see above). Should this rate of translocation, plus the flux of organic matter due to zooxanthellae mortality, exceed the maximum growth rate of coral host biomass, $\mu_{CH}^{max}CH$, then the coral host grows at its maximum rate, and the excess is released into the environment as mucus. Should the translocation rate and the particular organic matter flux be less than $\mu_{CH}^{max}CH$, then the coral host grows at the sum of the two. Finally, should the translocation rate and the particular organic matter flux be greater than $\mu_{CH}^{max}CH$, then the host will use all of the translocated organic matter, and a fraction captured particular organic matter, with the fraction being composed of fractions of each particulate components based on the relative concentration of organic matter in each category (Eq. 171).

4.4.8 Mortality of coral polyps

There are two mortality terms: the mortality of the entire polyp (ζ_{CH}), affecting both coral and zooxanthellae biomass, and mortality of the zooxanthellae (ζ_{CS}). The polyp mortality term has a quadratic mortality coefficient, ζ_{CH}, that stablises the biomass of coral tissue to μ_{CH}/ζ_{CH}. For a maximum growth rate of coral, $\mu_{CH}^{max} = 0.05$ d^{-1}, ζ_{CH} has been set to 0.01 (g N m^{-2})$^{-1}$ d^{-1}, so the biomass of coral tissue CH stabilises at 0.05 / 0.01 = 5 g N m^{-2}. As this biomass is per unit area, and includes a correction for corals being only be viable on A_{eff} of the area, ζ_{CH} needs to be divided by A_{eff} in the equations.

4.4.9 Coral calcification

The rate of coral calcification is a function of the water column aragonite saturation, Ω_a, and reserves of energy in the symbiont, E_q. The rates of change of DIC and total alkalinity, A_T, in the bottom water column layer of thickness h_{wc} due to calcification becomes:

$$\frac{\partial DIC}{\partial t} = -12gA_{eff}/h_{wc} \tag{179}$$

$$\frac{\partial A_T}{\partial t} = -2gA_{eff}/h_{wc} \tag{180}$$

$$g = k_{day}(\Omega_a - 1)\,(1 - E_q) + k_{night}(\Omega_a - 1) \tag{181}$$

where g is the rate of net calcification, k_{day} and k_{night} are defined in Table 26 with habitat-specific values (Anthony et al., 2011; Mongin and Baird, 2014). The fluxes are scaled by the effective projected area of the community, A_{eff}.

4.4.10 Dissolution of carbonate sands

Dissolution of carbonate sands, particular on a coral reef, affect water column DIC and alkalinity. At present the sediment model does not distinguish between carbonate and non-carbonate sands. To account for dissolution, the dissolution of carbonate sands is approximated as a source of DIC and alkalinity in areas with coral polyps present, and does not affect the properties (mass, porosity etc.) of the underlying sediments. Thus:

$$\frac{\partial DIC}{\partial t} = 12 d_{sand}/h_{wc} \tag{182}$$

$$\frac{\partial A_T}{\partial t} = 2 d_{sand}/h_{wc} \tag{183}$$

where d_{sand} is the dissolution rate of $CaCO_3$, and is the reverse reaction to calcification.

Calcification

$$\frac{\partial A_T}{\partial t} = -2gA_{eff}/h_{wc} \quad (184)$$

$$\frac{\partial DIC}{\partial t} = -12gA_{eff}/h_{wc} \quad (185)$$

$$g = k_{day}(\Omega_a - 1)\,(1 - E_q) + k_{night}(\Omega_a - 1) \quad (186)$$

$$\Omega_a = \frac{[\mathrm{CO_3^{2-}}][\mathrm{Ca^{2+}}]}{K_{sp}} \quad (187)$$

$$\mathrm{Ca^{2+}} + 2\mathrm{HCO_3^-} \longrightarrow \mathrm{CaCO_3} + \mathrm{CO_2} + \mathrm{H_2O} \quad (188)$$

Dissolution

$$\frac{\partial A_T}{\partial t} = 2d_{sand}/h_{wc} \quad (189)$$

$$\frac{\partial DIC}{\partial t} = 12d_{sand}/h_{wc} \quad (190)$$

(191)

$$\mathrm{CaCO_3} + \mathrm{CO_2} + \mathrm{H_2O} \longrightarrow \mathrm{Ca^{2+}} + 2\mathrm{HCO_3^-} \quad (192)$$

Table 27: Equations for coral polyp calcification and dissolution. The concentration of carbonate ions, $[\mathrm{CO_3^{2-}}]$, is determined from equilibrium carbon chemistry as a function of A_T, DIC, temperature and salinity, and the concentration of calcium ions, $[\mathrm{Ca^{2+}}]$, is a mean oceanic value. 12 g C mol $\mathrm{C^{-1}}$. Other constants and parameters are defined in Table 26.

5 Sediment processes

5.1 Brief summary of sediment model

The model contains particulate classes as summarised in Table 28.

Name	Nom. size μm	Sinking vel. m d^{-1}	Optically-active	Origin	Phosphorus adsorption
Gravel	10^4	60,480	N	I	N
Sand	10^2	172.8	N	I	N
Mud	30	17.2	Y	I	Y
FineSed	30	17.2	Y	C	Y
D_{Atk}	-	1,000	Y	OM	N
D_{Red}	-	1,000	Y	OM	N
D_C,D_N,D_P	-	1,000	Y	OM	N

Table 28: Characteristics of the particulate classes. Y - Yes, N - No, I - initial condition, C - catchment, OM - remineralistion from organic matter (Condie et al., 2009; Margvelashvili, 2009).

5.2 Sediment optical model

5.2.1 Light absorption by benthic microalgae

The light, as photons, below the epibenthos is integrated over the photosynthetically available radiation, and used to calculate light absorption by microalgae in the sediment layers using:

$$k_I = \frac{(10^9 hc)^{-1}}{A_V} n \alpha_{PAR} \int_{400}^{700} E_{d,\lambda} \lambda d\lambda \tag{193}$$

where A_V, h and c are fundamental constants (Table 26), E_d is the downwelling irradiance in energy units, n is the number of cells, α_{PAR} is the absorption cross-section of the cell assuming a quantum PAR-weighted pigment-specific attenuation coefficient of 0.04 m^{-1} (mg m^{-3})$^{-1}$, and using the geometric optics calculation for the absorption cross-section of spherical cell (Eq. 3).

This calculation assumes that benthic microalgae are the only attenuating components in the surface sediment layer, which effectively assumes the microalgae lie on the top of the top layer of sediment. No light penetrates through to the second sediment layer.

5.2.2 Bottom reflectance of macrophytes, benthic microalgae and sediment types

In order to calculate the importance of bottom reflectance, the integrated weighting of the water column must be calculated (Sec. 3.2.3), with the remaining being ascribed to the bottom. Thus, the weighting of the bottom reflectance as a component of surface reflectance is given by:

$$w_{\lambda,bot} = 1 - \frac{1}{z_{bot}} \int_0^{z_{bot}} \exp\left(-2K_{\lambda,z'}\right) dz' \tag{194}$$

where K_λ is the attenuation coefficient at wavelength λ described above, the factor of 2 accounts for the pathlength of both downwelling and upwelling light.

The bottom reflectance between 400 and 800 nm of $\sim$ 100 substrates (including turtles and giant clams!) have been measured on Heron Island using an Ocean Optics 2000 (Roelfsema and Phinn, 2012; Leiper et al., 2012). The data for selected substrates are shown in Fig. 9. When the bottom is composed of mixed communities, the surface reflectance is weighted by the fraction of the end members visible from above, with the assumption that the substrates are layered from top to bottom by macroalgae, seagrass (*Zostera* then *Halophila*), corals (zooxanthellae then skeleton), benthic microalgae, and then sediments. Since the sediment is sorted in the simulation by the sediment process, the sediments are assumed to be well mixed in surface sediment layer. Implicit in this formulation is that the scattering of one substrate type (i.e. benthic microalgae) does not contribute to the relectance of another (i.e. sand). This will hold true if the substrates are spatially segregated on the bottom. In terms of an individual photon, it implies that if it first intercepts substrate A, then it is only scattered and/or absorbed by A.

Calculation of bottom fraction.

The fraction of the bottom taken up by a benthic plant of biomass B is $A_{eff} = 1 - \exp(-\Omega_B B)$, with $\exp(-\Omega_B B)$ uncovered. Thus the fraction of the bottom covered by macroalgae, seagrass (Zostera then Halophila) and corals polyps is given by:

$$f_{MA} = 1 - \exp(-\Omega_{MA} MA) \tag{195}$$

$$f_{SG} = (1 - f_{MA})\,(1 - \exp(-\Omega_{SG} SG)) \tag{196}$$

$$f_{SGH} = (1 - f_{MA} - f_{SG})\,(1 - \exp(-\Omega_{SGH} SGH)) \tag{197}$$

$$f_{polyps} = (1 - f_{MA} - f_{SG} - f_{SGH})\,(1 - \exp(-\Omega_{CH} CH)) \tag{198}$$

Of the fraction of the bottom taken up by the polyps, f_{polyps}, zooxanthellae are first exposed. Assuming the zooxanthellae are horizontally homogeneous, the fraction taken up by the zooxanthellae is given by:

$$f_{zoo} = \min[f_{polyps}, \frac{\pi}{2\sqrt{3}} n \pi r_{zoo}^2] \tag{199}$$

where πr^2 is the projected area of the cell, n is the number of cells, and $\pi/(2\sqrt{3}) \sim 0.9069$ accounts for the maximum packaging of spheres. Thus the zooxanthellae can take up all the polyp area. The fraction, if any, of the exposed polyp area remaining is assumed to be coral skeleton:

$$f_{skel} = f_{polyps} - \min[f_{polyps}, \frac{\pi}{2\sqrt{3}} n\pi r_{zoo}^2] \tag{200}$$

The benthic microalgae overlay the sediments. Following the zooxanthellae calculation above, the fraction taken up by benthic microalgae is given by:

$$f_{MPB} = \min[(1 - f_{MA} - f_{SG} - f_{SGH} - f_{polyps}), \frac{\pi}{2\sqrt{3}} n\pi r_{MPB}^2] \tag{201}$$

Finally, the sediment fractions are assigned relative to their density in the surface layer:

$$M = \sum Sand + Mud + FineSed \tag{202}$$

$$f_{Sand} = (1 - f_{MA} - f_{SG} - f_{SGH} - f_{polyps} - f_{MPB}) \frac{Sand}{M} \tag{203}$$

$$f_{Mud} = (1 - f_{MA} - f_{SG} - f_{SGH} - f_{polyps} - f_{MPB}) \frac{Mud}{M} \tag{204}$$

$$f_{FineSed} = (1 - f_{MA} - f_{SG} - f_{SGH} - f_{polyps} - f_{MPB}) \frac{FineSed}{M} \tag{205}$$

with the porewaters not being considered optically-active. Now that the fraction of each bottom type has been calculated, the fraction of backscattering to absorption plus backscattering for the benthic surface as seen just below the surface, $u_{bot,\lambda}$, is given by:

$$\begin{aligned} u_{bot,\lambda} \quad = \quad & w_{\lambda,bot}(f_{MA}\rho_{MA,\lambda} \\ & + f_{SG}\rho_{SG,\lambda} \\ & + f_{SGH}\rho_{SGH,\lambda} \\ & + f_{zoo}\frac{b_{zoo,\lambda}}{a_{zoo,\lambda} + b_{zoo,\lambda}} \\ & + f_{skel}\rho_{skel,\lambda} \\ & + f_{MPB}\frac{b_{MPB,\lambda}}{a_{MPB,\lambda} + b_{MPB,\lambda}} \\ & + f_{Sand}\rho_{Sand,\lambda} + f_{Mud}\rho_{Mud,\lambda} + f_{FineSed}\rho_{FineSed,\lambda}) \end{aligned} \tag{206}$$

where the absorption and backscattering are calculated as given in Sec. 3.2.1, and ρ is the measured bottom refectance of each end member (Dekker et al., 2011; Reichstetter et al., 2015).

For the values of surface reflectance for sand and mud from Heron Island (Roelfsema and Phinn, 2012; Leiper et al., 2012), and microalgal optical properties calculated as per Sec. 3.2, a ternary plot can be used to visualise the changes in true colour with sediment composition (Fig. 8).

It is important to note that while the backscattering of light from the bottom is considered in the model for the purposes of calculating reflectance (and therefore comparing with observations), it is not included in the calculation of water column scalar irradiance, which would require a radiative transfer model (Mishchenko et al., 2002).

5.3 Sediment chemistry

5.3.1 Sediment nitrification - denitrification

Nitrification in the sediment is similar to the water-column, but with a sigmoid rather than hyperbolic relationship at low oxygen, for numerical reasons. Denitrification occurs only in the sediment.

Variable	Symbol	Units
Ammonia concentration	$[NH_4]$	mg N m^{-3}
Sediment Dissolved Inorganic Carbon (DIC)	DIC	mg C m^{-3}
Sediment Dissolved Inorganic Phosphorus (DIP)	P	mg P m^{-3}
Sediment Particulate Inorganic Phosphorus (PIP)	PIP	mg P m^{-3}
Sediment Immobolised Particulate Inorganic Phosphorus (PIPI)	$PIPI$	mg P m^{-3}
Sediment Non-Algal Particulates (NAP)	NAP	kg m^{-3}
Sediment dissolved oxygen concentration	$[O_2]$	mg O m^{-3}

Table 29: State and derived variables for the sediment inorganic chemistry model.

5.3.2 Sediment phosphorus absorption - desorption

Sediment phosphorus absorption - desorption is similar to water column.

There is an additional pool of immobilised particulate inorganic phosphorus, $PIPI$, which accumulates in the model over time as PIP becomes immobilised, and represents permanent sequestration.

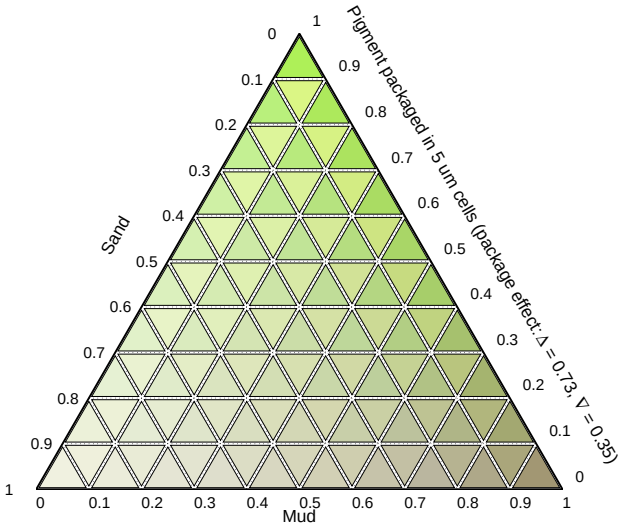

Figure 8: Modelled true colour surface reflectance for mixed sand, mud and microalgae sediment composition. The number of cells, n, required to fill the fraction without sand and mud, f_{MPB}, is calculated as $n = f_{MPB} / \left(\pi^2 r^2 / \left(2\sqrt{3}\right)\right)$ (from Eq. 201). The ternary plot shows cells of 5 μm radius with two internal concentrations of pigment (and therefore absorption). The generic parameter for the effect of cell pigment concentration on the reflectance is the packaging effect, $\alpha_\lambda/(\pi r^2)$, which varies between 0 and 1. A value of zero is a transparent cell with no self-shading, and a value of 1 is fully opaque at the specified wavelength. The upward pointing triangles, Δ, show the effect of cells with a package effect at 470 nm of 0.73, while the downward pointing triangles, ∇, show the effects of cells with a package effect at 470 nm of 0.35. Sand reflectance is based on observations from Heron Island (Roelfsema and Phinn, 2012), and mud from Janet (CLW). To read the counterclockwise ternary plot: At each point in the triangle the sum of sand, mud and microalgal fractions equals 1. Follow the grid in a SE direction from the sand axis, a NE from the mud axis, and W from the microalgae axis. Thus, the bottom left corner is 100 % light yellow sand, the bottom right corner is 100 % brown mud, and the top corner is 100 % green algal cells. The reflectance is enhanced using the MODIS true colour algorithm (Sec. B.2).

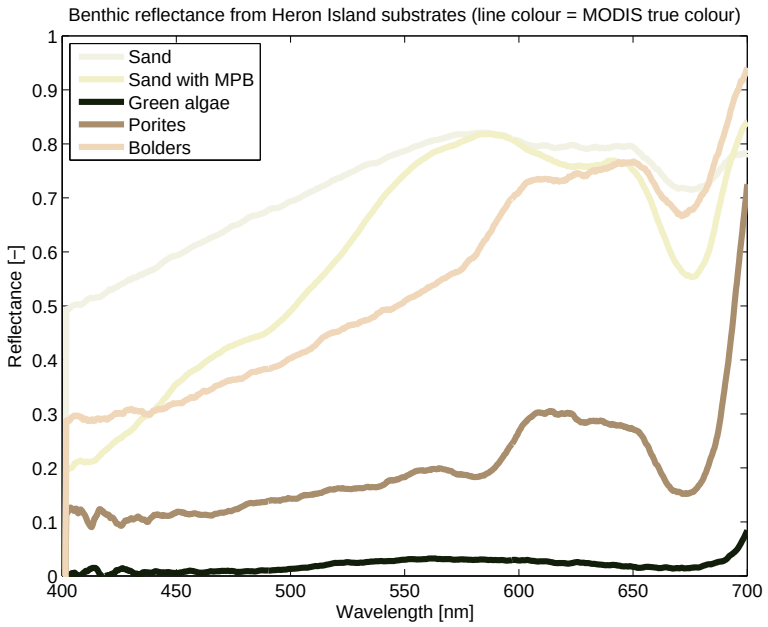

Figure 9: Observed substrate reflectance from 400 to 800 nm from Heron Island. Photos of the substrates, and the data, are available in Roelfsema and Phinn (2012). The line colour is calculated from the MODIS true colour algorithm (Gumley et al., 2010), giving the colour of the substrate lit by a spectrally-flat light source. Green algae appears almost black as there is low reflectance across all wavelengths, while sand is the whitest.

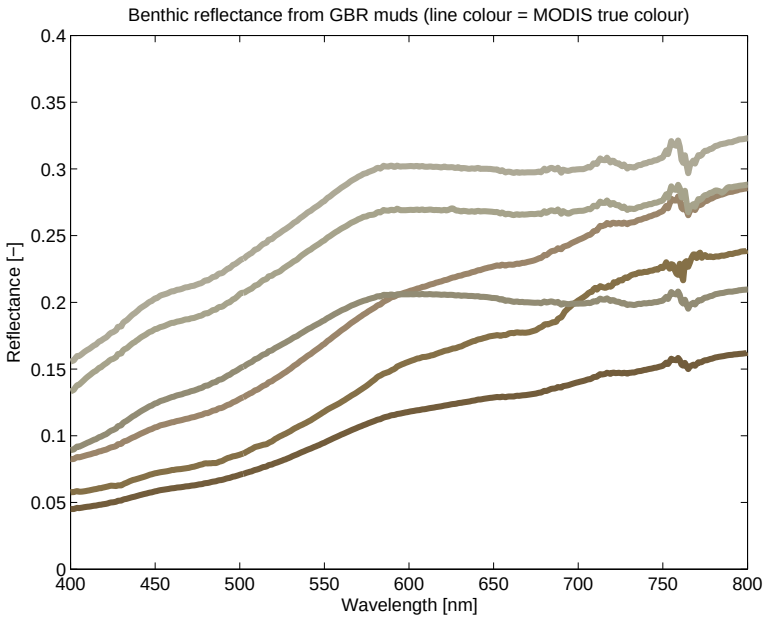

Figure 10: Observed substrate reflectance from 400 to 800 nm from terrestrial muds in the Whitsunday Islands region. The line colour is calculated from the MODIS true colour algorithm (Gumley et al., 2010), giving the colour of the substrate lit by a spectrally-flat light source. Reflectance measured as π [sr sr^{-1}] Lu [W m^{-2} nm^{-1} sr^{-1}] divided by Ed [W m^{-2} nm^{-1}], or percent reflectance.

6 Common water / epibenthic / sediment processes

6.1 Preferential uptake of ammonia

The model contains two forms of dissolved inorganic nitrogen (DIN), dissolved ammonia (NH_4) and dissolved nitrate (NO_3):

$$N = [\mathrm{NH_4}] + [\mathrm{NO_3}] \tag{216}$$

where N is the concentration of DIN, $[\mathrm{NH_4}]$ is the concentration of dissolved ammonia and $[\mathrm{NO_3}]$ is the concentration of nitrate. The rate of uptake of DIN by photosynthetic organisms is assumed to be function of DIN concentration, among other factors. In the model, the ammonia component of the DIN pool is assumed to be taken up first by all primary producers, followed by the nitrate, with the caveat that the uptake of ammonia cannot exceed the diffusion limit for ammonia. The underlying principle of this assumption is that photosynthetic organisms preference is at the upper limit of that which is physically possibly.

As the nitrogen uptake formulation varies for the different autotrophs, the formulation of the preference of ammonia also varies. As the diffusion coefficient of ammonia and nitrate are only 3 % different, the nitrate diffusion coefficient has been used for both.

Thus, for microalgae with internal reserves of nitrogen, the partitioning of nitrogen uptake is given by:

$$\frac{\partial N}{\partial t} = -\psi D_N N(1 - R_N^*)\,(B/m_N) \tag{217}$$

$$\frac{\partial [\mathrm{NH_4}]}{\partial t} = -\min\left(\psi D_N N(1 - R_N^*), \psi D_N [\mathrm{NH_4}]\right)(B/m_N) \tag{218}$$

$$\frac{\partial [\mathrm{NO_3}]}{\partial t} = -\left(\psi D_N N(1 - R_N^*) - \min\left(\psi D_N N(1 - R_N^*), \psi D_N [\mathrm{NH_4}]\right)\right)(B/m_N) \tag{219}$$

Tichodesmium has the same formulation for preferential ammonia uptake for $N > DIN_{crit}$ as non-fixing microalgae. Below the critical DIN concentration, *Trichodesmium* has no ammonia or nitrate uptake, and all nitrogen uptake is through nitrogen fixation (Sec. 3.4.1).

For macroalgae (and similarly for zooxanthellae), which also have diffusion limits to uptake, but are not represented with internal reserves of nitrogen, the terms are:

$$\frac{\partial N}{\partial t} = -\mu_{MA} MA \tag{220}$$

$$\frac{\partial [\mathrm{NH_4}]}{\partial t} = -\min\left[SA_{eff}[\mathrm{NH_4}], \mu_{MA} MA\right] \tag{221}$$

$$\frac{\partial [\mathrm{NO_3}]}{\partial t} = -\left(\mu_{MA} MA - \min\left[SA_{eff}[\mathrm{NH_4}], \mu_{MA} MA\right]\right) \tag{222}$$

In the case of nutrient uptake by seagrass, which has a saturating nitrogen uptake functional form, the terms are:

$$\frac{\partial N_s}{\partial t} = -\mu_{SG} SG \tag{223}$$

$$\frac{\partial [\mathrm{NH_4}]_s}{\partial t} = -\min\left[\mu_{SG} SG, \frac{\mu_{SG}^{max} [\mathrm{NH_4}]_s SG}{K_N + [\mathrm{NH_4}]_s}\right] \tag{224}$$

$$\frac{\partial [\mathrm{NO_3}]_s}{\partial t} = -\left(\mu_{SG} SG - \min\left[\mu_{SG} SG, \frac{\mu_{SG}^{max} [\mathrm{NH_4}]_s SG}{K_N + [\mathrm{NH_4}]_s}\right]\right) \tag{225}$$

where K_N is a function of the ratio of above ground to below ground biomass described above.

One feature worth noting is that the above formulation for preferential ammonia uptake requires no additional parameters, which is different to other classically applied formulations (Fasham et al., 1990) that require a new parameter, potentially for each autotroph. Given that there are at least 6 autotrophs, this simple formulation has an important role in reducing model complexity.

6.2 Temperature dependence of ecological rates

Physiological rate parameters (maximum growth rates, mortality rates, remineralisation rates) have a temperature dependence that is determined from:

$$r_T = r_{Tref} Q_{10}^{(T - T_{ref})/10} \tag{226}$$

where r_T is the physiological rate parameter (e.g. μ, ζ etc.) at temperature T, T_{ref} is the reference temperature (nominally 20°C for GBR), r_T the physiological rate parameter at temperature T_{ref}, Q_{10} is the Q10 temperature coefficient and represents the rate of change of a biological rate as a result of increasing temperature by 10°C.

Note that while physiological rates may be temperature-dependent, the ecological processes they are included in may not. For example, for extremely light-limited growth, all autotrophs capture light at a rate independent of temperature. With the reserves of nutrients replete, the steady-state realised growth rate, μ, becomes the rate of photon capture, k. This can be shown algebracially: $\mu = \mu^{max} R_I^* = k(1 - R^*)$, where R^* is the reserves of energy. Rearranging, $R^* = k/(\mu^{max} + k)$. At $k << \mu^{max}$, $R^* = k/\mu^{max}$, thus $\mu = \mu^{max} k/\mu^{max} = k$. This corresponds with observations of no temperature dependence of photosynthesis at low light levels (Kirk, 1994).

Similar arguments show that extremely nutrient limited autorophs will have the same temperature dependence to that of the diffusion coefficient. Thus, the autotroph growth model has a temperature-dependence that adjust appropriately to the physiological condition of the autotroph, and is a combination of constant, exponential, and polynomial expressions.

Physiological rates in the model that are not temperature dependent are: mass transfer rate constant for particulate grazing by corals, S_{Part}; net coral calcification g; maximum chlorophyll synthesis, k_{Chl}^{max};and rate of translocation between leaves and roots in seagrass, τ_{tran}.

6.3 Detritus remineralisation

The labile detritus has a pool at the Redfield ratio, D_{Red}, and at the Atkinson ratio, D_{Atk}, resulting from dead organic matter at these ratios. The labile detritus from both pools then breaks down into refractory detritus and dissolved organic matter. The refractory detritus and dissolved organic matter pools are quantified by individual elements (C, N, P), in order to account for the mixed source of labile detritus. Finally, a component of the breakdown of each of these pools is returned to dissolved inorganic components. The variables, parameters and equations can be found in Tables 32, 34 & 33 respectively.

6.3.1 Steady-state detritus and organic matter concentrations

The steady-state concentration of labile and refractory detritus and organic matter can be derived from equating derivatives in Tab. 33 to zero and adding net primary production as a source of labile detritus. Considering only carbon and labile detritus at the Redfield ratio, the equations at steady-state become:

$$-r_{Red}D_{Red} + PP = 0 \tag{240}$$

$$\frac{106}{16}\frac{12}{14}\zeta_{Red}r_{Red}D_{Red} - r_R D_C = 0 \tag{241}$$

$$\frac{106}{16}\frac{12}{14}\vartheta_{Red}r_{Red}D_{Red} + \vartheta_{Ref}r_R D_C - r_O O_C = 0 \tag{242}$$

where PP is net primary production in units of mg N m^{-3} d^{-1}. Solving for D_{Red}, D_C and O_C:

$$
\begin{aligned}
D_{Red} &= PP/r_{Red} && (243)\\
D_C &= \frac{106}{16}\frac{12}{14}\zeta_{Red} r_{Red} D_{Red}/r_R = \frac{106}{16}\frac{12}{14}\zeta_{Red} PP/r_R && (244)\\
O_C &= \left(\frac{106}{16}\frac{12}{14}\vartheta_{Red} r_{Red} D_{Red} + \vartheta_{Ref} r_R D_C\right)/r_O && (245)\\
&= \left(\frac{106}{16}\frac{12}{14}\vartheta_{Red} PP + \vartheta_{Ref}\zeta_{Red} PP\right)/r_O && (246)\\
&= \frac{106}{16}\frac{12}{14}\frac{PP}{r_O}\left(\vartheta_{Red} + \vartheta_{Ref}\zeta_{Red}\right) && (247)
\end{aligned}
$$

Thus, the steady state of O_C is proportional to the primary production divided by the breakdown rate of dissolved organic carbon, multiplied by the fractions of D_C, ϑ_{Ref} and D_{Red}, $\vartheta_{Ref}\zeta_{Red}$, that remain organics thought the breakdown process. Using values in Tab. 34, the pelagic-driven component of dissolved organic carbon, O_C, at the reference temperature for a primary production rate of 2 mg N m^{-3} d^{-1} is 767 mg C m^{-3}, which is within the range of 760-960 observed globally for tropical and sub-tropical systems (Hansell et al., 2009).

In order to have an absorption coefficient of DOC matter at 443 nm of 0.1 m^{-1}, requires a DOC-specific absorption coefficient, $k_{DOC,443}$ of 0.1/767 = 0.0013 m^{-2} mg C. Using these steady-state results, and assuming equal breakdown rates of all elements, the initial conditions detrital and dissolved organic C, N and P pools can be calculated (Tab. 35).

Description	Symbol	Units
Maximum rate of nitrification in the water column	$\tau_{nit,wc}$	0.1 d^{-1}
Maximum rate of nitrification in the sediment	$\tau_{nit,sed}$	20 d^{-1}
Oxygen half-saturation constant for nitrification	$K_{O_2,nit}$	500 mg O m^{-3}
Maximum rate of denitrification	τ_{denit}	5 d^{-1}
Oxygen half-saturation constant for de-nitrification	$K_{O_2,denit}$	10000 mg O m^{-3}
Rate of P adsorbed/desorbed equilibrium	τ_{Pabs}	0.04 d^{-1}
Isothermic const. P adsorption for NAP	$k_{Pads,wc}$	300 kg NAP^{-1}
Oxygen half-saturation for P adsorption	$K_{O_2,\text{abs}}$	500 mg O m^{-3}
Rate of P immobilisation	τ_{Pimm}	0.0012 d^{-1}

Table 30: Constants and parameter values used in the sediment inorganic chemistry.

$$\text{Nitrification} : NH_4^+ + 2O_2 \longrightarrow NO_3^- + H_2O + 2H^+ \quad (207)$$

$$\text{De} - \text{nitrification} : NO_3^- + \frac{1}{2}O_2 \longrightarrow \frac{1}{2}N_{2(g)} + 2O_2 \quad (208)$$

$$(209)$$

$$\frac{\partial[NH_4]}{\partial t} = -\tau_{nit,wc}[NH_4]\frac{[O_2]^2}{K_{O_2,nit}^2 + [O_2]^2} \quad (210)$$

$$\frac{\partial[O_2]}{\partial t} = -2\frac{32}{14}\tau_{nit,wc}[NH_4]\frac{[O_2]^2}{K_{O_2,nit}^2 + [O_2]^2} + 2\frac{32}{14}\tau_{denit}[NO_3]\frac{K_{O_2,denit}}{K_{O_2,denit} + [O_2]} \quad (211)$$

$$\frac{\partial[NO_3]}{\partial t} = \tau_{nit,wc}[NH_4]\frac{[O_2]^2}{K_{O_2,nit}^2 + [O_2]^2} - \tau_{denit}[NO_3]\frac{K_{O_2,denit}}{K_{O_2,denit} + [O_2]} \quad (212)$$

$$\frac{\partial P}{\partial t} = \left(\tau_{Pabs}\left(\frac{PIP}{k_{Pads,sed}NAP} - \frac{[O_2]P}{K_{O_2,\text{abs}} + [O_2]}\right)\right)/\phi \quad (213)$$

$$\frac{\partial PIP}{\partial t} = -\tau_{Pabs}\left(\frac{PIP}{k_{Pads,wc}NAP} - \frac{[O_2]P}{K_{O_2,\text{abs}} + [O_2]}\right) - \tau_{Pimm}PIP \quad (214)$$

$$\frac{\partial PIPI}{\partial t} = \tau_{Pimm}PIP \quad (215)$$

Table 31: Equations for the sediment inorganic chemistry.

Variable	Symbol	Units
Ammonia concentration	$[NH_4]$	mg N m^{-3}
Dissolved Inorganic Carbon (DIC)	DIC	mg C m^{-3}
Dissolved Inorganic Phosphorus (DIP)	P	mg P m^{-3}
Dissolved oxygen concentration	$[O_2]$	mg O m^{-3}
Labile detritus at Redfield ratio	D_{Red}	mg N m^{-3}
Labile detritus at Atkinson ratio	D_{Atk}	mg N m^{-3}
Refractory Detritus C	D_C	mg C m^{-3}
Refractory Detritus N	D_N	mg N m^{-3}
Refractory Detritus P	D_P	mg P m^{-3}
Dissolved Organic C	O_C	mg C m^{-3}
Dissolved Organic N	O_N	mg N m^{-3}
Dissolved Organic P	O_P	mg P m^{-3}
Chemical Oxygen Demand (COD)	COD	mg O m^{-3}

Table 32: State and derived variables for the detritus remineralisation model in both the sediment and water column.

$$\frac{\partial D_{Red}}{\partial t} = -r_{Red} D_{Red} \tag{227}$$

$$\frac{\partial D_{Atk}}{\partial t} = -r_{Atk} D_{Atk} \tag{228}$$

$$\frac{\partial D_C}{\partial t} = \frac{106}{16}\frac{12}{14}\zeta_{Red} r_{Red} D_{Red} + \frac{550}{30}\frac{12}{14}\zeta_{Atk} r_{Atk} D_{Atk} - r_R D_C \tag{229}$$

$$\frac{\partial D_N}{\partial t} = \zeta_{Red} r_{Red} D_{Red} + \zeta_{Atk} r_{Atk} D_{Atk} - r_R D_N \tag{230}$$

$$\frac{\partial D_P}{\partial t} = \frac{1}{16}\frac{31}{14}\zeta_{Red} r_{Red} D_{Red} + \frac{1}{30}\frac{31}{14}\zeta_{Atk} r_{Atk} D_{Atk} - r_R D_P \tag{231}$$

$$\frac{\partial O_C}{\partial t} = \frac{106}{16}\frac{12}{14}\vartheta_{Red} r_{Red} D_{Red} + \frac{550}{30}\frac{12}{14}\vartheta_{Atk} r_{Atk} D_{Atk} + \vartheta_{Ref} r_R D_C - r_O O_C \tag{232}$$

$$\frac{\partial O_N}{\partial t} = \vartheta_{Red} r_{Red} D_{Red} + \vartheta_{Atk} r_{Atk} D_{Atk} + \vartheta_{Ref} r_R D_N - r_O O_N \tag{233}$$

$$\frac{\partial O_P}{\partial t} = \frac{1}{16}\frac{31}{14}\vartheta_{Red} r_{Red} D_{Red} + \frac{1}{30}\frac{31}{14}\vartheta_{Atk} r_{Atk} D_{Atk} + \vartheta_{Ref} r_R D_P - r_O O_P \tag{234}$$

$$\frac{\partial [\mathrm{NH_4}]}{\partial t} = r_{Red} D_{Red}(1 - \zeta_{Red} - \vartheta_{Red}) + r_{Atk} D_{Atk}(1 - \zeta_{Atk} - \vartheta_{Atk}) + r_R D_N (1 - \vartheta_{Ref}) + r_O O_N \tag{235}$$

$$\frac{\partial DIC}{\partial t} = \frac{106}{16}\frac{12}{14} r_{Red} D_{Red}(1 - \zeta_{Red} - \vartheta_{Red}) + \frac{550}{30}\frac{12}{14} r_{Atk} D_{Atk}(1 - \zeta_{Atk} - \vartheta_{Atk}) + r_R D_C (1 - \vartheta_{Ref}) + r_O O_C \tag{236}$$

$$\frac{\partial P}{\partial t} = \frac{1}{16}\frac{31}{14} r_{Red} D_{Red}(1 - \zeta_{Red} - \vartheta_{Red}) + \frac{1}{30}\frac{31}{14} r_{Atk} D_{Atk}(1 - \zeta_{Atk} - \vartheta_{Atk}) + r_R D_P (1 - \vartheta_{Ref}) + r_O O_P \tag{237}$$

$$\frac{\partial [\mathrm{O_2}]}{\partial t} = -\frac{138}{106}\frac{32}{12}\frac{\partial DIC}{\partial t}\frac{[\mathrm{O_2}]^2}{K_{OA}^2 + [\mathrm{O_2}]^2} \tag{238}$$

$$\frac{\partial [COD]}{\partial t} = \frac{138}{106}\frac{32}{12}\frac{\partial DIC}{\partial t}\left(1 - \frac{[\mathrm{O_2}]^2}{K_{OA}^2 + [\mathrm{O_2}]^2}\right) \tag{239}$$

Table 33: Equations for detritus remineralisation in the water column and sediment.

Description	Symbol	Red	Atk	Refractory	Dissolved
Detritus breakdown rate (d^{-1})	$r_{Red,Atk,R,O}$	0.04	0.01	0.0036	0.00176
Fraction of detritus to refractory	$\zeta_{Red,Atk}$	0.19	0.19	-	-
Fraction of detritus to DOM	$\vartheta_{Red,Atk,Ref}$	0.1	0.1	0.05	

Table 34: Constants and parameter values used in the water column detritus remineralisation model. Red = Redfield ratio (C:N:P = 106:16:1); Atk = Atkinson ratio (C:N:P = 550:30:1); Ref = Refractory

	Labile Det., D_{Red}	Refractory Det., D	Dissolved Organic, O
Redfield	25	-	-
Carbon	-	27	767
Nitrogen	-	4.75	135
Phosphorus	-	0.66	18.7

Table 35: Steady-state detrital and dissolved organic C, N and P concentrations for primary production equal to 2 mg N m^{-1}

6.3.2 Anaerobic and anoxic respiration

The processes of remineralisation, phytoplankton mortality and zooplankton grazing return carbon dioxide to the water column. In oxic conditions, these processes consume oxygen in a ratio of $DIC : \frac{138}{106}\frac{32}{12}[O_2]$. At low oxygen concentrations, the oxygen consumed is reduced:

$$\frac{\partial [O_2]}{\partial t} = -\frac{\partial DIC}{\partial t}\frac{138}{106}\frac{32}{12}\frac{[O_2]^2}{K_{OA}^2 + [O_2]^2} \tag{248}$$

where $K_{OA} = 256$ mg O m^{-3} is the half-saturation constant for anoxic respiration (Boudreau, 1996). A sigmoid saturation term is used because it is more numerically stable as the oxygen concentration approaches 0. The anoxic component of remineralisation results in an increased chemical oxygen demand (COD):

$$\frac{\partial COD}{\partial t} = \frac{\partial DIC}{\partial t}\frac{138}{106}\frac{32}{12}\left(1 - \frac{[O_2]^2}{K_{OA}^2 + [O_2]^2}\right) \tag{249}$$

COD is a dissolved tracer, with the same units as oxygen.

When oxygen and COD co-exist they react to reduce both, following:

$$\frac{\partial [O_2]}{\partial t} = -\tau_{COD} COD \frac{[O_2]}{8000} \tag{250}$$

$$\frac{\partial COD}{\partial t} = -\tau_{COD} COD \frac{[O_2]}{8000} \tag{251}$$

where 8000 mg O m^{-3} is approximately the saturation concentration of oxygen in seawater, and τ_{COD} is the timescale of this reduction, and is set to 1 hr^{-1}.

7 Numerical integration

7.1 Splitting of physical and ecological integrations

The numerical solution of the time-dependent advection-diffusion-reaction equations for each of the ecological tracers is implemented through sequential solving of the partial differential equations (PDEs) for advection and diffusion, and the ordinary differential equations for reactions. This technique, called operator splitting, is common in geophysical science (Hundsdorfer and Verwer, 2003).

The time-step of the splitting is typically 15 min - 1 hour (Table 36). Under the sequential operator splitting technique used, first the advection-diffusion processes are solve for the period of the time-step. The value of the tracers at the end of this PDE integration, and the initial time, are then used as initial conditions for the ODE integration. After the ODE integration has run for same time period, the value of the tracers is update, and time is considered to have moved forward just one time-step. The integration continues to operate sequentially for the whole model simulation.

The PDE solutions are described in the physical model description available at:

`www.emg.cmar.csiro.au/www/en/emg/software/EMS/hydrodynamics.html` .

7.2 Diffusive exchange of dissolved tracers across sediment-water interface

Due to the thin surface sediment layer, and the potentially large epibenthic drawndown of porewater dissolved tracers, the exchange of dissolved tracers between the bottom water column layer and the top sediment layer is solved in the same numerical operation as the ecological tracers (other transport processes occurring between ecological timesteps). The flux, J, is given by:

$$J = k(C_s - C) \tag{252}$$

where C and C_s are the concentration in water column and sediment respectively, $k = 4.6 \times 10^{-7}$ m s^{-1} is the transfer coefficient. In the model parameterisation, $k = D/h$ where $D = 3 \times 10^{-9}$ m^2

s^{-1} is the diffusion coefficient and $h = 0.0065$ mm is the thickness of the diffusive layer.

While in reality k would vary with water column and sediment hydrodynamics as influenced by community type etc, these complexities has not been considered. In addition to the diffusive flux between the sediment and water column, particulate deposition entrains water column water into the sediments, and particulate resuspension releases porewaters into the water column.

7.3 Optical integration

The inherent and apparent optical properties are calculated between the physical and ecological integrations, at approximately 15 minute intervals. The spectral resolution of 25 wavebands has been chosen to resolve the absorption peaks associated with Chl *a*, and to span the optical wavelengths. As IOPs can be calculated at any wavelength given the model state, IOPs and AOPs at observed wavelengths are recalculated after the integration.

Additionally, the wavelengths integrated have been chosen such that the lower end of one waveband and the top end of another fall on 400 and 700 nm respectively, allowing precise calculation of photosynthetically available radiation (PAR).

7.4 Adaptive solution of ecological processes

A 5th-order Dormand-Prince ordinary differential equation integrator (Dormand. and Prince, 1980) with adaptive step control is used to integrate the local rates of changes due to ecological processes. This requires 7 function evaluations for the first step and 6 for each step after. A tolerance of 1×10^{-5} mg N m^{-3} is required for the integration step to be accepted.

For an n_{wc}-layer water column and n_{sed}-layer sediment, the integrator sequentially solves the top $n_{wc}-1$ water column layers; the nth water column layer, epibenthic and top sediment layer together; and then the $n_{sed}+1$ to bottom sediment layers.

7.5 Additional integration details

7.5.1 Mass conservation in water column and sediment porewaters

The model checks the conservation of Total C, TC, Total N, TN, Total P, TP, and oxygen, $[O_2]$, within each grid cell at each time step using the following conservation laws. To establish mass

conservation, the sum of the change in mass (of N, P, C and O) with time and the mass of sinks / sources (such as sea-air fluxes, denitrification) must equate to zero.

The total mass and conservation equations are same for the water column and porewaters, with the caveats that (1) air-sea fluxes only affect surface layers of the water, (2) denitrification only occurs in the sediment, and (3) the porosity, ϕ, of the water column is 1. In the sediment, the concentration of particulates is given in per unit volume of space, while the concentration of dissolved tracers is given in per unit volume of porewater. The concentration of dissolved tracer, X, per unit space is given by ϕX.

Thus the total carbon in a unit volume of space, and its conservation, are given by:

$$TC = \phi\left(DIC + O_C\right) + \left(\frac{550}{30}\frac{12}{14}D_{Atk} + D_C + \frac{106}{16}\frac{12}{14}\left(D_{red} + \sum B(1+R_I^*) + \sum Z\right)\right) \tag{253}$$

$$\frac{\partial TC}{\partial t} + \underbrace{k_{\mathrm{CO_2}}\left(\left[\mathrm{CO_2}\right] - \left[\mathrm{CO_2}\right]_{atm}\right)/h}_{\text{sea}-\text{air flux}} = 0 \tag{254}$$

The total nitrogen in a unit volume of space, and its conservation, are given by:

$$TN = \phi\left(\left[\mathrm{NO_3}\right] + \left[\mathrm{NH_4}\right] + O_N\right) + \left(D_{Atk} + D_{red} + D_N + \sum B(1+R_N^*) + \sum Z\right) \tag{255}$$

$$\frac{\partial TN}{\partial t} + \left(\text{denitrification} - \text{nitrogen fixation}\right)/\phi - \text{dust input}/h = 0 \tag{256}$$

The total phosphorus in a unit volume of space, and its conservation, are given by:

$$TP = \phi\left(DIP + O_P\right) + PIP + PIPI + \frac{1}{30}\frac{31}{14}D_{Atk} + D_P + \frac{1}{16}\frac{31}{14}\left(D_{red} + \sum B(1+R_P^*) + \sum Z\right) \tag{257}$$

$$\frac{\partial TP}{\partial t} - \text{dust input}/h = 0 \tag{258}$$

The concept of oxygen conservation in the model is more subtle than that of C, N and P due to the mass of oxygen in the water molecules themselves not being considered. When photosynthesis occurs, C is transferred from the dissolved phase to reserves within the cell. With both dissolved and particulate pools considered, mass conservation of C is straightforward. In contrast, when photosynthesis occurs, oxygen is drawn from the water molecules (i.e. H_2O), whose mass is not being considered, and released into the water column. Conversely, when organic matter is broken down oxygen is consumed from the water column and released as H_2O.

In order to obtain a mass conservation check of oxygen, the concept of Biological Oxygen Demand (BOD) is used. Often BOD represents the biological demand for oxygen in say a 5 day incubation,

BOD_5. Here, for the purposes of mass conservation checks, we use BOD_∞, the oxygen demand over an infinite time for breakdown. This represents the total oxygen removed from the water molecules for organic matter creation.

Anaerobic respiration reduces BOD_∞ without reducing O_2, but instead creating reduced-oxygen species. This is accounted for in the oxygen balance by the prognostic tracer Chemical Oxygen Demand (COD). In some other studies this is represented by a negative oxygen concentration.

Thus at any time point the biogeochemical model will conserve the oxygen concentration minus BOD_∞ minus COD, plus or minus any sources and sinks such as sea-air fluxes. The total oxygen minus BOD_∞ minus COD in a unit volume of water, and its conservation, is given by:

$$[\mathrm{O_2}] - BOD_\infty - COD =$$
$$\phi\left([\mathrm{O_2}] - COD + \frac{32}{12}O_C\right) - \left(\frac{716}{30}\frac{32}{14}D_{Atk} + \frac{32}{12}D_C + \frac{138}{16}\frac{32}{14}\left(D_{red} + \sum B_N(1+R_I^*)\right)\right) \quad (259)$$

$$\frac{\partial([\mathrm{O_2}] - BOD_\infty - COD)}{\partial t} + \mathcal{R} - \overbrace{\frac{k_{\mathrm{O_2}}\left([\mathrm{O_2}]_{sat} - [\mathrm{O_2}]\right)}{h}}^{sea-air\ flux} \underbrace{-2\frac{138}{16}\frac{32}{14}\tau_{nit,wc}[\mathrm{NH_4}]\frac{[\mathrm{O_2}]}{K_{nit,\mathrm{O}} + [\mathrm{O_2}]}}_{nitrification} = 0 \quad (260)$$

where $\mathcal{R}$ is respiration of organic matter.

7.5.2 Mass conservation in the epibenthic

Mass conservation in the epibenthos requires consideration of fluxes between the water column, porewaters and the epibenthic organisms (macroalgae, seagrass and coral hosts and symbionts).

The total carbon in the epibenthos, and its conservation, is given by:

$$TC = \frac{550}{30}\frac{12}{14}\left(MA + SG_A + SG_B\right) + \frac{106}{16}\frac{12}{14}\left(CS + CH\right) \quad (261)$$

$$\left.\frac{\partial TC}{\partial t}\right|_{epi} + h_{wc}\left.\frac{\partial TC}{\partial t}\right|_{wc} + h_{sed}\left.\frac{\partial TC}{\partial t}\right|_{sed} + \underbrace{12\left(gA_{eff} - d_{sand}\right)}_{coral\ calcification\ -\ dissolution} = 0 \quad (262)$$

where h_{wc} and h_{sed} are the thickness of the bottom water column and top sediment layers, $12g$ is the rate coral calcification per unit area of coral, A_{eff} is the area of the bottom covered by coral per m^{-2}, and the diffusion terms between porewaters and the water column cancel, so do not appear in the equations. Note the units of mass of CS needs to be in g N, and some configurations may have multiple seagrass and macroalgae species.

Similarly for nitrogen, phosphorus and oxygen in the epibenthos:

$$TN = MA + SG_A + SG_B + CS + CH \tag{263}$$

$$\left.\frac{\partial TN}{\partial t}\right|_{epi} + h_{wc}\left.\frac{\partial TN}{\partial t}\right|_{wc} + h_{sed}\left.\frac{\partial TN}{\partial t}\right|_{sed} = 0 \tag{264}$$

$$TP = \frac{1}{30}\frac{31}{14}\left(MA + SG_A + SG_B\right) + \frac{1}{16}\frac{31}{14}\left(CS + CH\right) \tag{265}$$

$$\left.\frac{\partial TP}{\partial t}\right|_{epi} + h_{wc}\left.\frac{\partial TP}{\partial t}\right|_{wc} + h_{sed}\left.\frac{\partial TP}{\partial t}\right|_{sed} = 0 \tag{266}$$

$$BOD_\infty = \frac{716}{30}\frac{32}{14}\left(MA + SG_A + SG_B\right) + \frac{138}{16}\frac{32}{14}\left(CS + CH\right) \tag{267}$$

$$-\left.\frac{\partial BOD_\infty}{\partial t}\right|_{epi} + h_{wc}\left.\frac{\partial([\mathrm{O}_2] - BOD_\infty)}{\partial t}\right|_{wc} + h_{sed}\left.\frac{\partial([\mathrm{O}_2] - BOD_\infty)}{\partial t}\right|_{sed} = 0 \tag{268}$$

where there is no dissolved oxygen in the epibenthos.

7.5.3 Wetting and drying

There is no wetting and drying in the large scale GBR models, but, depending on tides and bathymetry, there may be in the relocatable model.

7.5.4 Unconditional stability

In addition to the above standard numerical techniques, a number of innovations are used to ensure model solutions are reached. Should an integration step fail in a grid cell, no increment of the state variables occurs, and the model is allowed moves the next vertical column, with a warning flag registered (as `Ecology Error`). Generally the problem does not reoccur due to the transport of tracers alleviating the stiff point in phase space of the model.

8 Peer-review publications

The following list includes peer-reviewed papers using the biogeochemical and / or optical models of the EMS package.

Baird, M. E., Walker, S. J., Wallace, B. B., Webster, I. T., Parslow, J. S., 2003. The use of mechanistic descriptions of algal growth and zooplankton grazing in an estuarine eutrophication model. Est., Coastal and Shelf Sci. 56, 685–695.

Baird, M. E., Ralph, P. J., Rizwi, F., Wild-Allen, K. A., Steven, A. D. L., 2013. A dynamic model of the cellular carbon to chlorophyll ratio applied to a batch culture and a continental shelf ecosystem. Limnol. Oceanogr. 58, 1215–1226.

Baird, M. E., M. P. Adams, R. C. Babcock, K. Oubelkheir, M. Mongin, K. A. Wild-Allen, J. Skerratt, B. J. Robson, K. Petrou, P. J. Ralph, K. R. O'Brien, A. B. Carter, J. C. Jarvis, M. A. Rasheed (2016) A biophysical representation of seagrass growth for application in a complex shallow-water biogeochemical model. Ecol. Mod. 325, 13–27.

Baird, M. E., Cherukuru, N., Jones, E., Margvelashvili, N., Mongin, M., Oubelkheir, K., Ralph, P. J., Rizwi, F., Robson, B. J., Schroeder, T., Skerratt, J., Steven A. D. L., Wild-Allen, K. A. (2016). Remote-sensing reflectance and true colour produced by a coupled hydrodynamic, optical, sediment, biogeochemical model of the Great Barrier Reef, Australia: comparison with satellite data. Env. Model. Software. 78, 79–96.

Condie, S. A., Herzfeld, M., Margvelashvili, N., Andrewartha, J. R., 2009. Modeling the physical and biogeochemical response of a marine shelf system to a tropical cyclone. Geophys. Res. Lett. 36 (L22603).

Hadley, S., Wild-Allen, K. A., Johnson, C., Macleod, C., 2015. Modeling macroalgae growth and nutrient dynamics for integrated multi-trophic aquaculture. J. Appl. Phycol. 27, 901–916.

Hadley, S., Wild-Allen, K. A., Johnson, C., Macleod, C., 2015 online. Quantification of the impacts of finfish aquaculture and bioremediation capacity of integrated multi-trophic aquaculture using a 3D estuary model. J. Appl. Phycol. 28, 1875.

Jones, E. M., Baird, M. E., Mongin, M., Parslow, J., Skerratt, J., Lovell, J,. Margvelashvili, N., Matear, R. J., Wild-Allen, K., Robson, B., Rizwi, F., Oke, P., King, E., Schroeder, T., Steven, A., Taylor, J., 2016. Use of remote-sensing reflectance to constrain a data assimilating marine biogeochemical model of the Great Barrier Reef Biogeosciences 13, 6441–6469.

Margvelashvili, N., 2009. Stretched Eulerian coordinate model of coastal sediment transport. Computer Geosciences 35, 1167–1176.

Mongin, M., Baird, M. E., 2014. The interacting effects of photosynthesis, calcification and water circulation on carbon chemistry variability on a coral reef flat: a modelling study. Ecol. Mod. 284, 19–34.

Mongin, M., M. E. Baird, B. Tilbrook, R. J. Matear, A. Lenton, M. Herzfeld, K. A. Wild-Allen, J. Skerratt, N. Margvelashvili, B. J. Robson, C. M. Duarte, M. S. M. Gustafsson, P. J. Ralph, A. D. L. Steven (2016). The exposure of the Great Barrier Reef to ocean acidification. Nature Communications 7, 10732.

Robson, B. J., Baird, M., & Wild-Allen, K. (2013). A physiological model for the marine cyanobacteria, *Trichodesmium*. In MODSIM2013, 20th International Congress on Modelling and Simulation. Modelling and Simulation Society of Australia and New Zealand, ISBN (pp. 978-0).

Skerratt, J., Wild-Allen, K. A., Rizwi, F., Whitehead, J., Coughanowr, C., 2013. Use of a high resolution 3D fully coupled hydrodynamic, sediment and biogeochemical model to understand estuarine nutrient dynamics under various water quality scenarios. Ocean Coast. Man. 83, 52–66.

Wild-Allen, K., Herzfeld, M., Thompson, P. A., Rosebrock, U., Parslow, J., Volkman, J. K., 2010. Applied coastal biogeochemical modelling to quantify the environmental impact of fish farm nutrients and inform managers. J. Mar. Sys. 81, 134–147.

Wild-Allen, K., Skerratt, J., Whitehead, J., Rizwi, F., Parslow, J., 2013. Mechanisms driving estuarine water quality: a 3D biogeochemical model for informed management. Est. Coast. Shelf Sci. 135, 33–45.

Wild-Allen, K. and Andrewartha, J., in press. Connectivity between estuaries influences nutrient transport, cycling and water quality Mar. Chem.

Box 1. Comments on the model approach.

Throw up a handful of feathers, and all must fall to the ground according to definite laws; but how simple is this problem compared to the action and reaction of the innumerable plants and animals which have determined, in the course of centuries, the proportional numbers and kinds.

Charles Darwin, The Origin of Species (1859)

Darwin's thoughts while pondering the predictability of river bank flora and fauna says much to our problem. Firstly, we might expect to do a good job representing the sinking of a handful of different types of plankton! In fact, if an ecological process has a physical limit with a geometric origin that we can parameterise, we might expect to well represent the process. Physical limits that are used in the model include the diffusion of nutrients to the surface of microalgae and macroalgae, the capture of light by microalgae and macrophytes, and the encounter of plankton predators and prey.

Further, it seems reasonable to propose that at the bottom of the food chain, physical limits may be common. Natural selection will refine physiological processes, and even adapt organism anatomy to shapes with favourable physical limits. But paradoxically, the more refined the physiological processes, the more the organism is constrained by the physical limit.

Our greatest uncertainty lies in the physiological limits. Given this uncertainty, keeping the parameterisation of physiological processes simple is an advantage. Thus, physiological limits in the model are often parameterised with just one or two parameters for each organism, typically the maximum growth rate and the mortality / respiration rate. The maximum growth rate captures the organism's growth when all physical limits are faster than the organism's physiology requires. The model has ∼70 parameters that represent physiological and / or chemical processes and ∼30 that represent geometric properties. The model has about ∼60 state variables. Thus for such a complex model, it is relatively well constrained.

Finally, though every effort may be made to constrain the model, there is a time-limit to prediction of model state due to action and reaction (i.e. deterministic, non-linear interactions), that cannot be overcome through refinement of initial conditions and / or perfect model parameterisations (Baird and Suthers, 2010). But like weather and climate modelling, while the instantaneous state may be predictable for a finite time interval, statistical properties such as the mean and variability of model variables can be predictable over longer periods. Thus, Darwin saw past the problem of instantaneous state prediction of river bank ecology to see that the outcome of such actions and reactions could, over time, explain the origin of species ...

9 Acknowledgments

What models can do is make the most of existing scientific knowledge, a major undertaking by any standards.

A Reef in Time: The Great Barrier Reef from Beginning to End (Veron, 2008)

Many scientists and projects have contributed resources and knowhow to the development of this model over 15+ years. For this dedication we are very grateful.

Those who have contributed to the numerical code include (CSIRO unless stated):

Mike Herzfeld, Philip Gillibrand, John Andrewartha, Farhan Rizwi, Jenny Skerratt, Mathieu Mongin, Mark Baird, Karen Wild-Allen, John Parlsow, Emlyn Jones, Nugzar Margvelashvili, Pavel Sakov, Jason Waring, Stephen Walker, Uwe Rosebrock, Brett Wallace, Ian Webster, Barbara Robson, Scott Hadley (University of Tasmania), Malin Gustafsson (University of Technology Sydney, UTS), Matthew Adams (University of Queensland, UQ).

Collaborating scientists include:

Bronte Tilbrook, Andy Steven, Thomas Schroeder, Nagur Cherukuru, Peter Ralph (UTS), Russ Babcock, Kadija Oubelkheir, Bojana Manojlovic (UTS), Stephen Woodcock (UTS), Stuart Phinn (UQ), Chris Roelfsema (UQ), Miles Furnas (AIMS), David McKinnon (AIMS), David Blondeau-Patissier (Charles Darwin University), Michelle Devlin (James Cook University), Eduardo da Silva (JCU), Julie Duchalais, Jerome Brebion, Leonie Geoffroy, Yair Suari, Cloe Viavant.

Funding bodies: CSIRO Wealth from Oceans Flagship, Gas Industry Social & Environmental Research Alliance (GISERA), CSIRO Coastal Carbon Cluster, Derwent Estuary Program, INFORM2, eReefs, Great Barrier Reef Foundation, Australian Climate Change Science Program, University of Technology Sydney.

Description	Values
Timestep of hydrodynamic model	90 s (GBR4), 20 s (GBR1)
[a]Timestep of ODE ecological model	3600 s (GBR4), 1800 s (GBR1)
Timestep of optical and carbon chemistry models	3600 s
Optical model resolution in PAR	$\sim$ 20 nm
ODE integrator	5th order Dormand-Prince
ODE tolerance	10^{-5} mg N m^{-3}
Maximum number of ODE steps in ecology	2000
Maximum number of iterations in carbon chemistry	100
Accuracy of carbon chemistry calculations	$[H^+] = 10^{-12}$ mol

Table 36: Integration details. Optical wavelengths (nm): 290 310 330 350 370 390 410 430 440 450 470 490 510 530 550 570 590 610 630 650 670 690 710 800.[a]Since the integrator is 5th order, the ecological derivatives are evaluated at least every approximately 3600/5 = 900 s, and more regularly for stiff equations.

References

Alvarez-Romero, J. G., Devlin, M., da Silva, E. T., Petus, C., Ban, N. C., Pressey, R. L., Kool, J., Roberts, J. J., Cerdeira-Estrada, S., Wenger, A. S., Brodie, J., 2013. A novel approach to model exposure of coastal-marine ecosystems to riverine flood plumes based on remote sensing techniques. J. Enviro. Manage. 119, 194–207.

Anthony, K. R. N., Diaz-Pulido, G., Verlinden, N., Tilbrook, B., Andersson, A. J., 2013. Benthic buffers and boosters of ocean acidification on coral reefs. Biogeosciences 10, 4897–4909.

Anthony, K. R. N., Kleypas, J. A., Gattuso, J.-P., 2011. Coral reefs modify their seawater carbon chemistry - implications for impacts of ocean acidification. Glob. Change. Biol. 17, 3655–3666.

Atkinson, M. J., 1992. Productivity of Eniwetak atoll reef predicted from mass-transfer relationships. Cont. Shelf Res. 12, 799–807.

Atkinson, M. J., Bilger, B. W., 1992. Effects of water velocity on phosphate uptake in coral reef-flat communities. Limnol. Oceanogr. 37, 273–279.

Atkinson, M. J., Smith, S. V., 1983. C:N:P ratios of benthic marine plants. Limnol. Oceanogr. 28, 568–574.

Baird, M. E., 2003. Numerical approximations of the mean absorption cross-section of a variety of randomly oriented microalgal shapes. J. Math. Biol. 47, 325–336.

Baird, M. E., Emsley, S. M., 1999. Towards a mechanistic model of plankton population dynamics. J. Plankton Res. 21, 85–126.

Baird, M. E., Emsley, S. M., McGlade, J. M., 2001. Modelling the interacting effects of nutrient uptake, light capture and temperature on phytoplankton growth. J. Plankton Res. 23, 829–840.

Baird, M. E., Middleton, J. H., 2004. On relating physical limits to the carbon: nitrogen ratio of unicellular algae and benthic plants. J. Mar. Sys. 49, 169–175.

Baird, M. E., Oke, P. R., Suthers, I. M., Middleton, J. H., 2004a. A plankton population model with bio-mechanical descriptions of biological processes in an idealised 2-D ocean basin. J. Mar. Sys. 50, 199–222.

Baird, M. E., Ralph, P. J., Rizwi, F., Wild-Allen, K. A., Steven, A. D. L., 2013. A dynamic model of the cellular carbon to chlorophyll ratio applied to a batch culture and a continental shelf ecosystem. Limnol. Oceanogr. 58, 1215–1226.

Baird, M. E., Roughan, M., Brander, R. W., Middleton, J. H., Nippard, G. J., 2004b. Mass transfer limited nitrate uptake on a coral reef flat, Warraber Island, Torres Strait, Australia. Coral Reefs 23, 386–396.

Baird, M. E., Suthers, I. M., 2010. Increasing model structural complexity inhibits the growth of initial condition errors. Ecol. Comp. 7, 478486.

Baird, M. E., Timko, P. G., Suthers, I. M., Middleton, J. H., 2006. Coupled physical-biological modelling study of the East Australian Current with idealised wind forcing. Part I: Biological model intercomparison. J. Mar. Sys. 59, 249–270.

Baird, M. E., Timko, P. G., Wu, L., 2007. The effect of packaging of chlorophyll within phytoplankton and light scattering in a coupled physical-biological ocean model. Mar. Fresh. Res. 58, 966–981.

Baird, M. E., Walker, S. J., Wallace, B. B., Webster, I. T., Parslow, J. S., 2003. The use of mechanistic descriptions of algal growth and zooplankton grazing in an estuarine eutrophication model. Est., Coastal and Shelf Sci. 56, 685–695.

Blondeau-Patissier, D., Brando, V. E., Oubelkheir, K., Dekker, A. G., Clementson, L. A., Daniel, P., 2009. Bio-optical variability of the absorption and scattering properties of the Queensland inshore and reef waters, Australia. J. Geophys. Res. (Oceans) 114, C05003.

Bohren, C. F., Huffman, D. R., 1983. Absorption and scattering of light particles by small particles. John Wiley & Sons.

Boudreau, B. P., 1996. A method-of-lines code for carbon and nutrient diagenesis in aquatic sediments. Comp. Geosci. 22, 479–496.

Brando, V. E., Dekker, A. G., Park, Y. J., Schroeder, T., 2012. Adaptive semianalytical inversion of ocean color radiometry in optically complex waters. Applied Optics 51, 2808–2833.

Cambridge, M. L., Lambers, H., 1998. Specific leaf area and functional leaf anatomy in Western Australian seagrasses. In: Lambers, H., Poorter, H., Vuren, M. M. I. V. (Eds.), Inherent variations in plant growth: physiological mechanisms and ecological consequences. Backhuys, Leiden, pp. 88–99.

Chartrand, K. M., Ralph, P. J., Petrou, K., Rasheed, M. A., 2012. Development of a Light-Based Seagrass Management Approach for the Gladstone Western Basin Dredging Program. Tech. rep., DAFF Publication. Fisheries Queensland, Cairns 126 pp.

Condie, S. A., Herzfeld, M., Margvelashvili, N., Andrewartha, J. R., 2009. Modeling the physical and biogeochemical response of a marine shelf system to a tropical cyclone. Geophys. Res. Lett. 36 (L22603).

Cyronak, T., Santos, I. R., McMahon, A., Eyre, B. D., 2013. Carbon cycling hysteresis in permeable carbonate sands over a diel cycle: Implications for ocean acidification. Limnol. Oceanogr. 58, 131–143.

Dekker, A. G., Phinn, S. R., Anstee, J., Bissett, P., Brando, V. E., Casey, B., Fearns, P., Hedley, J., Klonowski, W., Lee, Z. P., Lynch, M., Lyons, M., Mobley, C., Roelfsema, C., 2011. Intercomparison of shallow water bathymetry, hydro-optics, and benthos mapping techniques in Australian and Caribbean coastal environments. Limnol. Oceanogr.: Methods 9, 396–425.

Devlin, M., da Silva, E., Petus, C., Wenger, A., Zeh, D., Tracey, D., Alvarez-Romero, J., Brodie, J., 2013. Combining in-situ water quality and remotely sensed data across spatial and temporal scales to measure variability in wet season chlorophyll-a: Great Barrier Reef lagoon (Queensland, Australia). Ecological Processes 2, 31.

Dormand., J. R., Prince, P. J., 1980. A family of embedded Runge-Kutta formulae. J. Comp. App. Math. 6, 19–26.

Duarte, C. M., Chiscano, C. L., 1999. Seagrass biomass and production: a reassessment. Aquat. Bot. 65, 159–174.

Duysens, L. N. M., 1956. The flattening of the absorption spectra of suspensions as compared to that of solutions. Biochim. Biophys. Acta 19, 1–12.

Everett, J. D., Baird, M. E., Suthers, I. M., 2007. Nutrient and plankton dynamics in an intermittently closed/open lagoon, Smiths Lake, south-eastern Australia: An ecological model. Est. Coast. Shelf Sci. 72, 690–702.

Falter, J. L., Atkinson, M. J., Merrifield, M. A., 2004. Mass-transfer limitation of nutrient uptake by a wave-dominated reef flat community. Limnol. Oceanogr. 49, 1820–1831.

Fasham, M. J. R., Ducklow, H. W., McKelvie, S. M., 1990. A nitrogen-based model of plankton dynamics in the oceanic mixed layer. J. Mar. Res. 48, 591–639.

Ficek, D., Kaczmarek, S., Stoń-Egiert, J., Woźniak, B., Majchrowski, R., Dera, J., 2004. Spectra of light absorption by phytoplankton pigments in the Baltic; conclusions to be drawn from a Gaussian analysis of empirical data. Oceanologia 46, 533–555.

Finkel, Z. V., 2001. Light absorption and size scaling of light-limited metabolism in marine diatoms. Limnol. Oceanogr. 46, 86–94.

Gentleman, W., 2002. A chronology of plankton dynamics *in silico*: how computer models have been used to study marine ecosystems. Hydrobiologica 480, 69–85.

Gillibrand, P. A., Herzfeld, M., 2016. A mass-conserving advection scheme for offline simulation of tracer transport in coastal ocean models. Env. Model. Soft. 101, 1–16.

Gras, A. F., Koch, M. S., Madden, C. J., 2003. Phosphorus uptake kinetics of a dominant tropical seagrass *Thalassia testudinum* . Aqu. Bot. 76, 299–315.

Griffies, S. M., Harrison, M. J., Pacanowski, R. C., Rosati, A., March 2004. A technical guide to MOM4 GFDL Ocean Group Technical Report No. 5 Version prepared on March 3, 2004. Tech. rep., NOAA/Geophysical Fluid Dynamics Laboratory.

Gumley, L., Descloitres, J., Shmaltz, J., 2010. Creating reprojected true color modis images: A tutorial, tech. rep 1.0.2, 17 pp. Tech. rep., Univ. of Wisconsin, Madison.

Gustafsson, M. S. M., Baird, M. E., Ralph, P. J., 2013. The interchangeability of autotrophic and heterotrophic nitrogen sources in scleractinian coral symbiotic relationships: a numerical study. Ecol. Model. 250, 183–194.

Gustafsson, M. S. M., Baird, M. E., Ralph, P. J., 2014. Modelling photoinhibition and bleaching in Scleractinian coral as a function of light, temperature and heterotrophy. Limnol. Oceanogr. 59, 603–622.

Hadley, S., Wild-Allen, K. A., Johnson, C., Macleod, C., 2015a. Modeling macroalgae growth and nutrient dynamics for integrated multi-trophic aquaculture. J. Appl. Phycol. 27, 901–916.

Hadley, S., Wild-Allen, K. A., Johnson, C., Macleod, C., 2015b. Quantification of the impacts of finfish aquaculture and bioremediation capacity of integrated multi-trophic aquaculture using a 3D estuary model. J. Appl. Phycol. 10.1007/s10811-015-0714-2.

Hansell, D. A., Carlson, C. A., Repeta, D. J., Schlitzer, R., 2009. Dissolved organic matter in the ocean. Oceanography 22, 202–211.

Hansen, J. W., Udy, J. W., Perry, C. J., Dennison, W. C., Lomstein, B. A., 2000. Effect of the seagrass *Zostera capricorni* on sediment microbial processes. Mar. Ecol. Prog. Ser. 199, 83–96.

Hansen, P. J., Bjornsen, P. K., Hansen, B. W., 1997. Zooplankton grazing and growth: Scaling within the 2-2,000 μm body size range. Limnol. Oceanogr. 42, 687–704.

Hermand, J.-P., Nascetti, P., Cinelli, F., 1998. Inversion of acoustic waveguide propagation features to measure oxygen synthesis by *Posidonia oceanica*. In: OCEANS '98 Conference Proceedings. Vol. 2. pp. 919–926.

Herzfeld, M., 2006. An alternative coordinate system for solving finite difference ocean models. Ocean Modelling 14 (34), 174 – 196.

Hill, R., Whittingham, C. P., 1955. Photosynthesis. Methuen, London.

Hundsdorfer, W., Verwer, J. G., 2003. Numerical solutions of time-dependent advection-diffusion-reaction equations. Springer.

Hurd, C. L., 2000. Water motion, marine macroalgal physiology, and production. J. Phycol. 36, 453–472.

Jackson, G. A., 1995. Coagulation of marine algae. In: Huang, C. P., O'Melia, C. R., Morgan, J. J. (Eds.), Aquatic Chemistry: Interfacial and Interspecies Processes. American Chemical Society, Washington, DC, pp. 203–217.

Kaldy, J. E., Brown, C. A., Andersen, C. P., 2013. *In situ* ^{13}C tracer experiments elucidate carbon translocation rates and allocation patterns in eelgrass *Zostera marina* . Mar. Ecol. Prog. Ser. 487, 27–39.

Kemp, W. M., Murray, L., Borum, J., Sand-Jensen, K., 1987. Diel growth in eelgrass *Zostera marina*. Mar. Ecol. Prog. Ser. 41, 79–86.

Kirk, J. T. O., 1975. A theoretical analysis of the contribution of algal cells to the attenuation of light within natural waters. I. General treatment of suspensions of pigmented cells. New Phytol. 75, 11–20.

Kirk, J. T. O., 1991. Volume scattering function, average cosines, and the underwater light field. Limnol. Oceanogr. 36, 455–467.

Kirk, J. T. O., 1994. Light and Photosynthesis in Aquatic Ecosystems, 2nd Edition. Cambridge University Press, Cambridge.

Kooijman, S. A. L. M., 2010. Dynamic Energy Budget theory for metabolic organisation, 3rd Edition. Cambridge University Press.

Lee, K.-S., Dunton, K. H., 1999. Inorganic nitrogen acquisition in the seagrass *Thalassia testudinum* : Development of a whole-plant nitrogen budget. Limnol. Oceanogr. 44, 1204–1215.

Lee, Z., Carder, K. L., Arnone, R. A., 2002. Deriving inherent optical properties from water color: a multiband quasi-analytical algorithm for optically deep waters. Applied Optics 41, 5755–5772.

Lee, Z., Shang, S., Hu, C., Du, K., Weidermann, A., Hou, W., Lin, J., Lin, G., 2015. Secchi disk depth: A new theory and mechanistic model for underwater visibility. Remote sensing of environment 169, 139–149.

Leiper, I., Phinn, S., Dekker, A. G., 2012. Spectral reflectance of coral reef benthos and substrate assemblages on Heron Reef, Australia. Int. J. of Rem. Sens. 33, 3946–3965.

Longstaff, B. J., 2003. Investigations into the light requirements of seagrasses in northeast Australia. Ph.D. thesis, University of Queensland.

Macdonald, H. S., Baird, M. E., Middleton, J. H., 2009. The effect of wind on continental shelf carbon fluxes off southeast Australia: a numerical model. J. Geophys. Res. 114, C05016,doi:10.1029/2008JC004946.

Mann, K. H., Lazier, J. R. N., 2006. Dynamics of Marine Ecosystems, 3rd Edition. Blackwell Scientific Publications Inc., Oxford.

Margvelashvili, N., 2009. Stretched Eulerian coordinate model of coastal sediment transport. Computer Geosciences 35, 1167–1176.

McKenzie, L. J., 1994. Seasonal changes in biomass and shoot characteristics of a *Zostera capricorni*Aschers. dominant meadow in Cairns Harbour, northern Queensland. Aust. J. Mar. Freshwater. Res. 45, 1337–52.

Miller, R. L., McKee, B. A., 2004. Using modis terra 250 m imagery to map concentrations of suspended matter in coastal waters. Remote Sens. Environ. 93, 259–266.

Mishchenko, M. I., Travis, L. D., Lacis, A. A., 2002. Scattering, Absorption and Emission of Light by Small Particles. Cambridge University Press.

Mobley, C. D., 1994. Light and Water. Academic Press.

Monbet, P., Brunskill, G. J., Zagorskis, I., Pfitzner, J., 2007. Phosphorus speciation in the sediment and mass balance for the central region of the Great Barrier Reef continental shelf (Australia). Geochimica et Cosmochimica Acta 71, 2762–2779.

Mongin, M., Baird, M. E., 2014. The interacting effects of photosynthesis, calcification and water circulation on carbon chemistry variability on a coral reef flat: a modelling study. Ecol. Mod. 284, 19–34.

Mongin, M., Baird, M. E., Tilbrook, B., Matear, R. J., Lenton, A., Herzfeld, M., Wild-Allen, K. A., Skerratt, J., Margvelashvili, N., Robson, B. J., Duarte, C. M., Gustafsson, M. S. M., Ralph, P. J., Steven, A. D. L., 2016. The exposure of the Great Barrier Reef to ocean acidification. Nature Communications 7, 10732.

Monismith, S. G., Davis, K. A., Shellenbarger, G. G., Hench, J. L., Nidzieko, N. J., Santoro, A. E., Reidenbach, M. A., Rosman, J. H., Holtzman, R., Martens, C. S., Lindquist, N. L., Southwell, M. W., Genin, A., 2010. Flow effects on benthic grazing on phytoplankton by a Caribbean reef. Limnol. Oceanogr. 55, 1881–1892.

Monsen, N., Cloern, J., Lucas, L., Monismith, S. G., 2002. A comment on the use of flushing time, residence time, and age as transport time scales. Limnol. Oceanogr. 47, 1545–1553.

Morel, A., Bricaud, A., 1981. Theoretical results concerning light absorption in a discrete medium, and application to specific absorption of phytoplankton. Deep Sea Res. 28, 1375–1393.

Muller-Parker, G., Cook, C. B., D'Elia, C. F., 1994. Elemental composition of the coral *Pocillopora damicornis* exposed to elevated seawater ammonium. Pac. Sci. 48, 234–246.

Munhoven, G., 2013. Mathematics of the total alkalinity-pH equation pathway - to robust and universal solution algorithms: the SolveSAPHE package v1.0.1. Geosci. Model Dev. 6, 1367–1388.

Najjar, R., Orr, J., 1999. Biotic-howto. internal ocmip report, lsce/cea saclay, gif-sur-yvette, france 15. Tech. rep.

Nielsen, M. V., Sakshaug, E., 1993. Photobiological studies of *Skeletonema costatum* adapted to spectrally different light regimes. Limnol. Oceanogr. 38, 1576–1581.

Pailles, C., Moody, P. W., 1992. Phosphorus sorption-desorption by some sediments of the Johnstone Rivers catchments, northern Queensland. Aust. J. Mar. Freshwater Res. 43, 1535–1545.

Pasciak, W. J., Gavis, J., 1975. Transport limited nutrient uptake rates in *Dictylum brightwellii*. Limnol. Oceanogr. 20 (4), 604–617.

Petrou, K., Jimenez-Denness, I., Chartrand, K., McCormack, C., Rasheed, M., Ralph, P. J., 2013. Seasonal heterogeneity in the photophysiological response to air exposure in two tropical intertidal seagrass species. Mar. Ecol. Prog. Ser. 482, 93–106.

Petus, C., Marieua, V., Novoac, S., Chust, G., Bruneau, N., Froidefond, J.-M., 2014. Monitoring spatio-temporal variability of the Adour River turbid plume (Bay of Biscay, France) with MODIS 250-m imagery. Cont. Shelf Res. 74, 35–49.

Redfield, A. C., Ketchum, B. H., Richards, F. A., 1963. The influence of organisms on the composition of sea-water. In: Hill, N. (Ed.), The sea, 2nd Edition. Wiley, pp. 26–77.

Reichstetter, M., Fearns, P. R., Weeks, S. J., McKinna, L. I., Roelfsema, C., Furnas, M., 2015. Bottom reflectance in ocean color satellite remote sensing for coral reef environments. Remote Sens. 7, 15852.

Ribes, M., Atkinson, M. J., 2007. Effects of water velocity on picoplankton uptake by coral reef communities. Coral Reefs 26, 413–421.

Roberts, D. G., 1993. Root-hair structure and development in the seagrass *Halophila ovalis* (R. Br.) Hook. f. Aust. J. Mar. Freshw. Res. 44, 85–100.

Robson, B. J., Baird, M. E., Wild-Allen, K. A., 2013. A physiological model for the marine cyanobacteria, *Trichodesmium*. In: Piantadosi, J. R. S. A., Boland, J. (Eds.), MODSIM2013, 20th International Congress on Modelling and Simulation. Modelling and Simulation Society of Australia and New Zealand, ISBN: 978-0-9872143-3-1, www.mssanz.org.au/modsim2013/L5/robson.pdf, pp. 1652–1658.

Roelfsema, C. M., Phinn, S. R., 2012. Spectral reflectance library of selected biotic and abiotic coral reef features in Heron Reef. Tech. rep., Centre for Remote Sensing and Spatial Information Science, School of Geography, Planning and Environmental Management, University of Queensland, Brisbane, Australia, doi:10.1594/PANGAEA.804589.

Sathyendranath, S., Stuart, V., Nair, A., Oke, K., Nakane, T., Bouman, H., Forget, M.-H., Maass, H., Platt, T., 2009. Carbon-to-chlorophyll ratio and growth rate of phytoplankton in the sea. Mar. Ecol. Prog. Ser. 383, 73–84.

Schroeder, T., Devlin, M. J., Brando, V. E., Dekker, A. G., Brodie, J. E., Clementson, L. A., McKinna, L., 2012. Inter-annual variability of wet season freshwater plume extent into the Great Barrier Reef lagoon based on satellite coastal ocean colour observations. Mar. Poll. Bull. 65, 210–223.

Smith, R. C., Baker, K. S., 1981. Optical properties of the clearest natural waters. Applied Optics 20, 177–184.

Straile, D., 1997. Gross growth efficiencies of protozoan and metazoan zooplankton and their dependence on food concentration, predator-prey weight ratio, and taxonomic group. Limnol. Oceanogr. 42, 1375–1385.

Subramaniam, A., Carpenter, E. J., Karentz, D., Falkowski, P. G., 1999. Bio-optical properties of the marine diazotrophic cyanobacteria *Trichodesmium* spp. I. Absorption and photosynthetic action spectra. Limnol. Oceanogr. 44, 608–617.

Vaillancourt, R. D., Brown, C. W., Guillard, R. R. L., Balch, W. M., 2004. Light backscattering properties of marine phytoplankton: relationship to cell size, chemical composition and taxonomy. J. Plank. Res. 26, 191–212.

Vermaat, J. E., Agawin, N. S. R., Duarte, C. M., Fortes, M. D., Marba, N., Uri, J. S., 1995. Meadow maintenance, growth and productivity of a mixed Philippine seagrass bed. Mar. Ecolo. Prog. Ser. 124, 215–225.

Veron, J. E. N., 2008. A Reef in Time: The Great Barrier Reef from Beginning to End. Harvard University Press.

von Liebig, J., 1840. Chemistry in its Application to Agriculture and Physiology. Taylor and Walton, London.

Wangpraseurt, D., Larkum, A. W. D., Ralph, P. J., Kühl, M., 2012. Light gradients and optical microniches in coral tissues. Frontiers Microbiol. 3 (316).

Wanninkhof, R., 1992. Relationship between wind speed and gas exchange over the ocean. J. Geophys. Res. 97 (C5), 7373–7382.

Wanninkhof, R., McGillis, W. R., 1999. A cubic relationship between air-sea CO_2 exchange and wind speed. Geophys. Res. Letts. 26, 1889–1892.

Weeks, S., Werdell, P. J., Schaffelke, B., Canto, M., Lee, Z., Wilding, J. G., Feldman, G. C., 2012. Satellite-derived photic depth on the Great Barrier Reef: spatio-temporal patterns of water clarity. Remote Sens. 4, 3781–3795.

Weiss, R., 1970. The solubility of nitrogen, oxygen and argon in water and seawater. Deep Sea Res. 17, 721–735.

Wild-Allen, K., Herzfeld, M., Thompson, P. A., Rosebrock, U., Parslow, J., Volkman, J. K., 2010. Applied coastal biogeochemical modelling to quantify the environmental impact of fish farm nutrients and inform managers. J. Mar. Sys. 81, 134–147.

Wyatt, A. S. J., Lowe, R. J., Humphries, S., Waite, A. M., 2010. Particulate nutrient fluxes over a fringing coral reef: relevant scales of phytoplankton production and mechanisms of supply. Mar. Ecol. Prog. Ser. 405, 113–130.

Zeebe, R. E., Wolf-Gladrow, D., 2001. CO_2 in seawater: equilibrium, kinetics isotopes. Elsevier.

Zhang, Z., Lowe, R., Falter, J., Ivey, G., 2011. A numerical model of wave- and current-driven nutrient uptake by coral reef communities. Ecol. Mod. 222, 1456–1470.

A State (prognostic) variables

The below table lists the 10 dissolved (Table 37), 22 living (Table 38) and 11 non-living (Table 39) particulate, and 6 epibenthic (Table 40) state variables.

Name	Symbol	Units	Description
Total alkalinity (alk)	A_T	mol kg^{-1}	Concentration of ions that can be converted to uncharged species by a strong acid. The model assumes A_T =[HCO_3^-] + [CO_3^{2-}], often referred to as carbonate alkalinity. Alkalinity and DIC together quantify the equilibrium state of the seawater carbon chemistry.
Nitrate (NO3)	[NO_3^-]	mg N m^{-3}	Concentration of nitrate. In the absence of nitrite [NO_2^-] in the model, nitrate represents [NO_3^-] + [NO_2^-].
Ammonia (NH4)	[NH_4^-]	mg N m^{-3}	Concentration of ammonia.
Dissolved Inorganic Phosphorus (DIP)	P	mg P m^{-3}	Concentration of dissolved inorganic phosphorus, also referred to as orthophosphate or soluble reactive phosphorus, SRP, composed chiefly of HPO_4^{2-} ions, with a small percentage present as PO_4^{3-}.
Dissolved inorganic carbon (DIC)	DIC	mg C m^{-3}	Concentration of dissolved inorganic carbon, composed chiefly at seawater pH of HCO_3^-, with a small percentage present as CO_3^{2-}.
Dissolved oxygen (Oxygen)	[O_2]	mg O m^{-3}	Concentration of oxygen.
Chemical Oxygen Demand (COD)	COD	mg O m^{-3}	Concentration of products of anoxic respiration in oxygen units. This represents products such as hydrogen sulfide, H_2S, that are produced during anoxic respiration and which, upon reoxidation of the water, will consume oxygen.
Dissolved Organic Carbon (DOR_C)	O_C	mg C m^{-3}	The concentration of carbon in dissolved organic compounds.
Dissolved Organic Nitrogen (DOR_N)	O_N	mg N m^{-3}	The concentration of nitrogen in dissolved organic compounds.
Dissolved Organic Phosphorus (DOR_P)	O_P	mg P m^{-3}	The concentration of phosphorus in dissolved organic compounds.

Table 37: Long name (and variable name) in model output files, symbol and units used in this document, and a description of all dissolved state variables. When the concentration of an ion is given, the chemical formulae appears in [] brackets.

Name	Symbol & Units	Description
Phytoplankton N (*_N)	B [mg N m^{-3}]	Total structural biomass of nitrogen of the phytoplankton population. All microalgae have a C:N:P ratio of the structural material of 106:16:1. Thus the mass of phosphorus in the structural material of a population with a biomass B is given by: $\frac{1}{16}\frac{31}{14}B$ and the mass of carbon by: $\frac{106}{16}\frac{12}{14}$ B. The number of cells is given by B/m_N.
Phytoplankton N reserves (*_NR)	BR_N^* [mg N m^{-3}]	Total non-structural biomass of nitrogen of the phytoplankton population. Phytoplankton N reserves divided by Phytoplankton N is a number between 0 and 1 and represents the factor by which phytoplankton growth is inhibited due to the internal reserves of nitrogen.
Phytoplankton P reserves (*_PR)	$\frac{1}{16}\frac{31}{14}BR_P^*$ [mg P m^{-3}]	Total non-structural biomass of phosphorus of the phytoplankton population. Phytoplankton P reserves divided by (Phytoplankton N $\times\frac{1}{16}\frac{31}{14}$) is a number between 0 and 1 and represent the factor by which phytoplankton growth is inhibited due to the internal reserves of phosphorus.
Phytoplankton I reserves (*_I)	$\frac{1060}{16}\frac{1}{14}BR_I^*$ [mmol photon m^{-3}]	Total non-structural biomass of fixed carbon of the phytoplankton population, quantified in photons. Phytoplankton I reserves divided by (Phytoplankton N $\times\frac{1060}{16}\frac{1}{14}$) is a number between 0 and 1 and represent the factor by which phytoplankton growth is inhibited due to the internal reserves of energy (or fixed carbon).
Phytoplankton chlorophyll (*_Chl)	nc_iV [mg m^{-3}]	Concentration of the chlorophyll a pigment of the population. The four phytoplankton classes have two pigments, a chlorophyll a-based pigment and an accessory pigment. As the pigment concentration adjusts to optimise photosynthesis, including the presence of the accessory pigment, the intracellular content, c_iV, represents only the chlorophyll a-based pigment. As the model does not distinguish between monovinyl and di-vinyl forms of chlorophyll, this c_i represents either form, depending on the phytoplankton type.
Zooplankton N (ZooS_N, ZooL_N)	Z [mg N m^{-3}]	Total biomass of nitrogen in animals. With only small and large zooplankton categories resolved, small zooplankton represents the biomass of unicellular fast growing animals (protozoans) and large zooplankton represents the biomass of all other animals (metazoans). All zooplankton have a C:N:P ratio of 106:16:1. Thus the mass of phosphorus of a population with a biomass Z is given by: $\frac{1}{16}\frac{31}{14}Z$ and the mass of carbon by: $\frac{106}{16}\frac{12}{14}$ Z.

Table 38: Long name (and variable name) in model output files, symbol and units used in this document, and description of all biological particulate state variables in the model. The model contains four categories of phytoplankton (bracket is variable name prefix): small (PhyS), $r < 2$ μm phytoplankton; large (PhyL): $e > 2$ μm phytoplankton; trichodesmium (Tricho): nitrogen fixing phytoplankton; and benthic microalgae (MPB): fast-sinking diatoms that are suspended primarily in the top layer of sediment porewaters. The elemental ratio of phytoplankton including both structural material and reserves is given by: C:N:P $= 106(1 + R_I^*) : 16(1 + R_N^*) : (1 + R_P^*)$.

Name	Symbol	Units	Description
Mud (Mud)	Mud	[kg m^{-3}]	Small sized, re-suspending particles with a sinking velocity of 17 m d^{-1}.
Fine Sediment (FineSed)	$FineSed$	[kg m^{-3}]	Identical to Mud, except that it is initialised to zero in the model domain, and enters only from the catchments.
Sand (Sand)	$Sand$	[kg m^{-3}]	Medium sized, re-suspending particles with a sinking velocity of 173 m d^{-1}.
Gravel (Gravel)	$Gravel$	[kg m^{-3}]	Large, non-resuspending particles.
Particulate Inorganic Phosphorus (PIP)	PIP	[mg P m^{-3}]	Phosphorus ions that are absorbed onto particles. It is considered a particulate with the same properties as Mud.
Immobilised Particulate Inorganic Phosphorus (PIPI)	$PIPI$	[mg P m^{-3}]	Phosphorus that is permanently removed from the system through burial of PIP.
Labile Detritus Nitrogen Plank (DetPL_N)	D_{Red}	[mg N m^{-3}]	Concentration of N in labile (quickly broken down) organic matter with a C:N:P ratio of 106:16:1 derived from living microalgae, zooplankton, coral host tissue and zooxanthellae with the same C:N:P ratio. Thus the mass of phosphorus in D_{Red} is given by: $\frac{1}{16}\frac{31}{14}D_{Red}$ and the mass of carbon by: $\frac{106}{16}\frac{12}{14}D_{Red}$.
Labile Detritus Nitrogen Benthic (DetBL_N)	D_{Atk}	[mg N m^{-3}]	Concentration of N in labile (quickly broken down) organic matter with a C:N:P ratio of 550:30:1 derived from living seagrass and macroalgae with the same C:N:P ratio. Thus the mass of phosphorus in D_{Atk} is given by: $\frac{1}{30}\frac{31}{14}D_{Atk}$ and the mass of carbon by: $\frac{550}{30}\frac{12}{14}D_{Atk}$.
Refractory Detritus Carbon (DetR_C)	D_C	[mg C m^{-3}]	Concentration of carbon as particulate refractory (slowly breaking down) material. It is sourced only from the breakdown of labile detritus, and from rivers.
Refractory Detritus Nitrogen (DetR_N)	D_N	[mg N m^{-3}]	Concentration of nitrogen as particulate refractory (slowly breaking down) material. It is sourced only from the breakdown of labile detritus, and from rivers.
Refractory Detritus Phosphorus (DetR_P)	D_P	[mg P m^{-3}]	Concentration of phosphorus as particulate refractory (slowly breaking down) material. It is sourced only from the breakdown of labile detritus, and from rivers.

Table 39: Long name (and variable name) in model output files, symbol, unit used in this document, and description of all non-biological particulate state variables in the model.

Name	Symbol	Description
Macroalgae (MA)	MA [g N m^{-2}]	Concentration of nitrogen biomass per m^2 of macrolagae. Macroalgae (or seaweed) grows above all other benthic plants (corals, seagrasses, benthic microalgae). It is parameterised as a non-calcifying leafy algae, with a C:N:P ratio of 550:30:1, and a formulation for calculating the percentage of the bottom covered as $1 - \exp(-\Omega_{MA}\ MA)$. In the model, in the absence of both calcifying macroalgae (particularly *Halimeda*) and unicellular epiphytes, macroalgae represents the biomass of all seaweeds and epiphytes.
Seagrass (SG)	SG [g N m^{-2}]	Concentration of nitrogen biomass per m^2 of a seagrass form parameterised to be similar to *Zostera*. This form captures light after it has passed through macroalgae and before it passes through *Halophila*. This form is better adapted to high light, low nutrient conditions than *Halophila* as a result of a deeper root structure and being able to shade it. See macroalgae for elemental ratio and bottom cover.
Halophila (SGH)	SG [g N m^{-2}]	Concentration of nitrogen biomass per m^2 of a seagrass form parameterised to be similar to *Halophila*. This form captures light after it has passed through the *Zostera* seagrass form. The *Halophila* form is batter adapted to low light conditions than *Zostera*, having a faster growth rate and lower minimum light requirement. See macroalgae for elemental ratio and bottom cover.
Coral host N (CH_N)	CH [g N m^{-2}]	Concentration of nitrogen biomass per m^2 of coral host tissue in the entire grid cell. Unlike other epibenthic variables, corals area is assumed to exist in communities that are potentially smaller than the grid size. The fraction of the grid cell covered by corals is given by A_{CH}. Thus the biomass in the occupied region is given by CH/A_{CH}. The percent coverage of the coral of the bottom for the whole cell is given by $A_{CH}\,(1 - \exp(-\Omega_{CH}\ CH/A_{CH}))$. With only one type of coral resolved, CH represents the biomass of all symbiotic corals. Since the model contains no other benthic filter-feeders, CH best represent the sum of the biomass of all symbiotic filter-feeding organisms such as corals, sponges, clams etc. C:N:P is 106:16:1.
Coral symbiont N (CS_N)	CS [mg N m^{-2}]	Concentration of nitrogen biomass per m^2 of coral symbiont cells, or zooxanthellae. To determine the density of cells, use $n = CS/m_N$. The percentage of the bottom covered is given by $\frac{\pi}{2\sqrt{3}} n \pi r_{zoo}^2$ where πr^2 is the projected area of the cell, n is the number of cells, and $\pi/(2\sqrt{3}) \sim 0.9069$ accounts for the maximum packaging of spheres. C:N:P is 106:16:1.
Coral symbiont chl (CS_Chl)	nc_iV [mg chl m^{-2}]	Concentration of chlorophyll biomass per m^2 of coral symbiont cells. As chlorophyll is the only pigment resolved in the coral symbiont, c_i represents the sum of the concentration of all photosynthetic pigments within the cell and has an absorption spectrum of divinyl chlorophyll *a*.

Table 40: Long name (and variable name) in model output files, units, symbol used in this document, and description of all epibenthic state variables in the model. The order in the above table corresponds to their vertical position, and therefore the order in which they access light. Benthic microalage, being suspended in porewaters, is consider

B Diagnostic outputs

Name	Units	Description
Absorption at 440 nm (at_440)	m^{-1}	Total absorption due to clear water, CDOM, microalgae and suspended sediments at 440 nm.
Scattering at 550 nm (bt_550)	m^{-1}	Total scattering due to clear water, microalgae and suspended sediments at 550 nm.
Vertical attenuation at 490 nm (Kd_490)	m^{-1}	Vertical attenuation (along z axis not along zenith angle) of light at 490 nm.
Average PAR in layer (PAR)	mol photon m^{-2} d^{-1}	Mean downwelling photosynthetically available radiation (400 - 700 nm) within the layer.
Light intensity above seagrass (EpiPAR_sg)	mol photon m^{-2} d^{-1}	Mean downwelling photosynthetically available radiation (400 - 700 nm) above seagrass canopy.
Light intensity above sediment layer (EpiPAR)	mol photon m^{-2} d^{-1}	Mean downwelling photosynthetically available radiation (400 - 700 nm) at the sediment-water interface.
Vertical attenuation of heat (K_heat)	m^{-1}	Vertical attenuation (along z axis not along zenith angle) of heat energy.
Bicarbonate (HCO3)	mmol m^{-3}	Concentration of bicarbonate ions [HCO_3^-] calculated from carbon chemistry equlibra at water column values of T, S, DIC and A_T.
Carbonate (CO3)	mmol m^{-3}	Concentration of carbonate ions [CO_3^{2-}] calculated from carbon chemistry equlibra at water column values of T, S, DIC and A_T.
Oxygen % saturation (Oxy_sat)	%	Dissolved oxygen concentration as a percentage of the saturation concentration at atmospheric pressure and local T and S.
pH (PH)	$\log_{10}$ mol m^{-3}	pH based on [H^+] calculated from carbon chemistry equlibra at water column values of T, S, DIC and A_T.
Sea-air CO_2 flux (CO2_flux)	mg C m^{-2} s^{-1}	Flux of carbon from sea to air (positive from sea to air). The value is given in the layer in which it was deposited (must be thicker than 20 cm), but still represents an areal flux.
Sea-air O_2 flux (O2_flux)	mg O m^{-2} s^{-1}	Flux of oxygen from sea to air (positive from sea to air). The value is given in the layer in which it was deposited (must be thicker than 20 cm), but still represents an areal flux.
Delta pCO_2 (dco2star)	ppmv	Partial pressure of CO_2 in the ocean minus that of the atmosphere (396 ppmv).
Oceanic pCO_2 (pco2surf)	ppmv	Partial pressure of CO_2 in the ocean.

Table 41: Long name (and variable name) in model output files, units, and description of gas and optical diagnostic variables. Unless otherwise stated quantities are cell centred vertical averages.

Name	Units	Description
Total C, N, P (TC, TN, TP)	mg m^{-3}	Sum of dissolved and particulate C, N, and P.
Total chlorophyll a (Chl_a_sum)	mg m^{-3}	Sum of chlorophyll concentration of the four microalgae types ($\sum nc_i V_i$).
Ecology Fine Inorganics (EFI)	kg m^{-3}	Sum of fine sediment and mud concentrations.
Ecology Particulate Organics (EPO)	kg m^{-3}	Weight of carbon in microalgae, zooplankton, and particulate detritus.
Large phytoplankton net production (PhyL_N_pr)	mg C m^{-3} d^{-1}	Rate of large phytoplankton organic matter synthesis from inorganic constituents.
Small phytoplankton net production (PhyS_N_pr)	mg C m^{-3} d^{-1}	Rate of small phytoplankton organic matter synthesis from inorganic constituents.
Trichodesmium net production (Tricho_N_pr)	mg C m^{-3} d^{-1}	Rate of *Trichodesmium* organic matter synthesis from inorganic constituents.
Microphytobenthos net production (MPB_N_pr)	mg C m^{-3} d^{-1}	Rate of microphytobenthos organic matter synthesis from inorganic constituents.
Total phytoplankton net production (P_prod)	mg C m^{-3} d^{-1}	Rate of total phytoplankton organic matter synthesis from inorganic constituents.
Large zooplankton removal rate from small zooplankton	mg C m^{-3} d^{-1}	Rate of carnivory of large zooplankton on small zooplankton.
Small zooplankton removal rate from small phytoplankton	mg C m^{-3} d^{-1}	Secondary production of small zooplankton.
Large zooplankton removal rate from large phytoplankton	mg C m^{-3} d^{-1}	Secondary production of large zooplankton.
Zooplankton total grazing (Z_grazing)	mg C m^{-3} d^{-1}	Total secondary pelagic production - feeding of both zooplankton classes on phytoplankton.
N_2 fixation (Nfix)	mg N m^{-3} s^{-1}	Nitrogen fixation by *Trichodesmium*.

Table 42: Long name (and variable name) in model output files, units, and description of pelagic diagnostic variables.

Name	Units	Description
Total epibenthic C, N, P (EpiTC, EpiTN, EpiTP)	mg m^{-2}	Sum of C, N, and P in epibenthic plants and corals.
Coral inorganic supply (Coral_IN_up)	mg N m^{-2} s^{-1}	Flux of dissolved inorganic nitrogen into coral polyps from the water column, absorbed by zooxanthellae. Note that the flux is averaged over the whole grid cell, while the fraction of the bottom that is responsible for this uptake is given by A_{eff} (Eq. 152)
Coral organic supply (Coral_ON_up)	mg N m^{-2} s^{-1}	Flux of particulate organic nitrogen into coral polyps from the water column, consumed by the coral host. See coral organic supply.
Net calcification (Gnet)	mg C m^{-2} s^{-1}	Net calcification (calcification minus dissolution) at the sediment-water column interface leading to a change in the water column properties.
Halophila production (SGH_N_pr)	g N m^{-2} d^{-1}	Gross production of nitrogen in *Halophila*, where N fluxes are not accounted for in respiration.
Halophila growth rate (SGH_N_gr)	s^{-1}	Turnover time of above-ground *Halophila* biomass.
Seagrass growth rate (SG_N_gr)	s^{-1}	Turnover time of above-ground *Zostera* biomass.
Seagrass production (SG_N_pr)	g N m^{-2} d^{-1}	Gross production of nitrogen in *Zostera*, where N fluxes are not accounted for in respiration.
Macroalgae growth rate (MA_N_gr)	s^{-1}	Turnover time of macroalgae biomass.
Macroalgae production (MA_N_pr)	g N m^{-2} d^{-1}	Gross production of nitrogen in macroalgae, where N fluxes are not accounted for in respiration.

Table 43: Long name (and variable name) in model output files, units and description of benthic diagnostic variables.

B.1 Diagnostic age tracer

Tracer 'age' is a diagnostic tracer (Monsen et al., 2002; Macdonald et al., 2009) use to quantify the spatially-resolved residence time of water in different regions. The age tracer, τ, is advected and diffused by the hydrodynamic model using the same numerical schemes as other tracers such as salinity. When inside the region of interest, the age increases at the rate of 1 d d^{-1}. When the age tracer is outside the region of interest, its age decays (or anti-ages) at the rate of Φ d^{-1}. Thus, the local rate of change over the whole domain is given by:

$$\frac{\partial \tau}{\partial t} = 1 \tag{269}$$

$$\frac{\partial \tau}{\partial t} = -\Phi\tau \qquad \text{outside ageing region} \tag{270}$$

$$\tag{271}$$

In some applications the age is held to zero outside the region to represent time since water moved within the area of interested (such as the surface mixed layer (Baird et al., 2006)). For more information see Mongin et al. (2016).

B.2 Simulated true colour

True color images are often used in the geophysical sciences to provide a broad spatial view of a phenomenon such as cyclones, droughts or river plumes. Their strength lies in the human experience of natural colors that allows three 'layers' of information, and the interaction of these information streams, to be contained within one image. Spectacular true color images of, for example, the Great Barrier Reef (GBR), simultaneously depict reef, sand and mud substrates, sediment-laden river plumes and phytoplankton blooms. Further, the advection of spatially-variable suspended coloured constituents reveals highly-resolved flow patterns.

For these reasons and more, true color imagery has become a valued communication tool within both the geosciences and wider community. Here we demonstrate that the power of true colour images can be harnessed for interpreting geophysical models if the model output includes remote-sensing reflectance, or normalised water leaving radiance, at the red, green and blue wavelengths.

In order to interpret simulated true colour images, a palette of true colours from the model optical relationships has been painted (Fig. 11), for varying values of water column CDOM, NAP and chlorophyll concentration. The green hues produced for varying IOPs are quite similar, demonstrating the difficulty in ocean colour analysis. The most obvious trend in the image is that Chl produces a greener hue than NAP (top panels vs bottom panels). The difference between increasing

CDOM and chlorophyll (right panels vs left panels) is more subtle, which is a significant challenge in remote sensing of chlorophyll in high CDOM coastal waters (Schroeder et al., 2012).

The important role of scattering can be seen in Fig. 11. At low chl and / or NAP, the colour becomes dark at moderately low CDOM concentration. In reality CDOM is usually associated with either chlorophyll or NAP, hence natural waters rarely appear black.

As the model calculates remote-sensing reflectance at any wavelength, it is possible to reproduce simulated true colour images using the same algorithms as the MODIS processing (Fig. 12). The comparison of observed and modelled true colour images is particular insightful because the impact of multiple spectrally-distinct events (such as a sediment plume and a phytoplankton bloom) can be viewed on one image (Fig. 13). Furthermore, the colour match-up provides an intuitive and challenging test for parameterisation of the spectrally-resolved optical coefficients.

True colour images use intensity in the red, green and blue wavebands. We use the centre wavelengths of MODIS bands 1 (645 nm), 2 (555 nm) and 4 (470 nm). Simulated true colour image brightness is adjusted using the MODIS approach by linearly scaling the above surface remote-sensing reflectance at each wavelength so that the brightest band has an intensity of approximately 1. This requires multiplication of between 20 to 30. The scaled intensity is intensified in the darker bands by scaling [0 30 60 120 190 255]/255 onto [0 110 160 210 240 255]/255. The final image is rendered in MATLAB.

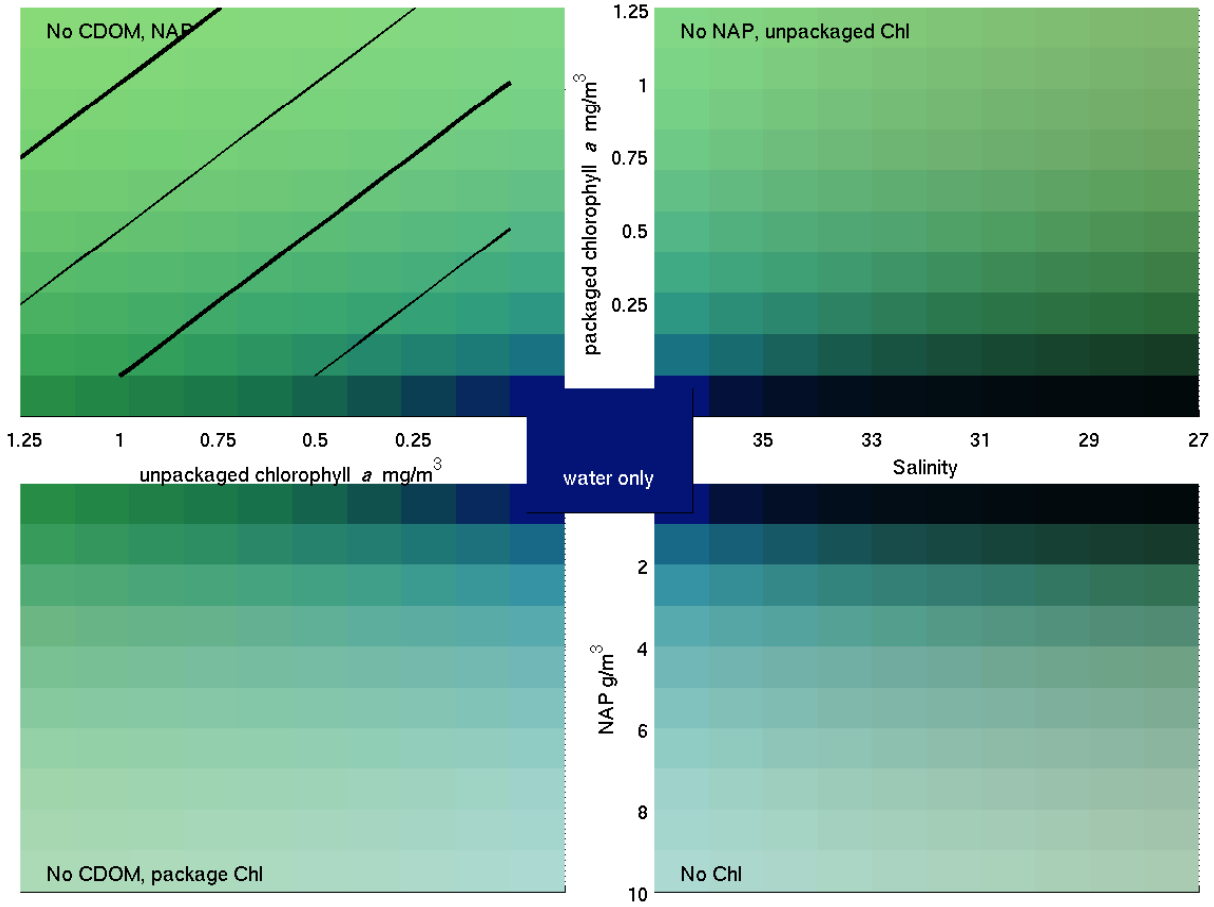

Figure 11: Palette of true colours from IOP relationships. The true colours are produced from the MODIS algorithm (Sec. B.2), and IOP relationships in Sec. 3.2.1. The centre box is the colour produced by clear water absorption and scattering alone. From the centre, moving right is increasing CDOM (as quantified by salinity), down is increasing NAP, and left and up are increasing chlorophyll in cells package by 0.35 and 0.73 respectively. The line contours in the top left panel are 0.5, 1, 1.5 and 2 mg Chl m^{-3}. Note that packaged chlorophyll is not plotted with NAP and unpackaged is not plotted with CDOM.

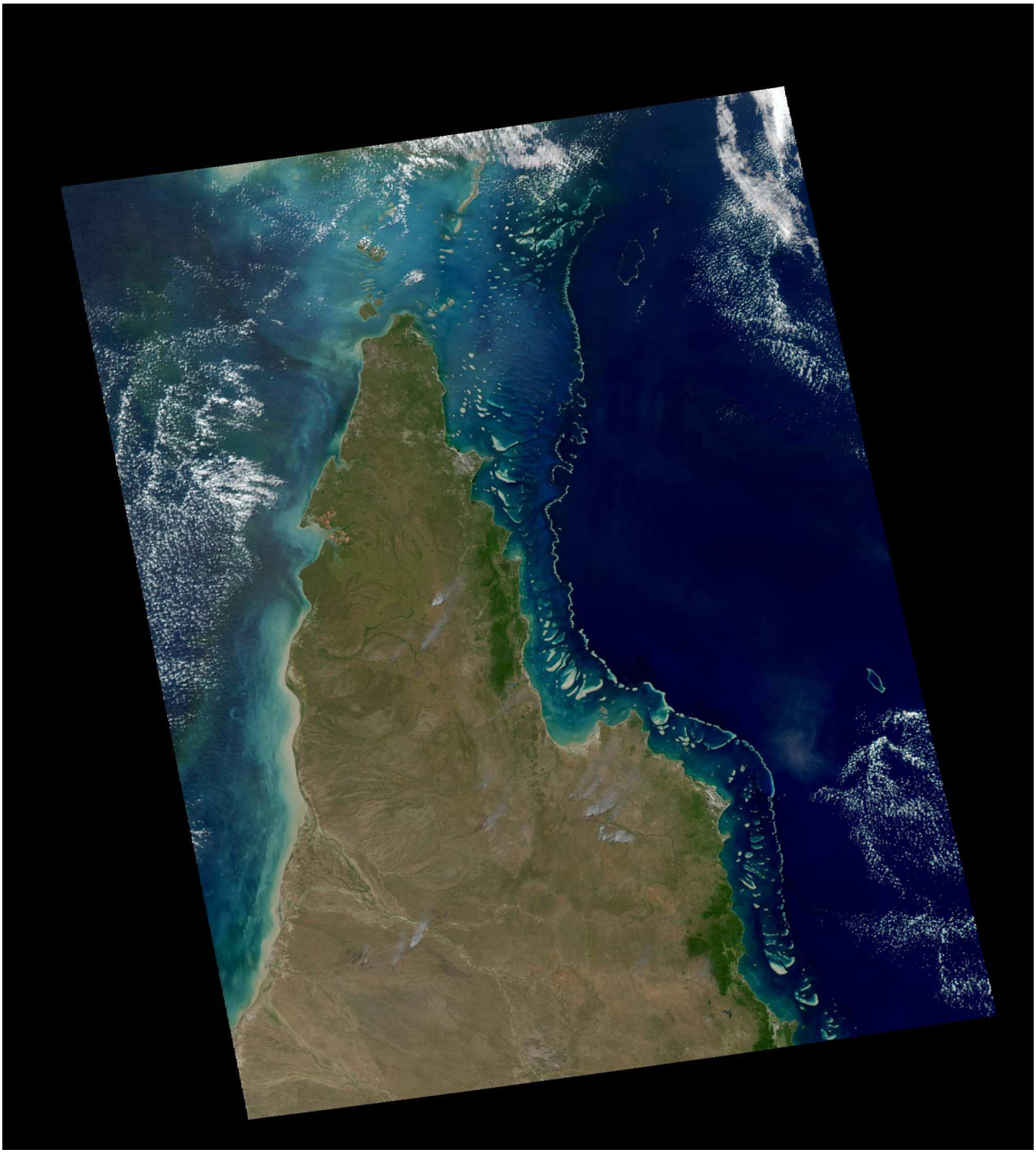

Figure 12: Observed true colour from MODIS using reflectance at 670, 555 and 470 nm.

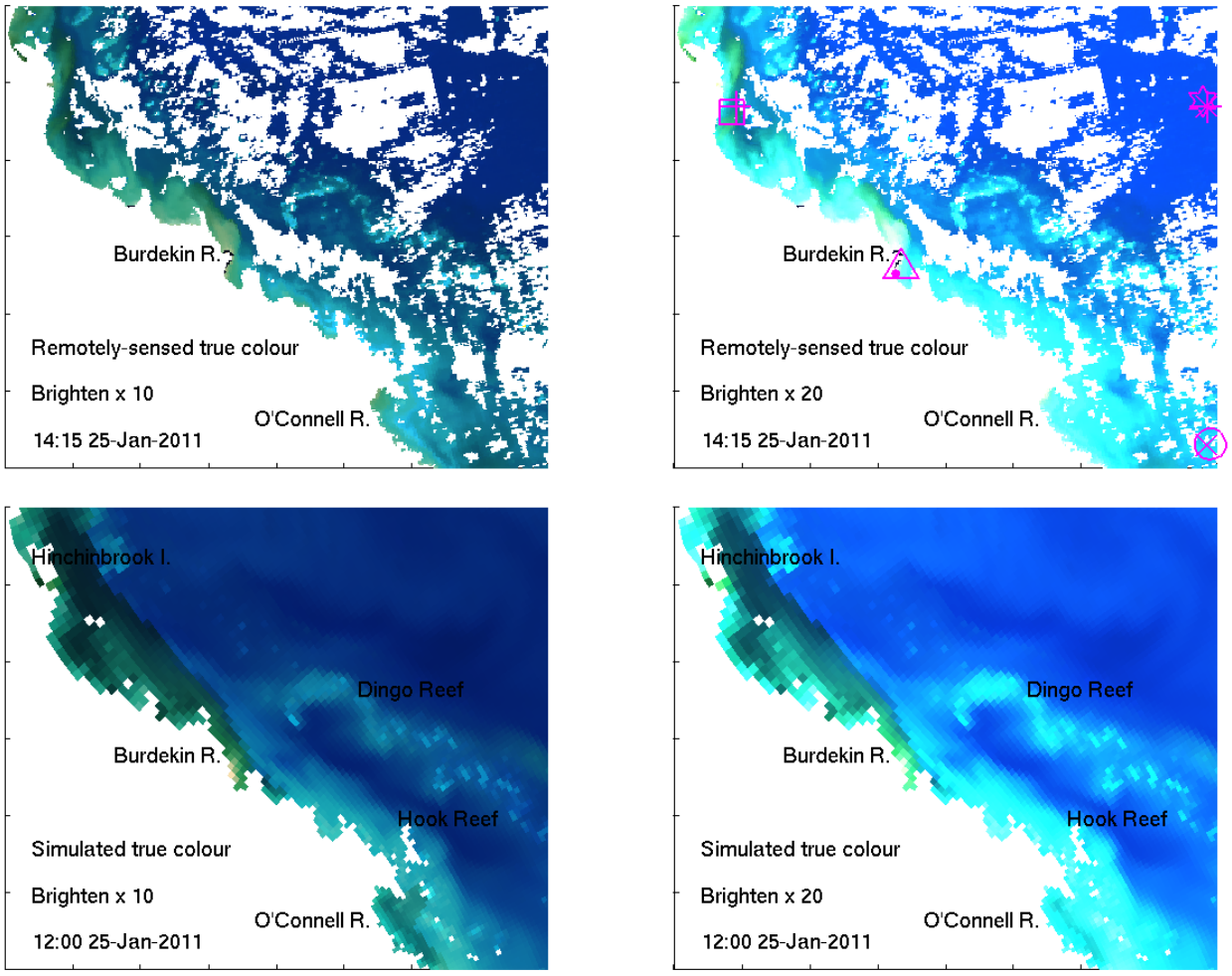

Figure 13: Observed (top) and simulated (bottom) true colour from simulated remote-sensing reflectance at 670, 555 and 470 nm in the GBR4 model configuration in the region of the Burdekin River. A brightening of 10 (left) and 20 (right) was applied for comparison.

B.3 Estimates of chlorophyll using the OC3 algorithm

The ratio of above-surface remote-sensing reflectance as a combination of three wavelengths, R', is given by:

$$R' = \log_{10}\left(\max\left[R_{rs,443}, R_{rs,488}\right]/R_{rs,551}\right) \tag{272}$$

The ratio R' is used in the MODIS OC3 algorithm to estimate surface chlorophyll, Chl_{OC3}, with coefficients from the 18 March 2010 reprocessing:

$$\mathrm{Chl}_{OC3} = 10^{0.283+R'(-2.753+R'(1.457+R'(0.659-1.403R')))} \tag{273}$$

obtained from `http://oceancolor.gsfc.nasa.gov/REPROCESSING/R2009/ocv6/` .

B.4 Estimates of vertical attenuation using the $K_{d,490}$ algorithm

The ratio of above-surface remote-sensing reflectance as a combination of two wavelengths, R', is given by:

$$R' = \log_{10}\left(R_{rs,488}/R_{rs,547}\right) \tag{274}$$

The ratio R' is used in the MODIS algorithm to estimate vertical attenuation at 490 nm, $K_{d,490}$, with coefficients from the 18 March 2010 reprocessing:

$$K_{d,490} = 10^{-0.8813+R'(-2.0584+R'(2.5878+R'(-3.4885-1.5061R')))} \tag{275}$$

obtained from `http://oceancolor.gsfc.nasa.gov/REPROCESSING/R2009/ocv6/` .

B.5 Estimates of particulate organic carbon using the POC algorithm

The ratio of above-surface remote-sensing reflectance as a combination of two wavelengths, R', is given by:

$$R' = \log_{10}\left(R_{rs,488}/R_{rs,555}\right) \tag{276}$$

The ratio R' is used in the MODIS algorithm to estimate concentration of particulate organic carbon, POC, with coefficients from the 18 March 2010 reprocessing:

$$POC = 308.3R'^{-1.639} \tag{277}$$

obtained from `http://oceancolor.gsfc.nasa.gov/REPROCESSING/R2009/ocv6/` .

B.6 Simulated turbidity from $b_{b,570}$

Turbidity is a measure of water clarity. The units of turbidity from a calibrated nephelometer are called Nephelometric Turbidity Units (NTU). Turbidity is often directly related to total suspended solids. However, as turbidity is measured optically (in the case of the three-wavelength Wetlabs sensor the scattering at 700 nm at a measured angle of 124°), it is better to produce a simulated turbidity - a calculation of what the optical model predicts an optical turbidity sensor would measure. Simulated turbidity, like simulated remote-sensing reflectance, is an example of "taking the model to the observations".

Thus, simulated turbidity (NTU) is given by:

$$\mathcal{T} = 47.02\,(b_{b,570} - 0.5 b_{b,clear,570}) + 0.13 \tag{278}$$

where $b_{b,570}$ is the backscattering coefficient at 570 nm, and the linear coefficient and offset were obtained from comparison of a BB9 backscattering sensor and a Wetlabs NTU at Lucinda Jetty, north Queensland. The coefficients are an empirical fit to the factory calibration of NTU standards. The clear water backscatter is removed because it was also removed in the output of the BB9.

B.7 Estimates of total suspended matter using 645 nm

We use a local relationship between the remote-sensing reflectance at 645 nm, $R_{rs,645}$ [sr^{-1}], and total suspended matter, TSM (Petus et al., 2014):

$$TSM = \left(12450 R_{rs,645}^2 + 666 R_{rs,645} + 0.48\right)/1000 \tag{279}$$

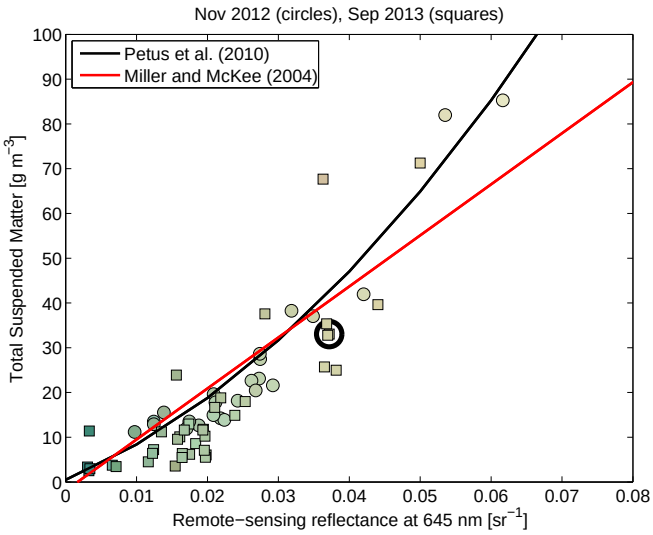

Figure 14: Relationship between the remote-sensing reflectance at 645 nm, $R_{rs,645}$, [sr^{-1}], and total suspended matter, TSM, in the samples taken during November 2012 (circles) and September 2013 (squares), compared to the empirical relationship of Petus et al. (2014) for the Bay of Biscay and Miller and McKee (2004) for the Mississippi. The symbols are coloured by true color, showing browner sites with higher TSM and remote-sensing reflectance. The black circle represents the site used for the model parameterisation of TSM optical properties.

B.8 Secchi depth

Over 5000 measurements of Secchi depth have been undertaken in the GBR and used to develop a satellite algorithm for Secchi depth (Weeks et al., 2012). We adopt this approach to define a simulated remotely-sensed Secchi depth, Z_{SD}:

$$Z_{SD,sim,rs} = 10^{\left(\log_{10}\left(2.303/K_{d,490}\right)-0.529\right)/0.816} \tag{280}$$

where $2.303/K_{d,490}$ gives the 10 percent light depth and the empirical constants come from Weeks et al. (2012).

Secchi depth is often calculated using:

$$Z_{SD} = 1.7/K_d \tag{281}$$

where K_d is a vertical attenuation of light, typically energy-weighted PAR. At particular wavelength the constant 1.7 varies. In a recent study (Lee et al., 2015), it was shown that the constant has a value of approximately 1.0 when the colour of human perception of the disk surface is used as the wavelength. This varies in different waters, from 486 to 475 nm, as the water clarity improves. Even though this value is slightly bluer than 490 nm, we found a good match with observations for:

$$Z_{SD,490} = 1/K_{d,490} \tag{282}$$

Finally these can be compared to the observed in situ Secchi depth, $Z_{SD,obs}$, and the remotely-sensed Secchi depth, $Z_{SD,rs}$.

B.9 Optical plume classification

Optical properties have been used to classify the extend of plumes (Devlin et al., 2013; Alvarez-Romero et al., 2013). Here we use a similar approach on simulated plumes. First we determine from observations the spectra of 6 standard plume classes (Fig. 15), as adopted by Alvarez-Romero et al. (2013). Using these standard plume classifications, we determine the dissimilarity between an observed or simulated spectra and the spectra of each standard class. The cosine dissimilarity between standard class c and the observed or simulated spectra, $S(c)$, is determined by:

$$S(c) = \cos^{-1}\left(\frac{\sum_{\lambda=1}^{W} R_{rs,c,\lambda} R_{rs,sim,\lambda}}{\sqrt{\sum_{\lambda=1}^{W} R_{rs,c,\lambda}^2}\sqrt{\sum_{\lambda=1}^{W} R_{rs,sim,\lambda}^2}}\right) \tag{283}$$

where $R_{rs,c,\lambda}$ is the remote-sensing reflectance of class c at wavelength λ, $R_{rs,sim,\lambda}$ is the remote-sensing reflectance of the simulation at wavelength λ and W is the number of wavelengths considered.

The observed or simulated spectra is then assigned to the standard class c with the minimum dissimilarity, S, between the standard class and the observed or simulated spectra.

A simplier spectra matching scheme using the rms difference between the spectra is also employed.

Using this classification technique we can compare the extent of plumes in an observed scene (Fig. 16 left), and a simulated scene (Fig. 16 right) of the same day. The areal extent of the observed and simulated plume classes can also be calculated, noting that the observed area is less due to clouds.

As a metric of the recent history of plume exposure, we propose a metric the plume exposure, $\mathcal{P}$, which is given by:

$$\mathcal{P} = \int_{t-t_{c<6}}^{t} (1/c)\, dt \tag{284}$$

where c is the plume class determined from Eq. 283. The plume exposure is calculated for each model grid cell. The metric is calculated from the most recent time that c for a grid cell was less than 6 (i.e. impacted by a plume class 1, 2, 3, 4 or 5). The metric is a weighted-running mean, such that exposure to plume class 1 for 10 days would give a value of 10, plume class 2 for 10 days 5, plume class 3 for 10 days would give 10/3 etc.

An additional concept is the annual plume extent, or the mean plume area over the year.

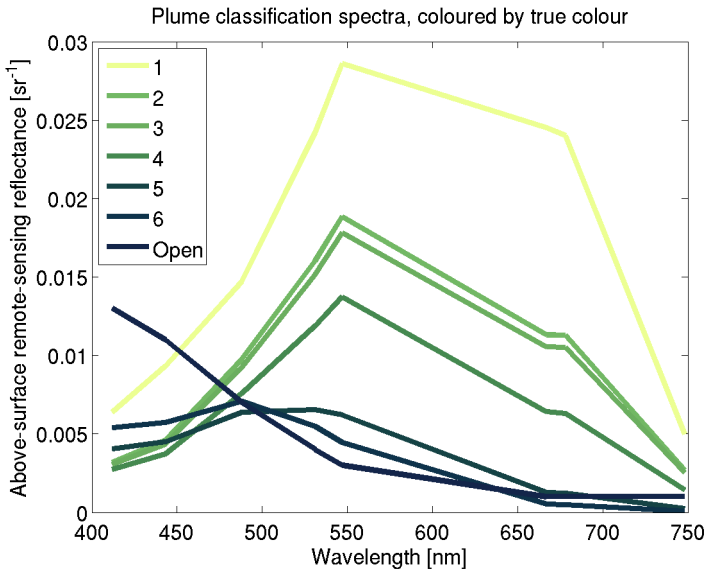

Figure 15: Spectra of each of the optical plume classifications (1-6) and the open ocean. The area in km^2 for each plume class within the region plotted is given on the left for both the observed and simulated classes.

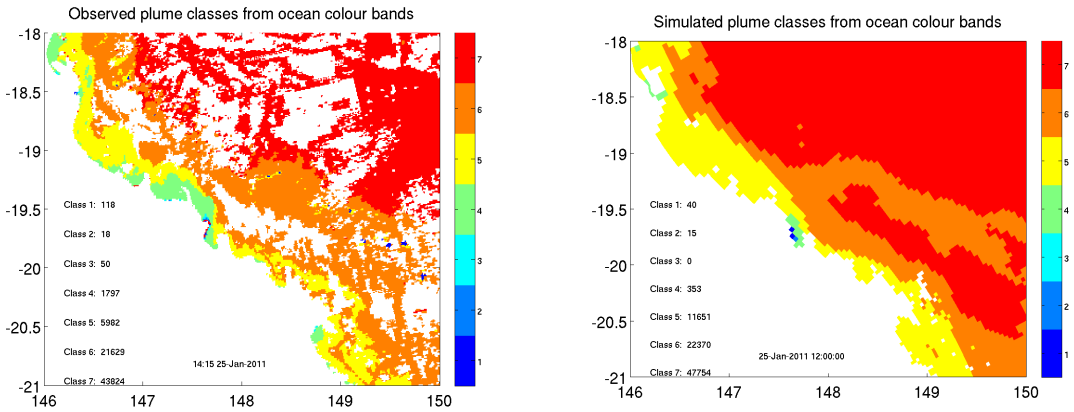

Figure 16: Observed and simulated optical plume classification on the 25 Jan 2011 in the Burdekin River region. See Fig. 15 for spectra of individual classes.

Description	Calculation	Application
Monthly bottom light (eqival. to daily dose]	1 hourly running-mean $\frac{1}{\tau}\int_0^t E_{d,\lambda,t}\exp(-\tau t)dt$ [mol m^{-2} d^{-1}]	seagrass viability
Aragonite dissolution exposure	$\int_{t-t_{\Omega<3}}^{t}(3-\Omega)\,dt$ reset time 1 day, [unit days]	acidification stress
Monthly net calcification rate	1 hourly running-mean $\frac{1}{\tau}\int_0^t g_{net,t}\exp(-\tau t)dt$	calcification index coral accretion
Temperature exposure (degree heating weeks)	$\int_{t-t_{T>T_{clim}}}^{t}(T-T_{clim})\,dt$ rest time 7 day, [°C weeks]	thermal coral bleaching
Weekly inorganic N uptake by corals	1 hourly running-mean $\frac{1}{\tau}\int_0^t G_t\exp(-\tau t)dt$	oxidative stress
Salinity exposure	$\int_{t-t_{S<28}}^{t}(28-S)\,dt$ reset time 1 day, [PSU days]	freshwater coral bleaching
Weekly net deposition rate (sinking / resuspension / diffusion)	1 hourly running-mean $\frac{1}{\tau}\int_0^t D_t\exp(-\tau t)dt$ [cm d^{-1}]	coral smothering
Hypoxic exposure	$\int_{t-t_{[O_2]<2000}}^{t}(2000-[O_2])\,dt$ rest time 1 hour, [mg O m^{-3} d^{-1}]	low oxygen stress
Weekly bottom light attenuation (approx. from 490 nm)	1 hourly running-mean $\frac{1}{\tau}\int_0^t K_{d,490,t}\exp(-\tau t)dt$ [m^{-1}]	predator visibility prey behaviour
Remote-sensing reflectance R_{rs}	see Section 3.2.2 412, 443, 488, 531, 547, 648, 667, 748 nm	comparison with ocean colour products
MODIS algorithms - Kd, OC3, TSS, POC - Kd, OC3, TSS, POC	empirical algorithms using remote-sensing reflectance	comparison with ocean colour products
Simulated true colour	RGB additive colour model using remote-sensing reflectance	water quality non-expert communication
Plume classification (1-6) + clear water	categorical from spectra matching using RMS errors on OC bands 1-7	plume extent

Table 44: Diagnostic variables. In addition to 60+ state variables, derived diagnostic variables have been developed in consultation with researchers and managers that provide metrics for improve understanding and application. For those metrics with a time scale, τ, the coefficient represents an exponential decay time - thus for a weekly running average, the impact of the value 1 week earlier on the running average is $100 \times \exp(-1)$, or 37 % of the impact of the present value.

C Parameter values used in eReefs GBR4 BGC

The below five tables of parameters are specified for each run, and are automatically generated by the EMS software after a run. All other parameters are hard-wired into the code.

Description	Name in code	Symbol	Value	Units
Reference temperature	Tref	T_{ref}	20.000000	Deg C
Temperature coefficient for rate parameters	Q10	$Q10$	2.000000	none
Nominal rate of TKE dissipation in water column	TKEeps	ϵ	0.000001	$m^2\ s^{-3}$
Atmospheric CO2	xco2_in_air	pCO_2	396.480000	ppmv
Concentration of dissolved N2	N2	$[N_2]_{gas}$	2000.000000	mg N m^{-3}
DOC-specific absorption of CDOM 443 nm	acdom443star	$k_{CDOM,443}$	0.000130	m^2 mg C^{-1}

Table 45: Environmental parameters in GBR4 BGC

Description	Name in code	Symbol	Value	Units
Maximum growth rate of PL at Tref	PLumax	μ_{PL}^{max}	1.400000	d^{-1}
Radius of the large phytoplankton cells	PLrad	r_{PL}	0.000004	m
Natural (linear) mortality rate, large phyto.	PhyL_mL	$m_{L,PL}$	0.100000	d^{-1}
Natural (linear) mortality rate in sediment, large phyto.	PhyL_mL_sed	$m_{L,PL,sed}$	1.000000	d^{-1}
Maximum growth rate of PS at Tref	PSumax	μ_{PL}^{max}	1.600000	d^{-1}
Radius of the small phytoplankton cells	PSrad	r_{PS}	0.000001	m
Natural (linear) mortality rate, small phytoplankton	PhyS_mL	$m_{L,PS}$	0.100000	d^{-1}
Natural (linear) mortality rate in sediment, small phyto.	PhyS_mL_sed	$m_{L,PS,sed}$	1.000000	d^{-1}
Maximum growth rate of MB at Tref	MBumax	μ_{MPB}^{max}	0.839000	d^{-1}
Radius of the MPB cells	MBrad	r_{MPB}	0.000010	m
Natural (quadratic) mort. rate of MPB in sediment	MPB_mQ	$m_{Q,MPB}$	0.000100	$d^{-1}(mg\ N\ m^{-3})^{-1}$
Ratio of xanthophyll to chl a of PS	PSxan2chl	$\Theta_{xan2chl,PS}$	0.510000	mg mg $^{-1}$
Ratio of xanthophyll to chl a of PL	PLxan2chl	$\Theta_{xan2chl,PL}$	0.810000	mg mg $^{-1}$
Ratio of xanthophyll to chl a of MPB	MBxan2chl	$\Theta_{xan2chl,MPB}$	0.810000	mg mg $^{-1}$
Maximum growth rate of *Trichodesmium* at Tref	Tricho_umax	μ_{MPB}^{max}	0.240000	d^{-1}
Radius of *Trichodesmium* colonies	Tricho_rad	r_{MPB}	0.000005	m
Sherwood number for the Tricho dimensionless	Tricho_Sh	Sh_{Tricho}	1.000000	none
Linear mortality for Tricho in sediment	Tricho_mL	$m_{L,Tricho}$	0.140000	d^{-1}
Quadratic mortality for Tricho due to phages in wc	Tricho_mQ	$m_{Q,Tricho}$	0.200000	$d^{-1}(mg\ N\ m^{-3})^{-1}$
Critical Tricho above which quadratic mortality applies	Tricho_crit		0.000200	mg N m^{-3}
Minimum density of *Trichodesmium*	p_min	$\rho_{min,Tricho}$	990.000000	kg m^{-3}
Maximum density of *Trichodesmium*	p_max	$\rho_{max,Tricho}$	1060.000000	kg m^{-3}
DIN conc below which Tricho N fixes	DINcrit	DIN_{crit}	10.000000	mg N m^{-3}
Ratio of xanthophyll to chl a of *Trichodesmium*	Trichoxan2chl	$\Theta_{xan2chl,Tricho}$	0.500000	mg mg $^{-1}$
Chl-specific scattering coef. for microalgae	bphy	b_{phy}	0.200000	$m^{-1}(mg\ Chla\ m^{-3})^{-1}$
Nominal N:Chl a ratio in phytoplankton by weight	NtoCHL	$R_{N:Chl}$	7.000000	g N(g Chla)$^{-1}$
Minimum carbon to chlorophyll a ratio	C2Chlmin	θ_{min}	20.000000	wt/wt

Table 46: Phytoplankton parameters GBR4 BGC.

Description	Name in code	Symbol	Value	Units
Maximum growth rate of ZS at Tref	ZSumax	μ_{max}^{ZS}	4.000000	d^{-1}
Radius of the small zooplankton cells	ZSrad	r_{ZS}	0.000005	m
Swimming velocity for small zooplankton	ZSswim	U_{ZS}	0.000200	m s^{-1}
Grazing technique of small zooplankton	ZSmeth		rect	none
Maximum growth rate of ZL at Tref	ZLumax	μ_{max}^{ZL}	1.330000	d^{-1}
Radius of the large zooplankton cells	ZLrad	r_{ZL}	0.000320	m
Swimming velocity for large zooplankton	ZLswim	U_{ZL}	0.003000	m s^{-1}
Grazing technique of large zooplankton	ZLmeth		rect	none
Growth efficiency, large zooplankton	ZL_E	E_{ZL}	0.426000	none
Growth efficiency, small zooplankton	ZS_E	E_{ZS}	0.462000	none
Natural (quadratic) mortality rate, large zooplankton	ZL_mQ	$m_{Q,ZL}$	0.012000	d^{-1}(mg N m^{-3})$^{-1}$
Natural (quadratic) mortality rate, small zooplankton	ZS_mQ	$m_{Q,ZS}$	0.007000	d^{-1}(mg N m^{-3})$^{-1}$
Fraction of growth inefficiency lost to detritus, large zooplankton	ZL_FDG	γ_{ZL}	0.500000	none
Fraction of mortality lost to detritus, large zooplankton	ZL_FDM	N/A	1.000000	none
Fraction of growth inefficiency lost to detritus, small zooplankton	ZS_FDG	γ_{ZS}	0.500000	none
Fraction of mortality lost to detritus, small zooplankton	ZS_FDM	N/A	1.000000	none

Table 47: Zooplankton parameters GBR4 BGC.

Description	Name in code	Symbol	Value	Units
Fraction of labile detritus converted to refractory detritus	F_LD_RD	ζ_{Red}	0.190000	none
Fraction of labile detritus converted to dissolved organic matter	F_LD_DOM	ϑ_{Red}	0.100000	none
fraction of refractory detritus that breaks down to DOM	F_RD_DOM	ϑ_{Ref}	0.050000	none
Breakdown rate of labile detritus at 106:16:1	r_DetPL	r_{Red}	0.040000	d^{-1}
Breakdown rate of labile detritus at 550:30:1	r_DetBL	r_{Atk}	0.001000	d^{-1}
Breakdown rate of refractory detritus	r_RD	r_R	0.001000	d^{-1}
Breakdown rate of dissolved organic matter	r_DOM	r_O	0.000100	d^{-1}
Respiration as a fraction of umax	Plank_resp	ϕ	0.025000	none
Oxygen half-saturation for aerobic respiration	KO_aer	K_{OA}	256.000000	mg O m^{-3}
Maximum nitrification rate in water column	r_nit_wc	$\tau_{nit,wc}$	0.100000	d^{-1}
Maximum nitrification rate in water sediment	r_nit_sed	$\tau_{nit,sed}$	20.000000	d^{-1}
Oxygen half-saturation for nitrification	KO_nit	$K_{O_2,nit}$	500.000000	mg O m^{-3}
Rate at which P reaches adsorbed/desorbed equilibrium	Pads_r	τ_{Pabs}	0.040000	d^{-1}
Freundlich Isothermic Const P adsorption to TSS in water column	Pads_Kwc	$k_{Pads,wc}$	300.000000	mg P kg TSS^{-1}
Freundlich Isothermic Const P adsorption to TSS in sediment	Pads_Ksed	$k_{Pads,sed}$	74.000000	mg P kg TSS^{-1}
Oxygen half-saturation for P adsorption	Pads_KO	$K_{O_2,abs}$	2000.000000	mg O m^{-3}
Exponent for Freundlich Isotherm	Pads_exp	N/A	1.000000	none
Maximum denitrification rate	r_den	τ_{denit}	5.000000	d^{-1}
Oxygen half-saturation constant for denitrification	KO_den	$K_{O_2,denit}$	10000.000000	mg O m^{-3}
Rate of conversion of PIP to immobilised PIP	r_immob_PIP	τ_{Pimm}	0.001200	d^{-1}

Table 48: Detritus parameters GBR4 BGC.

Description	Name in code	Symbol	Value	Units
Sediment-water diffusion coefficient	EpiDiffCoeff	D	0.000000	$m^2\ s^{-1}$
Thickness of diffusive layer	EpiDiffDz	h	0.006500	m
Maximum growth rate of MA at Tref	MAumax	μ_{MA}^{max}	1.000000	d^{-1}
Natural (linear) mortality rate, macroalgae	MA_mL	ζ_{MA}	0.010000	d^{-1}
Nitrogen-specific leaf area of macroalgae	MAleafden	Ω_{MA}	1.000000	$m^2\ g\ N^{-1}$
Respiration as a fraction of umax	Benth_resp	ϕ	0.025000	none
net dissolution rate of sediment without coral	dissCaCO3_sed	d_{sand}	0.000700	$mmol\ C\ m^{-2}\ s^{-1}$
Grid scale to reef scale ratio	CHarea	A_{CH}	0.100000	$m^2\ m^{-2}$
Nitrogen-specific host area of coral polyp	CHpolypden	Ω_{CH}	2.000000	$m^2\ g\ N^{-1}$
Max. growth rate of Coral at Tref	CHumax	μ_{CH}^{max}	0.050000	d^{-1}
Max. growth rate of zooxanthellae at Tref	CSumax	μ_{CS}^{max}	0.400000	d^{-1}
Radius of the zooxanthellae	CSrad	r_{CS}	0.000005	m
Quadratic mortality rate of coral polyp	CHmort	ζ_{CH}	0.010000	$(g\ N\ m^{-3})^{-1}\ d^{-1}$
Linear mortality rate of zooxanthellae	CSmort	ζ_{CS}	0.040000	d^{-1}
Fraction of coral host death translocated.	CHremin	f_{remin}	0.500000	-
Rate coefficent for particle uptake by corals	Splank	S_{part}	3.000000	$m\ d^{-1}$
Maximum daytime coral calcification	k_day_coral	k_{day}	0.013200	$mmol\ C\ m^{-2}\ s^{-1}$
Maximum nightime coral calcification	k_night_coral	k_{night}	0.006900	$mmol\ C\ m^{-2}\ s^{-1}$
Carbonate sediment dissolution rate on shelf	dissCaCO3_shelf	d_{shelf}	0.000100	$mmol\ C\ m^{-2}\ s^{-1}$
Age tracer growth rate per day	ageing_decay	n/a	1.000000	$d\ d^{-1}$
Age tracer decay rate per day outside source	anti_ageing_decay	Φ	0.100000	d^{-1}

Table 49: Benthic parameters GBR4 BGC, excluding seagrass

Description	Name in code	Symbol	Value	Units
Maximum growth rate of SG at Tref	SGumax	μ_{SG}^{max}	0.400000	d^{-1}
Half-saturation of SG N uptake in SED	SG_KN	$K_{SG,N}$	420.000000	mg N m^{-3}
Half-saturation of SG P uptake in SED	SG_KP	$K_{SG,P}$	96.000000	mg P m^{-3}
Natural (linear) mortality rate aboveground seagrass	SG_mL	ζ_{SG_A}	0.040000	d^{-1}
Natural (linear) mortality rate belowground seagrass	SGROOT_mL	ζ_{SG_B}	0.004000	d^{-1}
Fraction (target) of SG biomass below-ground	SGfrac	$f_{below,SG}$	0.500000	-
Time scale for seagrass translocation	SGtransrate	$\tau_{tran,SG}$	0.033300	d^{-1}
Nitrogen-specific leaf area of seagrass	SGleafden	Ω_{SG}	1.500000	m^2 g N^{-1}
Seagrass seed biomass as fraction of 63 % cover	SGseedfrac	$f_{seed,SG}$	0.010000	-
Sine of nadir Zostera canopy bending angle	SGorient	$\sin\beta_{blade,SG}$	0.500000	-
Compensation irradiance for Zostera	SGmlr	$E_{comp,SG}$	4.500000	mol m^{-2}
Maximum depth for Zostera roots	SGrootdepth	$z_{root,SG}$	-0.150000	m
Maximum growth rate of SGH at Tref	SGHumax	μ_{SGH}^{max}	0.400000	d^{-1}
Half-saturation of SGH N uptake in SED	SGH_KN	$K_{SGH,N}$	420.000000	mg N m^{-3}
Half-saturation of SGH P uptake in SED	SGH_KP	$K_{SGH,P}$	96.000000	mg P m^{-3}
Nitrogen-specific leaf area of SGH	SGHleafden	Ω_{SGH}	1.900000	m^2 g N^{-1}
Natural (linear) mortality rate, aboveground SGH	SGH_mL	ζ_{SGH_A}	0.080000	d^{-1}
Natural (linear) mortality rate, belowground SGH	SGHROOT_mL	ζ_{SGH_B}	0.004000	d^{-1}
Fraction (target) of SGH biomass below-ground	SGHfrac	$f_{below,SGH}$	0.250000	-
Time scale for seagrass translocation	SGHtransrate	$\tau_{tran,SGH}$	0.033300	d^{-1}
Halophila seed biomass as fraction of 63 % cover	SGHseedfrac	$f_{seed,SGH}$	0.010000	-
Sine of nadir Halophila canopy bending angle	SGHorient	$\sin\beta_{blade,SGH}$	1.000000	-
Compensation irradiance for Halophila	SGHmlr	$E_{comp,SGH}$	2.800000	mol m^{-2}
Maximum depth for Halophila roots	SGHrootdepth	$z_{root,SGH}$	-0.080000	m

Table 50: Seagrass parameters GBR4 BGC.